

ISSN 0352-9045

# *Informacije* MIDEM

*Journal of Microelectronics,  
Electronic Components and Materials*  
**Vol. 42, No. 4 (2012), December 2012**

*Revija za mikroelektroniko,  
elektronske sestavne dele in materiale*  
**letnik 42, številka 4 (2012), December 2012**



# Informacije MIDE M 4-2012

Journal of Microelectronics, Electronic Components and Materials

VOLUME 42, NO. 4(144), LJUBLJANA, DECEMBER 2012 | LETNIK 42, NO. 4(144), LJUBLJANA, DECEMBER 2012

Published quarterly (March, June, September, December) by Society for Microelectronics, Electronic Components and Materials - MIDE M.  
Copyright © 2012. All rights reserved. | Revija izhaja trimesečno (marec, junij, september, december). Izdaja Strokovno društvo za mikroelektroniko, elektronske sestavne dele in materiale – Društvo MIDE M. Copyright © 2012. Vse pravice pridržane.

## Editor in Chief | Glavni in odgovorni urednik

Marko Topič, University of Ljubljana (UL), Faculty of Electrical Engineering, Slovenia

## Editor of Electronic Edition | Urednik elektronske izdaje

Kristijan Brecl, UL, Faculty of Electrical Engineering, Slovenia

## Associate Editors | Odgovorni področni uredniki

Vanja Ambrožič, UL, Faculty of Electrical Engineering, Slovenia  
Slavko Amon, UL, Faculty of Electrical Engineering, Slovenia  
Danjela Kuščer Hrovatin, Jožef Stefan Institute, Slovenia  
Matjaž Vidmar, UL, Faculty of Electrical Engineering, Slovenia  
Andrej Žemva, UL, Faculty of Electrical Engineering, Slovenia

## Editorial Board | Uredniški odbor

Mohamed Akil, ESIEE PARIS, France  
Giuseppe Buja, University of Padova, Italy  
Gian-Franco Dalla Betta, University of Trento, Italy  
Martyn Fice, University College London, United Kingdom  
Ciprian Iliescu, Institute of Bioengineering and Nanotechnology, A\*STAR, Singapore  
Malgorzata Jakubowska, Warsaw University of Technology, Poland  
Marc Lethiecq, University of Tours, France  
Teresa Orłowska-Kowalska, Wrocław University of Technology, Poland  
Luca Palmieri, University of Padova, Italy

## International Advisory Board | Časopisni svet

Janez Trontelj, UL, Faculty of Electrical Engineering, Slovenia - Chairman  
Cor Claeys, IMEC, Leuven, Belgium  
Denis Donlagič, University of Maribor, Faculty of Elec. Eng. and Computer Science, Slovenia  
Zvonko Fazarinc, CIS, Stanford University, Stanford, USA  
Leszek J. Golonka, Technical University Wrocław, Wrocław, Poland  
Jean-Marie Haussonne, EIC-LUSAC, Octeville, France  
Marija Kosec, Jožef Stefan Institute, Slovenia  
Miran Mozetič, Jožef Stefan Institute, Slovenia  
Stane Pejovnik, UL, Faculty of Chemistry and Chemical Technology, Slovenia  
Giorgio Pignatelli, University of Perugia, Italy  
Giovanni Soncini, University of Trento, Trento, Italy  
Iztok Šorli, MIKROIKS d.o.o., Ljubljana, Slovenia

## Headquarters | Naslov uredništva

Uredništvo Informacije MIDE M  
MIDE M pri MIKROIKS  
Stegne 11, 1521 Ljubljana, Slovenia  
T. +386 (0)1 513 37 68  
F. + 386 (0)1 513 37 71  
E. info@midem-drustvo.si  
www.midem-drustvo.si

Annual subscription rate is 100 EUR, separate issue is 25 EUR. MIDE M members and Society sponsors receive current issues for free. Scientific Council for Technical Sciences of Slovenian Research Agency has recognized Informacije MIDE M as scientific Journal for micro-electronics, electronic components and materials. Publishing of the Journal is cofinanced by Slovenian Book Agency and by Society sponsors. Scientific and professional papers published in the journal are indexed and abstracted in COBIS and INSPEC databases. The Journal is indexed by ISI® for Sci Search®, Research Alert® and Material Science Citation Index™.

Letna naročnina je 100 EUR, cena posamezne številke pa 25 EUR. Člani in sponzorji MIDE M prejema jo posamezne številke brezplačno. Znanstveni svet za tehnične vede je podal pozitivno mnenje o reviji kot znanstveno-strokovni reviji za mikroelektroniko, elektronske sestavne dele in materiale. Izdajo revije sofinancirajo JAKRS in sponzorji društva. Znanstveno-strokovne prispevke objavljene v Informacijah MIDE M zajemamo v podatkovne baze COBIS in INSPEC. Prispevke iz revije zajema ISI® v naslednje svoje produkte: Sci Search®, Research Alert® in Materials Science Citation Index™.

Po mnenju Ministrstva za informiranje št.23/300-92 se šteje glasilo Informacije MIDE M med proizvode informativnega značaja.

## Content | Vsebina

<i>Original scientific papers</i>		<i>Izvirni članki</i>
Editorial	210	Uvodnik
F. Bechtold: Innovation Steps Towards A Novel and Cost Efficient LTCC Packaging Technology for High End Applications	211	F. Bechtold: Inovativni koraki proti novi in ceneni LTCC tehnologiji pakiranja za visokotehnoške aplikacije
L. J. Golonka, K. Malecha: LTCC Fluidic Microsystems	225	L. J. Golonka, K. Malecha: Tekočinski LTCC mikrosistemi
T. Maeder, C. Slater, B. Jiang, F. Vecchio, C. Jacq, P. Ryser: 3D Structuration of LTCC and Related Technologies for Thermal Management and Microfluidic Structures	234	T. Maeder, C. Slater, B. Jiang, F. Vecchio, C. Jacq, P. Ryser: 3D strukturiranje LTCC in sorodnih tehnologij za termično upravljanje in mikro tekočinske strukture
A. Karbasi, W. K. Jones: Cofired Platinum /Alumina Microsystems for Implantable Medical Applications	245	A. Karbasi, W. K. Jones: Žgani mikrosistemi platina/aluminijev oksid za implantacijske medicinske naprave
R. Bermejo: Mechanical Properties of Low Temperature Co-fired Ceramics: Testing Methodologies for Strength Characterization	254	R. Bermejo: Mehanske lastnosti keramike z nizko temperaturo žganja: metodologije testiranja trdnosti
U. Partsch, C. Lenz, S. Ziesche, C. Lohrberg, H. Neubert, T. Maeder: LTCC-based Sensors for Mechanical Quantities	260	U. Partsch, C. Lenz, S. Ziesche, C. Lohrberg, H. Neubert, T. Maeder: Senzorji mehanskih veličin na osnovi LTCC
G. Radosavljević: Wireless LTCC sensors for monitoring of pressure, temperature and moisture	272	G. Radosavljević: Brezžični LTCC senzorji za merjenje pritiska, temperature in vlage
D. Nesić, I. Jokić, M. Frantlović, M. Sarajlić: Wide Band-Stop Microwave Microstrip Filter on High-Resistivity Silicon	282	D. Nesić, I. Jokić, M. Frantlović, M. Sarajlić: Širokopasovni zaporni mikrovalovni mikrotrakasti filter na visoko uporovnem siliciju
In memoriam: Marija Kosec	287	V spomin: Marija Kosec
Announcement and Call for Papers: 49 <sup>th</sup> International Conference on Microelectronics, Devices and Materials With the Workshop on Digital Electronic Systems	289	Napoved in vabilo k udeležbi: 49. Mednarodna konferenca o mikroelektroniki, napravah in materialih z delavnico o digitalnih elektronskih sistemih
Front page : Attendees of the 48 <sup>th</sup> International Conference on Microelectronics, Devices and Materials, Otočec, Slovenia, 2012		Naslovnica: Udeleženci 48. mednarodne konference MIDEM, Otočec, 2012

---

## *Editorial | Uvodnik*

Dear Reader,

Year 2012 is running out. Last December days bring festive atmosphere in each home, office or research laboratory. Let last December days bring joy and peacefulness to all. It is the time to look back to the whole 2012, but also to look ahead and make plans for the coming year.

In the last December days Society MIDEEM has lost an outstanding member Professor Marija Kosec. After several months of fight against incurable illness Professor Marija Kosec passed away on 23 Dec 2012. She was a wonderful person, scientist, innovator, leader and mentor. She had been the head of Electronic Ceramics Department of Institute »Jozef Stefan« and led the Centre of Excellence NAMASTE, member of several committees, societies and two academies: Slovenian Academy of Engineering and World Academy of Ceramics, and recipient of several national and international awards. She is past president and past vice-president of the Society MIDEEM (Society for Microelectronics, Electronic Devices and Materials) and the Chairperson of the MIDEEM 2012 – the 48<sup>th</sup> International Conference on Microelectronics, Devices and Materials with the Workshop on Ceramic Microsystems that was held in September 19-21, 2012 in Otočec, Slovenia.

For more on her work, you can read In memoriam of Prof. Kosec at the end of this issue or browse VideoLectures.net (an EU supported project of the Institute "Jozef Stefan"), where nine of her lectures are posted.

Marija Kosec was named Ambassador of Science of the Republic of Slovenia in 2003, but she had been acting as ambassador of our society since 1989, when she became a vice-president. She was a bright star on the sky of Slovenian Science, a bright star that will keep shining on our society. We will keep a lasting memory of her.

This issue brings seven papers contributed from distinguished invited speakers at the MIDEEM 2012 Conference that were selected by co-chairpersons Prof. Marija Kosec and Darko Belavič to present the state-of-the-art achievements from the broad field of Ceramic Microsystems.

Merry Christmas and a Happy and Prosperous New Year!

Marko Topič  
Editor-in-Chief

P.S.

All papers published in Informacije MIDEEM (since 1986) can be access electronically at <http://midem-drustvo.si/journal/home.aspx>.

# *Innovation steps towards a novel and cost efficient LTCC packaging technology for high end applications*

*Franz Bechtold*

*VIA electronic GmbH, Hermsdorf, Germany*

**Abstract:** The emerging of a new MEMS, MOEMS and BioMEMS in the field of Sensors and a new GaN based generation of RF semiconductors in the field of RF Communication create new challenges for the packaging technology. In order to provide adequate packaging solutions for high end applications, manufacturers today are requested for high flexibility, excellent performance and reasonable costs.

Requirements with respect to advanced circuit functionality and enhanced thermal management, low dielectric losses, low parasitic effects and crosstalk, SiP integration, thermal management, miniaturisation and reliability have to be fulfilled. Today LTCC provides a proven packaging solution for Standard MEMS, GaAs devices and MCMs. Increasing frequencies; increasing power and increasing functionality of the systems are the driving forces to investigate into novel packaging solutions.

This paper describes the different steps how LTCC technology can cope with these requirements. Based on a comparison of the different available LTCC systems and a benchmark between them, the packaging performance of several LTCC systems is investigated in detail. Technological features, relevant for miniaturisation, System in package integration and RF performance, like cavities, conductor line resolution, via diameter and flatness are considered. Process capability, relevant for thermal management, SiP integration and hermeticity like brazing of heat sinks, integration of heat pipes, integrated capacitors and resistors are analysed.

The impact of novel and low cost materials for metallization, heat sink and brazing will be evaluated with respect to weight and cost. Compatibility with RoHS and REACH regulations will be discussed. The progress beyond the state of the art will be demonstrated by packaging solutions recently developed for industrial applications and in the frame of research programmes.

**Keywords:** LTCC, sensors, RF packaging, System in Package, reliability

## *Inovativni koraki proti novi in ceneni LTCC tehnologiji pakiranja za visokotehnološke aplikacije*

**Izvleček:** Združevanje MEMS, MOEMS in BioMEMS na področju senzorjev z RF polprevodniki na osnovi nove GaN tehnologije predstavlja nove izzive za tehnologijo pakiranja. Visoka fleksibilnost, izjemne lastnosti in sprejemljiva cena so zahteve proizvajalcem za izdelovanje ustreznih rešitev pakiranja visokotehnoloških izdelkov.

Današnje LTCC predstavljajo preizkušene rešitve za pakiranje standardnih MEMS, GaAs elementov in MCMjev. Povečanje moči, funkcionalnosti in frekvenc zahtevajo razvoj novih rešitev.

Članek opisuje različne korake rešitev teh zahtev s pomočjo LTCC tehnologije. Različni LTCC sistemi so medsebojno primerjani in njihove lastnosti natančno raziskane. Opisane so tehnološke značilnosti pomembne za proces miniaturizacije, integracije sistemov v ohišje in RF lastnosti. Analizirane so sposobnosti procesa termičnega upravljanja, SiP integracije in hermetičnosti.

Vpliv novih in cenениh materialov za metalizacijo, hladilnike in spajkanja bodo ocenjene glede na težo in ceno. Opisana bo združljivost z RoHS in REACH regulativami. Predstavljene bodo napredne rešitve novega pakiranja za industrijske aplikacije v okviru raziskovalnih programov.

**Ključne besede:** LTCC, senzori, nizke izgube, nizka teža, RF ohišja

\* Corresponding Author's e-mail: bechtold@via-electronic.de

## 1. Introduction

New microsystems, microsensors and microelectronic devices like MEMS, MOEMS, BIOMEMS and GaN based high power/high frequency semiconductors are emerging. These devices show an outstanding performance with respect to miniaturisation, functionality and power. Adequate packaging solutions, encapsulating heterogeneously the different components have to take into account that some of these devices are sensitive to environmental conditions like thermal cycling, heat dissipation and humidity. In addition good electrical stability and good EMC performance together with excellent high frequency and high power performances have to be obtained and hermetic or quasi hermetic packaging is requested in different cases. These requirements create new challenges to the packaging technology with respect to electrical performance, SiP integration, thermal management and reliability.

## 2. State of the Art LTCC Packaging solutions

Today LTCC provides an established and proven packaging solution for automotive applications, mobile phone circuits, industrial sensors; GaAs based MMICs and RF MEMS. Passive functional elements like miniaturised antennas, filters, couplers, temperature sensors, heating elements, resistors, capacitors and inductors can be monolithically embedded. Depending on the power dissipation and the reliability requirements those packaging solutions cover the whole range from low power quasi-hermetic packages to high power near hermetic packages and fully hermetic packaged high power MMICs. Glob top and transfer moulding protection, adhesive bonded heat sink and cavity shielded MMICs as well as brazing technology for heat sink and ring frame attachment are used. The type of packaging chosen is related to the lifetime, the reliability and the volumes of the different application.

## 3. Packaging solutions in the low volume industrial market

The low and medium volume market for LTCC is mainly represented by customized packages in the field of industrial sensors, medical devices and high end rf modules for telecommunication and satellite communication. Driving forces for all of those applications are the technical performance at acceptable cost for the individual customer solution. In the following example (Fig.1) the complete package of an x-ray detector is shown.

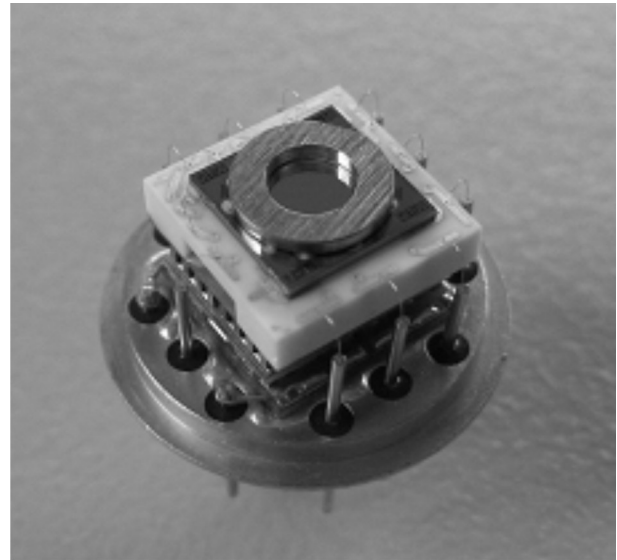


**Figure 1:** KETEK: x-ray detector

The key benefits with LTCC is the high miniaturisation, the capability of thermal management which includes a channel for heat transfer and thermal vias for power dissipation, the spectroscopic neutrality and the full Hermeticity with 0 outgassing.

In Fig. 2 different customized packages for X-Ray detectors and pressure sensors demonstrate the benefits of specific shapes; several wire bond levels, integrated fluidic channels and the capability of dedicated material systems.

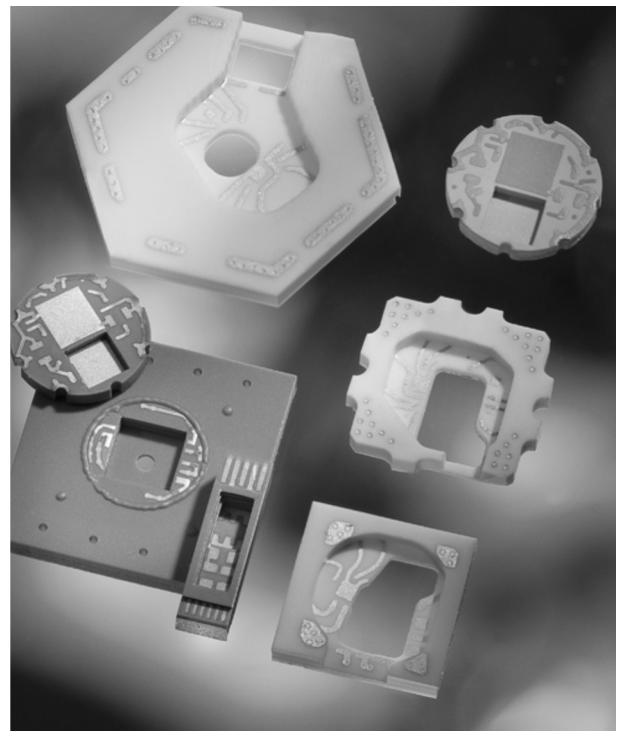


**Figure 2:** VIA: Customized sensor packages

Key benefits shown are specific shapes, several wire bond levels and Integrated fluidic channels Dedicated material systems

#### 4. Packaging solutions in the high volume automotive market

Cost together with reliability and Miniaturisation are the driving forces in the automotive business. LTCC in Germany's automotive market today is a business of about 250 Mio €. Typical under the hood applications are Antilocking, Gear control or Steer by wire systems.

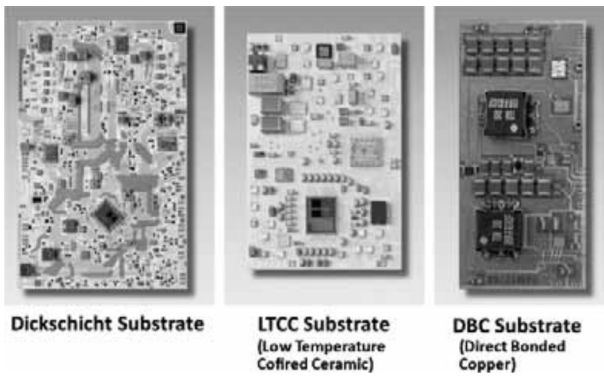


Figure 3: TEMIC: Technology platform

All of them request heterogeneous integration of highly miniaturised signal electronics together with thickfilm and DCB high power substrates into the same package.



Figure 4: TEMIC: Gear control unit

#### 5. Packaging solutions in the high volume mobile phone market

In the high volume market of mobile phones a fast evolution of miniaturisation using LTCC packaging technology can be observed.

Front end (Fig. 5) is realized today in LTCC. The key benefit of LTCC is the possibility to integrate passive RF functions at substrate level. Using a material system which consists of two different dielectric materials, one for signals with  $K= 8$  and the other with  $K= 20$  (the so called electronic ceramic) enables to integrate a number of such functions like filters, baluns, matching networks and others.

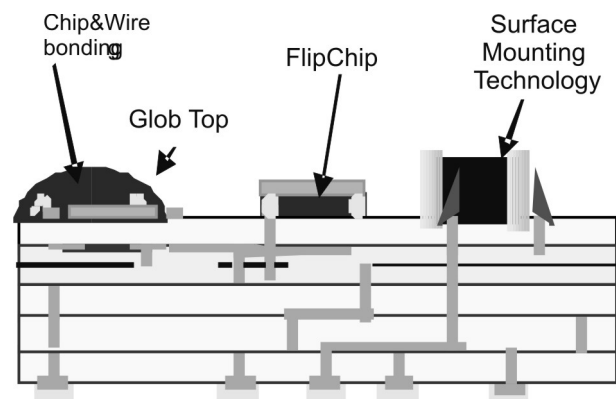


Figure 5: Epcos: Schematic of a LTCC frontend,

Fig. 6 depicts the top view of a dual-band WiMAX LTCC module. Active components like PA, switch and even some power management (PM), functionality are soldered on the top of the module while the RFIC is connected by means of wire bonds.

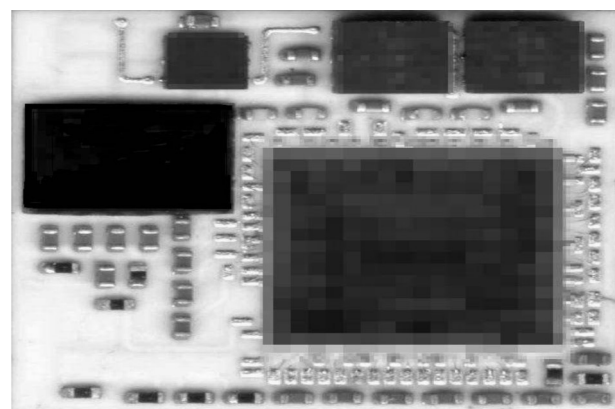


Figure 6: TDK-EPC: WiMAX SiP

The worldwide smallest All-in-one Frontend-Modul for Bluetooth- and WLAN-application has been published by Epcos 2008. With a height of 1,4mm it requests only

a small area of 4,5 x 3,2 mm<sup>2</sup> on the PCB. This module integrates the power amplifier, the switch, the receive-balun and the bias network with EMW protection. Furthermore, the integrated coexistence filter allows simultaneous operation of WLAN and Bluetooth having all standards of mobile communication and realises all requested functions between WLAN and Bluetooth.



**Figure 7:** Epcos D 601: The world smallest All in One Module

The most actual development is an advanced frontend, based on the co-design of Frontend and Antenna by combining flex foil and LTCC. This module combines the advantages of LTCC and Flexible board technology and results in a game-changing 16-band antenna, including Japanese frequency bands in the 1.5 GHz range. It is a single hardware-serving operator worldwide.

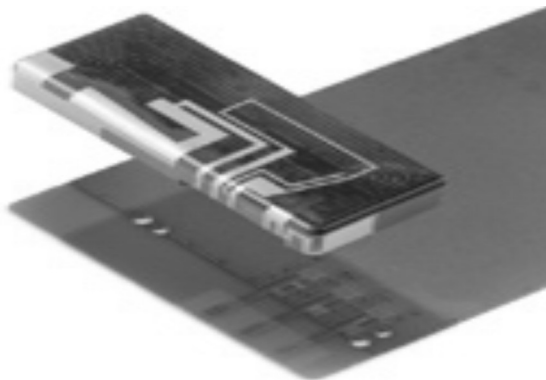


**Figure 8:** TDK-EPC: Advanced multi-feed RF front-end

## 6. RF Packaging solutions in other applications

The telecommunication market requests also for high end solutions at medium volumes. High power T/R modules, antenna- and phase shifting modules, RF-MEMs Switches are widely applied in active antennas for satellite communication and radio links. Radar detection systems are used in defence applications. Radar sensors have been successfully introduced in the automotive business and industrial applications are

following. The following pictures show a 60GHz-band 500-Mpbs transmitter and receiver multi-chip modules (MCMs), in which MMICs and filters are mounted into a LTCC package using flip-chip technique. A Lid protects the IC's and the MCMs are directly bonded with printed wiring boards using ball grid array technique, achieving connections for signals and biasing.

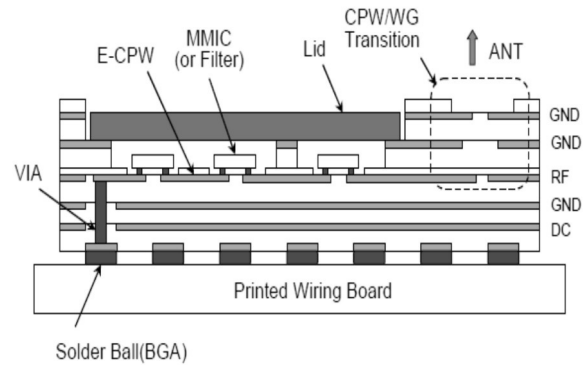


**Figure 9:** NEC: Schematic of the NEC 60 TR module

The transceiver is applied to the IEEE1394 wireless adapter, which demonstrates 17-mcommunication distance in line of sight.

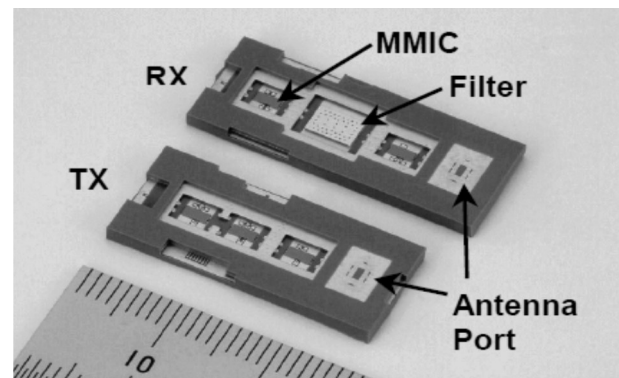


**Figure 10:** NEC 60 TX and RX Module

LTCC is offering again numerous advantages like the rf performance and the capability of passive integration. Another one is the design flexibility combined with the approach of modularity. Ericsson has demonstrated how to develop a number of T/R modules working at different frequencies from 15 to 39, using the same or similar RF building blocks for the realisation of the circuit. Filters, waveguide transition and other RF functions were successfully integrated at substrate level together with buried resistors. The other advantage is the high reliability performance.

**High integrated Microwave Transceiver Modules**  
RF module in LTCC

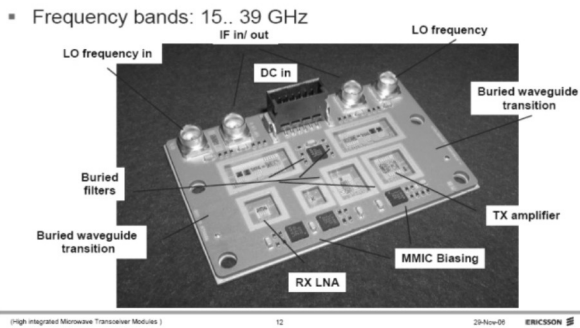


**Figure 11:** Ericsson: Modular kit of LTCC T/R modules, 15 to 39 GHz

LTCC circuits perform a lifetime of more the 20 years, they are stable under harsh environment and they are capable for full hermeticity according to Mil Std. Those substrates can be sourced from foundries like VIA on the free market in Europe.

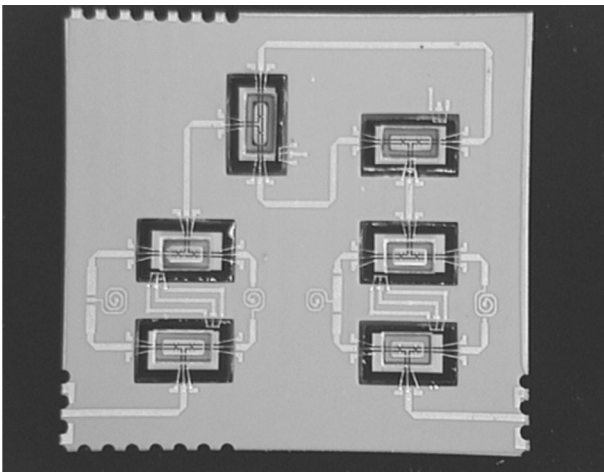


**Figure 12:** Thales: 3-bit phase shifters for phased array antenna

For space and military applications hermeticity is a must. Weight plays an important role and also cost is a key issue for success. Efficiency in packaging and miniaturisation in order to reduce cost, weight and size are key benefits of the LTCC technology.

According to the high energy requested for transmission, power dissipation and thermal management are integral part of the packaging requirements and components like heat sinks and ring frames as well as the attachment of those elements to LTCC are in the focus of this paper.

The following picture shows the TNO design of a state of the art packaging solution for a TR module working at K- band for nautical application.

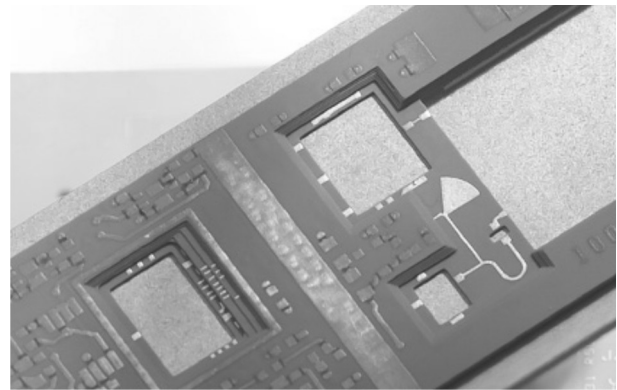


**Figure 13:** TNO: Design of a LTCC Transmit Receive Module

The package contains a rather complex stepped cavity structure for MMIC, Circulator and IC integration. The LTCC is adhesive bonded to the Molybdenum heat sink and then populated with SMT and chip and wire technology.

A further step towards reliability has to be made if full hermeticity of the packaged dies is required. This is the case in space and defence radar applications. An example is given in the following package of a TR module for phased radar antennas. Molybdenum heat sink and Kovar ring frame are AuSn brazed to the LTCC substrate. This package type shows extremely good thermal and reliability behaviour and it fulfils the MIL specification for hermeticity ( $>5 \times 10^{-8} \text{ atmcm}^3/\text{s}$ )

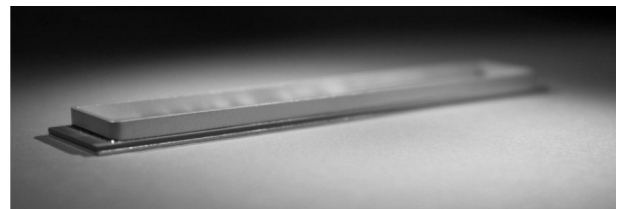


**Figure 14:** EADS: LTCC T/R Package

Another approach to achieve full hermeticity and good heat dissipation is shown in the following example, in which a Kovar frame is AuSn brazed to achieve hermeticity and a BGA is used on the backside for PCB assembly.



**Figure 15:** SELEX: RF package Kovar ring and BGA

## 7. Future system requirements

Increasing frequencies, power and functionality of systems are the driving forces to investigate novel packaging solutions. In the following pictures typical T/R modules for x-band and wide band are shown.

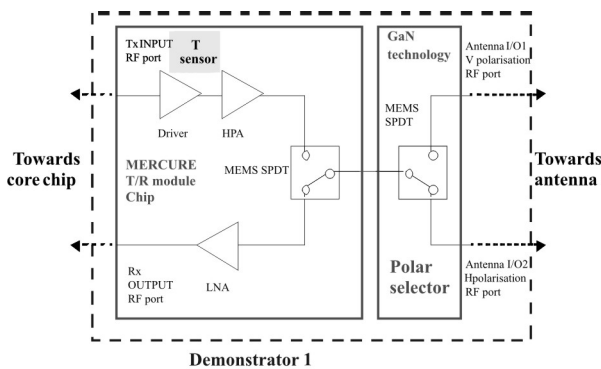


**Figure 16:** Thales: Block Diagram Wide Band T/R module

Typical functions and sizes to be integrated are:

- HPA: 20 mm<sup>2</sup>
- Driver: 5 to 10 mm<sup>2</sup>
- LNA: 5 mm<sup>2</sup>
- MEMS: 2 mm<sup>2</sup>
- Decoupling capacitors and others about 30 mm<sup>2</sup> in total
- Temperature sensor

In order to have a smart package, the internal room for components is thus typically estimated from 100 to 250 mm<sup>2</sup> for wideband and 150 to 400mm<sup>2</sup> for x-band. The developed package must be compatible with a cold plate cooled by fluid.

Power to be dissipated is up to 80 watts peak dissipated power, pulsed with a pulse time from 1 to 20µs associated to a duty cycle of up to 20%.

Materials with excellent thermal conductivity are required. These materials must be compatible with high temperature gold tin brazing. Return loss of one microwave transition must be better than -25 dB and the isolation between the antenna access and the LNA access must be better than -80 dB. The isolation between biasing and /or control ports must be typically 50 dB, which is typically realised by a metallic wall.

As sensitive devices are encapsulated a good hermeticity must be by enclosure obtained. Typically a 5x10-8 Atmcm<sup>3</sup>/s (air) is required. The package must withstand -55 +125°C 500 cycles without lack of hermeticity or electrical performances degradations.

## 8. Steps to cope with these requirements

The expertise in the technology together with the relevant application know how of the customer is the backbone of the small and medium sized European LTCC Foundries like VIA in order to service the free market with high flexibility and medium to low volumes.

## 9. Understand materials and their properties

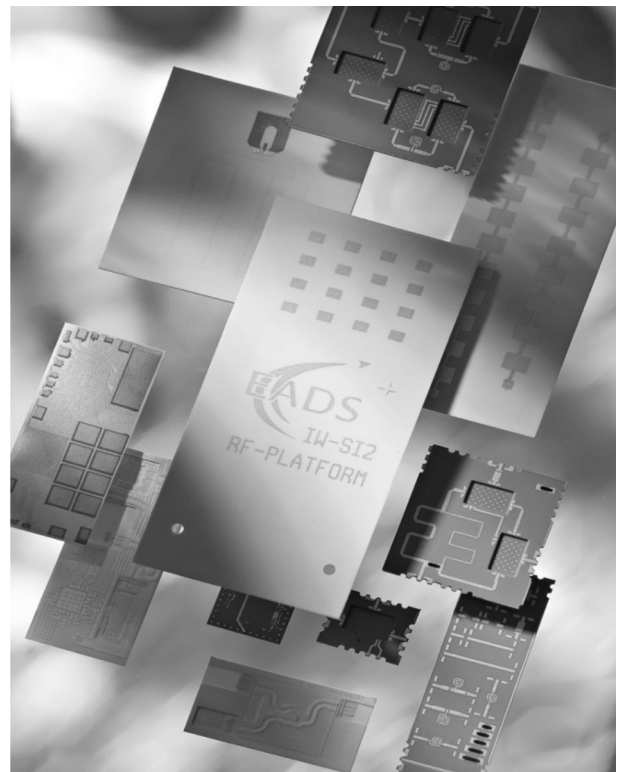


**Figure 17:** VIA: LTCC RF packages transition from DuPont 951 towards DuPont 9K7.

## 10. Overview

One of the most mature systems used is DuPont 951. The RF capability of this system is limited to about 10 GHz, dependent from design and application. For RF applications above 10 GHz specific low loss materials are available from different suppliers. RF Properties and characteristics are listed in table 1, in comparison with DuPont 951:

**Table 1:**

	Commercial LTCC materials for High Frequency				
	951 DuPont	943 DuPont	9K7 DuPont	9K5 DuPont*	A6M-E Ferro
Permittivity $\epsilon$					
$\leq 1$ GHz	7,8	7,5	7,1	5,8	5.9+/-0.20
1-20 GHz	7,4	7,4	7,1	5,8	5.9+/-0.20
20-40 GHz	-	7,4			5.9+/-0.20
Dielectric losses $\tan \delta$ [10 <sup>-3</sup> ]					
$\leq 1$ GHz	< 2	< 1	< 1	$\leq 1$	$\leq 1$
1-20 GHz	5	1	<1	$\leq 1$	$\leq 2$
20-40 GHz	<15	< 2			$\leq 2$
Insertion loss [dB inch <sup>-1</sup> ]					
Conductor	Ag	Ag	Ag		
1- 20 GHz	$\leq 1,4$	$\leq 0,3$	$\leq 0,3$		

\* Published October 2011, available in Europe end of 2012

And in table 2 physical properties and available tape thicknesses, relevant for RF designs, are as given and compared to DuPont 951

**Table 2:**

Physical Property	DuPont 951	DuPont 943	DuPont 9k7	DuPont 9K5	Ferro A6ME
	Value	Value	Value	Value	Value
Unfired thickness [ $\mu\text{m}$ ]	50 $\pm$ 3 114 $\pm$ 8 165 $\pm$ 11 254 $\pm$ 13	51 $\pm$ 4 127 $\pm$ 9 254 $\pm$ 13	127 $\pm$ 9 254 $\pm$ 14	127* 254*	127 254
X,Y, shrinkage, [%]	12.7 $\pm$ 0.3	9.5 $\pm$ 0.3	9.1 $\pm$ 0.3	9.1*	15.4 $\pm$ 0.3
Z shrinkage, [%]	15.0 $\pm$ 0.5	10.3 $\pm$ 0.5	11.8 $\pm$ 0.5	11,8*	24.0 $\pm$ 0.3
Dielectric constant, (40GHz)	7.4	7.4	7.1 $\pm$ 0.2		5.9 $\pm$ 0.2
TCE $\alpha$ [ppm K <sup>-1</sup> ] (25-300°C)	5,8	4,5	4,4	4,4*	5,6
Environmental		Lead-free	Lead-free	Lead-free	

Large entities like the big Japanese and Bosch are dealing only with high volume markets. Bosch is focussing on automotive and Epcos on the telecom business. They all have their proprietary material systems either provided by external partners or made by themselves. Constrained sintering and plating are key process for cost and performance reasons. All these processes are dedicated to automate high volume production. A summary is given in table 3:

**Table 3:**

Murata	TDK-EPC	Kyocera
K8.8/K15.1 for telecom K7.7 for automotive Plating Pressure assisted sintering (0-Shrinkage)	K8/K20 for telecom Plating Pressure assisted sintering (0-Shrinkage) DuPont 943 for automotive	K9,4/K18,7 for telecom K7,7 Cu K5,7 Cu K5,7 Cu K5,2 Cu Plating

It is obvious, that a deep understanding of materials and processes as well as a good knowledge about the application requirements have to meet together in order to provide proper cost efficient LTCC packaging solutions.

### 11. Benchmark DP 943/9K7

In order to understand deeply the different materials, VIA made a detailed manufacturability benchmark between DP 943 and DP 9K7. The impact of thermal and post processes parameters on RF characteristics and geometrical properties of LTCC was investigated. Radar front ends also including calibration structures and test vehicles were fabricated using Du Pont Green Tape<sup>®</sup> 943 and 9k7 material systems. The following parameters have been investigated:

- The x- and y- dimensions both after co-firing and re-firing
- Warping of the whole substrate
- Warping of cavities
- Characterization of electrical properties up to 110 GHz
- Influence of re-firing on the dielectric constant.

The LTCC wafer has been a multi-project wafer, having a particularly complicated package combining several features with unfavourable impact on even and homogeneous shrinkage. Uniformity of the shrinkage is constricted by perforations, clusters with more metal content, cavities or cut-outs. The following Figure shows the test vehicle MPW1 to visualize the local differences of metallization.

The left part of the substrate contains 80% of the vias and 70% of the co-fired conductors, while the right side has larger metallization of inner layers and cavities as chip pockets or decoupling features. Both parts of the substrates were measured separately in x- and y-axis in order to quantify possible differences in the local and overall shrinkage. The results are shown in table 4. Shrinkage values are given in % deviation from the mean value. Warping is given in  $\mu\text{m}$  of maximum to

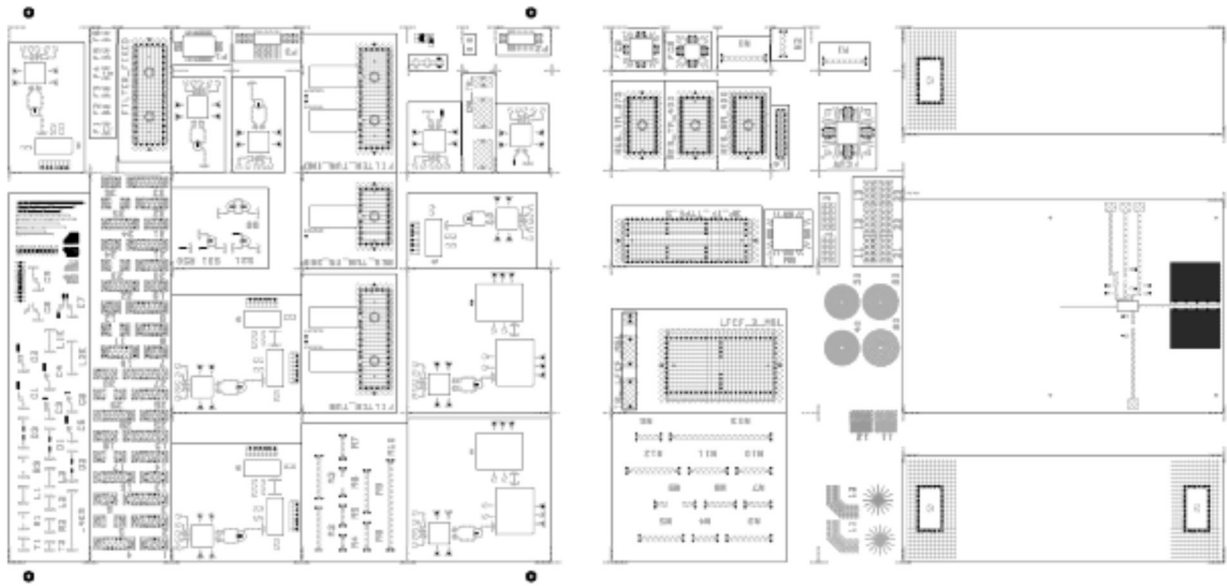


**Figure 18:** VIA: Multiwafer design

minimum value using a 40mm long scanning line. Re-firing stability in % expansion after re-firing.

**Table 4:**

Investigation	measurement	DuPont 943	DuPont 9K7
Shrinkage sensitivity	Shrinkage around cavity areas	-0,175%	-0,19%
	Shrinkage in dense metallisation area	-0,02 to -0,040%	-0,02 to -0,03%
	Shrinkage in low metallisation area	0,02 to 0,035	0,02 to 0,035%
Shrinkage accuracy	Overall substrate area	+/- 0,16%	+/- 0,13%
Planarity sensitivity	Warping around cavity	-3 to 17µm	-3 to 17µm
	Warping in dense metallisation area	9-15µm	10 – 14µm
	Warping in low metallisation area	15-22µm	16 – 17µm
Dimensional Stability vs. re-firing	Expansion after 3 refrings	0,07-0,11%	0,07-0,11%
	Expansion after 5 refrings	0,14-0,17%	0,13-0,15%
	Expansion after 8 refrings	0,17-0,21%	0,16-0,18%
Dielectric Constant vs. re-firing (20-60GHz)	Deviation of the Dielectric constant after 5 refrings	-0,10 to -0,12	-0,02 – 0,02

The 9K7 LTCC material shows excellent RF performance up to 100 GHz and above. Comparing to the previ-

ous generation 943, process stability, higher accuracy in its shrinkage behaviour and RF stability have been improved. Due to these benefits it allows SiP solutions with complex structures and a high accuracy of co-fired features.

## 12. Understand the requirements

Table 5 gives an overview of the different systems available concerning the aspects of miniaturisation and process capability, which impact cost and performance. Datas are based on the experience of VIA..

**Table 5:**

Investigation	DuPont 951	DuPont 9K7	Ceram tape	Heraeus CT 700
Available sheet thickness µm	50			100
	114	127		
	165		320	320
	254	254		
Shrinkage tolerance %	Standard	0,6	0,6	0,8
	Minimum	0,3	0,3	0,5
	Cavities	1,0	1,0	1,0
0-Shrinkage Capability	++	+	++	++
Line width µm	100	100	100	100
Line spaces µm	100	100	100	100
Dimension Stability	Green, µm	30-70	<20	<30
	Refring, in %	0,1-0,15	<0,1	0,1
Embedding capability	lines >30µm	+	-	+++
	resistors	++	-	---
	high k capacitors	+-	-	---

Process sensitivity				
Warpage	++	+	++	-
Waviness	+	+	++	+-
Metallisation impact	+-	-	+-	+-
Maximum density of metallisation %	75	75	75	75
Line density				
Width	100	100	100	100
Spaces	100	100	100	100
VIA density				
Diameter $\mu\text{m}$	100	100	150	150
Distance $\mu\text{m}$	250	250	250	250
Postfired resistors	+++	+	-	-
Embedded Fluidic Channels	+++	++	++	++
Chambers	+++	++	++	++
Bonding				
Al	++	++	++	+
Au	++	++	+-	++
Al heavy wire	++	-	-	++
Cavity bonding				
Al	++	--	--	--
Au	++	++	+	++
Soldering				
PbSn 95-5	++	++	--	++
SnAg	++	++	--	++
Brazing				
AuSn	++	+	--	--
GeSn	++		--	--
Laser processing				
Green	+++	+++	+++	+++
Fired	+-	+	++	+++
RoHS/REACH compatibility	In process	Yes	Yes	In process
Lead-free	no	yes	yes	yes

In order to provide adequate packaging solutions for high end applications, manufacturers today are requested for high flexibility and excellent performance at acceptable costs. Also RoHS and REACH compatibility have to be considered.

### 13. Introduction and impact of novel and low cost materials

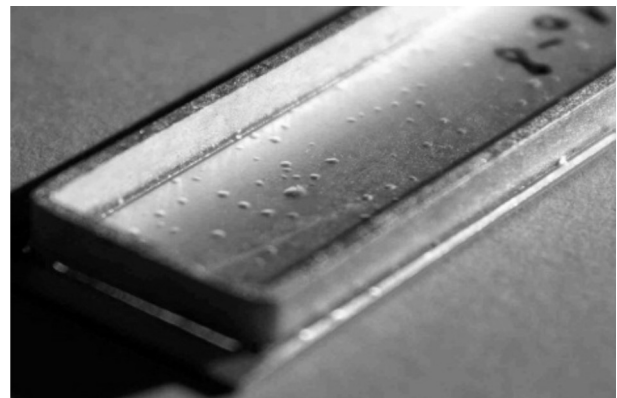
To improve weight and cost, VIA did investigations in alternative materials for heat sinks, brazing and mixed metal wiring. This work is initially focused on the mature DuPont 951 material system and then expanded to the new 9K7 system. The criterions for materials investigated were availability, thermo mechanical properties, weight and cost. All materials and components investigated were introduced on an existing functional RF design. Hermeticity was tested and compared with standard package performance.

### 14. Carbon-fibre Aluminum Composite (CarfAl)

This material is very promising concerning weight, machinability and costs. The following pictures are demonstrating that customer designed heat sink and ring frame elements can be easily realized. Solder experiments have been carried out using the same AuSn performs as they are used with conventional Kovar and Molybdenum Components. The solderability was excellent and no difference to conventional components could be observed. Hermeticity tested was according to MIL Standard at  $5 \times 10^{-9}$ , comparable to conventional components.

After Hermeticity tests some defects were identified: small blisters occurred on the plated surface, which could be eliminated at the supplier side by improvements in the plating process.

**Figure 19:** CarfAl heat sink and ring frame after hermeticity tests



### 15. Solder performs

AuSn brazing using solder performs is well established for high hermetic packages required in space and defence industry. It is obvious that Au is a cost-driving element in these packages. Promising alternatives are high lead containing solder materials, which are widely used for soldering of power devices or sealing of ceramic sensor packages. Additionally SnAg alloyed performs have been investigated..

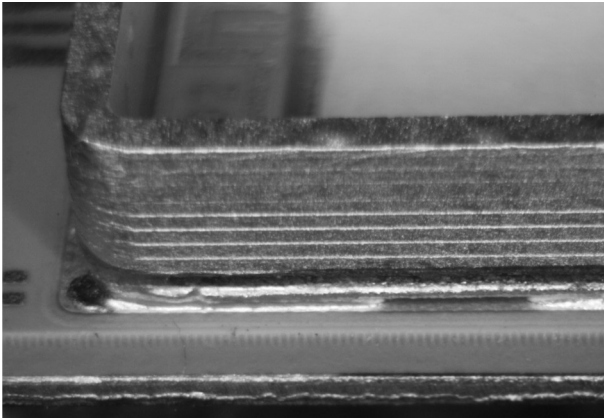


**Figure 20:** Preform Pb92.5Sn5Ag2.5 on AgPt, CarFAL ring frame

Table 6 shows some promising results:

Pre form	Liquid. temp. °C	Pad	Ring	Herm. atm	Result
Au80Sn20	278	AgPt	Kovar	3x10 <sup>-9</sup>	Excellent
		AgPd	Kovar	3x10 <sup>-9</sup>	Good
		AgPd	Kovar	3x10 <sup>-9</sup>	Good
		Au/AuPd	Kovar	3x10 <sup>-9</sup>	Good
		AgPt	Kovar	3x10 <sup>-9</sup>	Good
Pb92.5Sn5Ag2.5	287	AgPt	CarFAL	6x10 <sup>-9</sup>	Bad
		AgPd	Kovar	leaky	bad
		Au/AuPd	Kovar	5x10 <sup>-9</sup>	acceptable
		AgPd	Kovar	2x10 <sup>-9</sup>	acceptable
		AgPd	Kovar	leaky	bad
Sn96.5Ag3.5	221	AgPt	CarFAL	leaky	bad
		AgPd	CarFAL	leaky	bad
		Au/AuPd	CarFAL	leaky	bad
		AgPt	Kovar	leaky	bad
Sn99.1Ag0.4Cu0.5	228	AgPt	CarFAL	6x10 <sup>-9</sup>	acceptable
		AgPd	CarFAL	leaky	bad
		AgPd	Kovar	5x10 <sup>-9</sup>	good
		Au/AuPd	CarFAL	5x10 <sup>-9</sup>	acceptable
		AgPt	CarFAL	4x10 <sup>-9</sup>	acceptable

### 16. Mixed metal LTCC

With respect to LTCC, changing from AuSn to high lead and tin/silver alloys require a change in the thickfilm metallisation beneath. Expensive Au/AuPd metallisation systems shall be replaced by more economic Ag/AgPd systems or even simple AgPt solder pads. Consequently, Ag shall replace external and internal Au wiring, and AgPd and only pads for wire bonding have to

be fabricated with gold. Unfortunately Ag has very low activation energy and tends to migration. Therefore a proper diffusion barrier system has to be introduced in order to avoid silver migration problems.

In the past, diffusion barriers made of AgPd inks were used between Au and Ag conductors. As far as vias are concerned connecting a silver conductor with an Au pad, AgPd transition vias are used. These transition vias show the disadvantage to expand during firing and to create a non-negligible posting of via, which arrives up to 30µm. Those postings are a problem of accurate die attach and should be avoided as far as possible. DuPont recently published a new recipe for transition vias for the mixed metal system, which is under investigation. Measurements show a significant reduction of the posting from around 20 to about 10µm using the new ink.

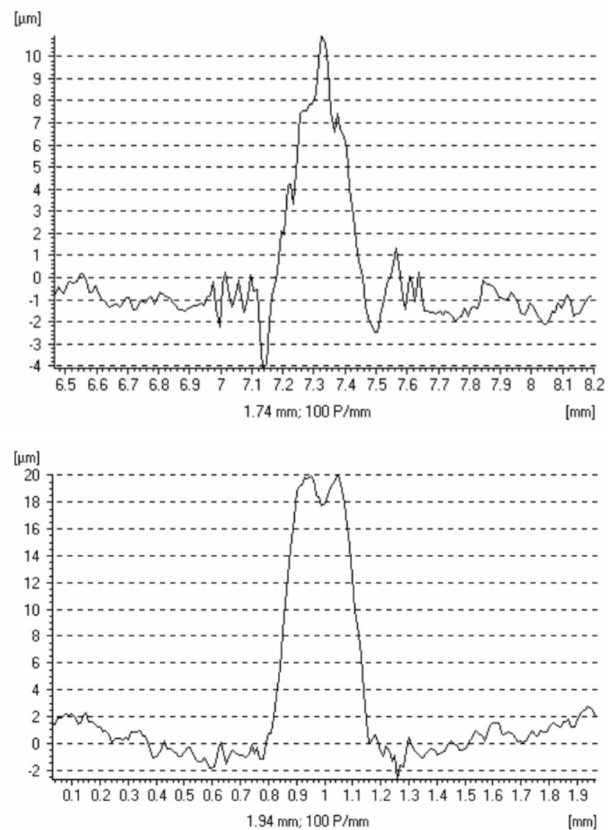


**Figure 21:** Posting effect: 10µm, new transition via compared to 20µm Conventional AgPd transition via

The progress beyond the state of the art is demonstrated by new packaging solutions recently developed at VIA for RF and non RF industrial applications and in the frame of research programmes.

### 17. 77 GHz Radar Front end

To introduce the new 9K7 LTCC material system into the manufacturing line to qualify the processes and to validate the system, it was decided to use the new system for the development of a very challenging 77 GHz Radar Front-end. This development was carried out in the frame of a joint cooperation research project, funded by the German BMWI/AiF.

The sensor developed aims at applications where the sensor is mounted very close - but contactless - to the target. The target can be measured by using the continuous wave (CW) mode of operation. Since the phase is ambiguous the measurement range is limited to half the wavelength. For example, in the case of a frequency of 77 GHz, these measurements range of  $\lambda/2 = 1.95 \text{ mm}$  might be located at 1cm distance to the sensor with measurement accuracy in the  $\mu\text{m}$  range. The sensor's centre frequency is therefore a trade off between the measurement range, which decreases with frequency, and the precision, which increases. A very important point for the design is the available space for the sensor. The LTCC frontend takes only 1.4mm x 30mm x 12mm including a broadband Vivaldi antenna. The 9K7 LTCC process has been chosen for its RF capability, miniaturization capabilities and robustness in harsh environments. The key features of the Frontend, designed by IMST, are as the following:

Frequency	77 GHz (72 ... 77 GHz)
Operation	CW and FMCW
Output Power	5 dBm
Antenna	Vivaldi
Module Size	30 x 12 x 1.4 mm <sup>3</sup>
Material	DuPont 9k7

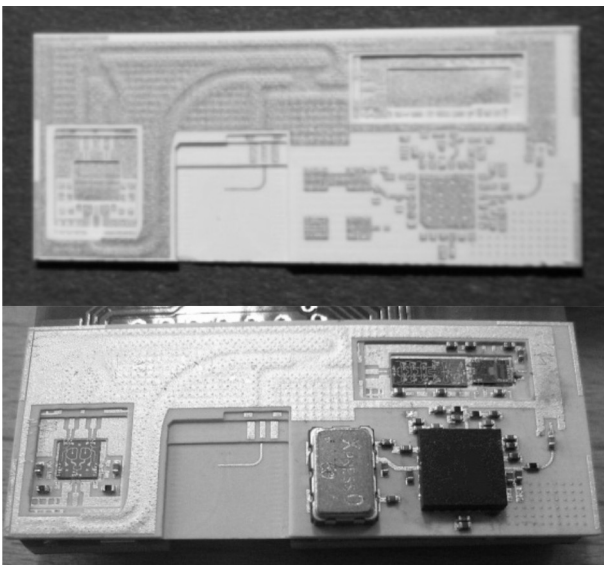


**Figure 22:** VIA/IMST: 77 GHz Radar Front end, Substrate and assembled package

The following pictures are showing the radar module in different stages of the development:

### 18. Light weighted TR Module using CarfAl heat sinks

In the first run (compare Fig. 13) a conventional Molybdenum heat sink was bonded to the LTCC substrate, assembled and qualified.

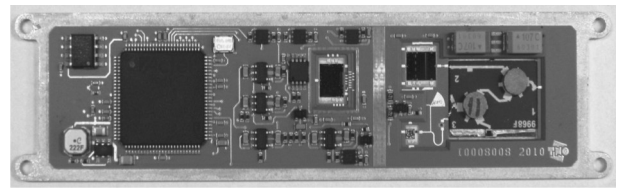


**Figure 23:** TNO: TR-Module using CarfAl heat sink

Introducing the CarfAl material has led to a weight saving of 80 % of the complete module!

### 19. High Speed Optical Router

A LTCC substrate has been used as an optical bench to integrate and optically interconnect a high speed data transmission chip. The accuracy challenges were extreme:

cavity with  $\pm 50\mu\text{m}$ , blind holes  $\pm 25\mu\text{m}$ , Vias  $90\mu\text{m}$  diameter, Via position over the whole substrate  $\pm 50\mu\text{m}$ , thickness  $1,5\text{mm}$   $5\pm \mu\text{m}$ , Signal speed 10 Gbit/s, Flip chip pitch  $100\mu\text{m}$ , BGA Pitch  $500\mu\text{m}$ .

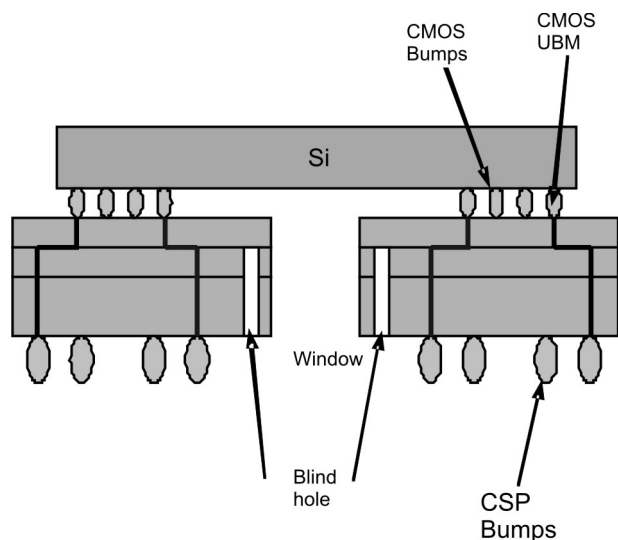


**Figure 24:** CEA: Optical Router, Schematic

A solution could be found by applying the 0-Shrinkage process, picosecond laser drilling, grinding and lapping the substrate and interconnecting with thinfilm on top and thickfilm on bottom to provide a full high accuracy solution.

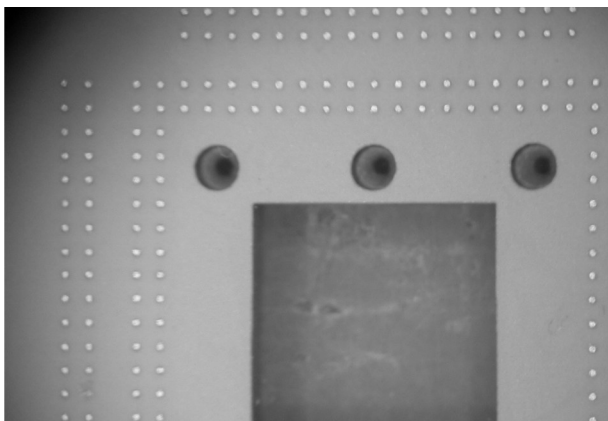


**Figure 25:** Optical Router Package

## 20. One way DSC-Chip

A complete differential scanning calorimetric system was developed and integrated into a LTCC substrate. The key features have been:

- Integrated Temperature sensors
- Integrated heater elements
- Pinout in chip card format
- Total mass of the chip: 1,43g
- Measuring head: 400mg

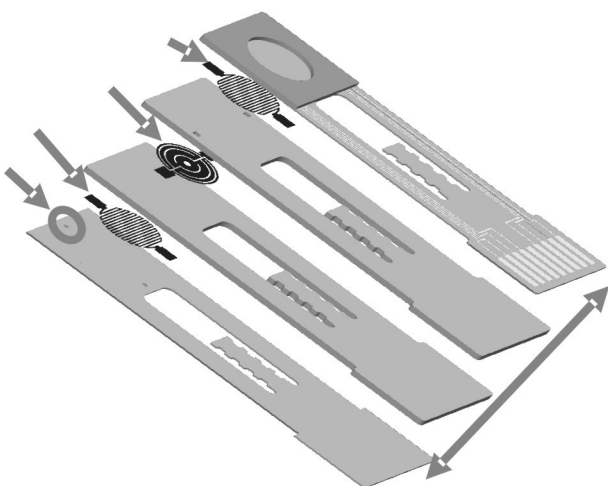


**Figure 26:** One way DSC Chip

The system has been realised at VIA in Heraeus CT 700 and HL 800 material system.

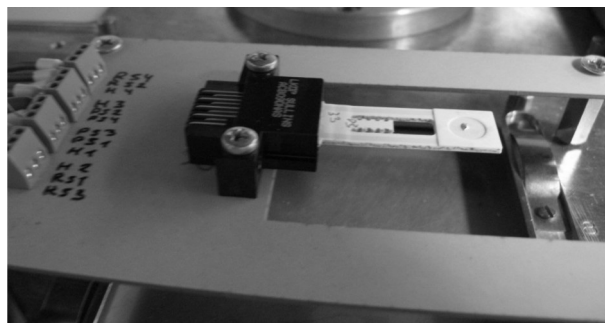


**Figure 27:** DSC Chip in test fixture (University of Bayreuth)

## 21. Ceramic Microreaktor

BioMEMS and biosensors, Lab on chip systems and similar devices are in development and under investigation since a couple of years. One of the elements which VIA has developed is a highly integrated micro reactor, shown in the following figures.

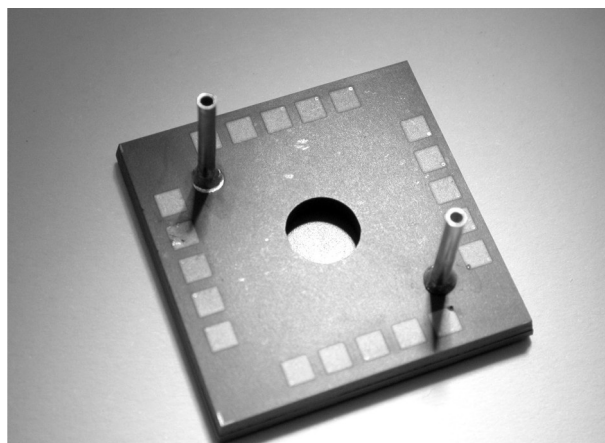


**Figure 28:** LTCC Micro reactor

The micro reactor contains fully integrated fluidics and soldered fluidic interfaces. The key features are the 50 $\mu$ l reactor with a fluidic system allowing a flow rate of 1 $\mu$ l per minute.

Enzymes were immobilised onto a 0,1x0,4mm 3d channel. The cell growth in the reactor has been verified.

## Conclusions

LTCC is providing manifold advantages for packaging tasks in the field of high-end applications. Applying new materials like 9K7, new light weighted materials for packaging components like CarfAl, low cost materials for brazing like SnAg together with a proper man-

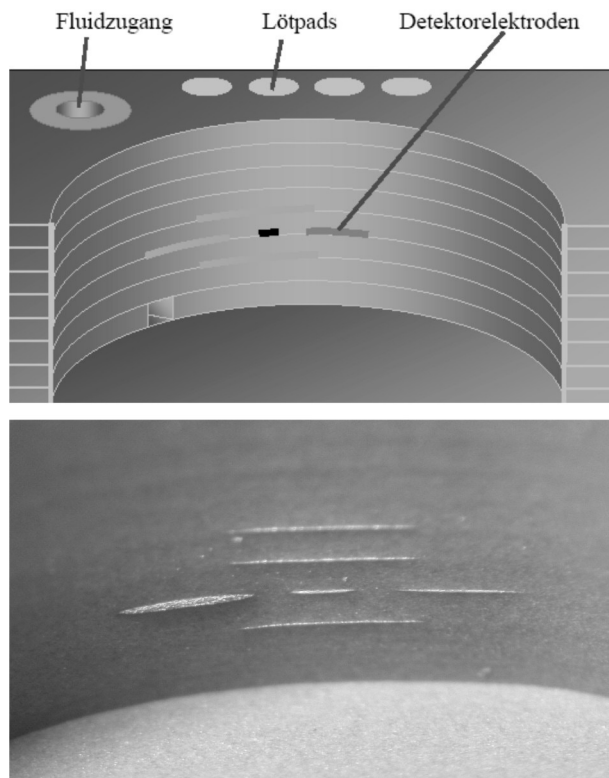


**Figure 29:** Micro reactor, schematic of the sensor and detail

agement of mixed metal processing; the LTCC technology will make a significant step ahead towards a cost efficient packaging technology. In addition with the well-known integration capabilities and its superior reliability performance it provides innovative and novel RF packaging solutions.

## References

1. J. John, "A Fine Presentation", Proceedings of the 1993 Electronic Components and Technology Conference (ECTC), Atlanta, Georgia, August 12-15, pp. 21-33, 1993.
2. F. Bechtold, "Innovative Integrationslösungen für Sensoren mit LTCC", Sensor Magazin Vol.2 pp 16-20, Juni, 2008
3. M.Kallenbach e.a., "High-Inductive Small-Size Micro coils with High Ampacity", Proceedings of the 2007 Smart System Integration Conference, Paris, 27-28.3., pp.505ff, 2007
4. J. Töpfer e.a., "Soft Ferrites for multilayer inductors", Int. J. Appl. Ceram. Technol., 3[6], pp 455-462, 2006
5. F.Bechtold, "A Specialist Manufacturer's Outlook on the Future of Ceramics and Ceramic Microsystems", Keynote Presentation at the 2<sup>nd</sup> International Conference on Ceramic Interconnect and Ceramic Microsystems Technologies Denver, April 2006
6. T. Kraft, H. Riedel, D. Schwanke und E. Müller: „Simulation von Rissbildung und Verzug in der Mikroelektronik“, PLUS, Bd.7 (2005) 883-886
7. T. Bartnitzek, "MATCH-X-LTCC-Packages for Modular Microsystems", Proceedings of the 14th European Microelectronics and Packaging Conference, Friedrichshafen, 23. -25. June pp. 2003
8. F.Bechtold, "Innovative Integrationslösungen für Sensoren mit LTCC", Sensor Magazin Vol.2 pp 16-20, Juni, 2008
9. J. Töpfer e.a. "Soft Ferrites for multilayer inductors", Int. J. Appl. Ceram. Technol., 3[6], pp 455-462, 2006
10. F.Bechtold, "A Specialist Manufacturer's Outlook on the Future of Ceramics and Ceramic Microsystems", Keynote Presentation at the 2<sup>nd</sup> International Conference on Ceramic Interconnect and Ceramic Microsystems Technologies Denver, April 2006
11. Thomas Bartnitzek e.a.: "An Investigation of the Process Stability of RF SiP Made of DuPont 943 and 9K7, Proceedings CICMT San Diego, April 2011
12. Franz Bechtold e.a.: "Comparison of Ceramic Multilayer Technologies for RF Integration HTCC/LTCC, Imaps Congress Munich, October 2010
13. Franz Bechtold, "A Comprehensive Overview on Today's Ceramic Substrate Technologies", Imaps Europe Proceedings Rimini 2009
14. Thomas Bartnitzek, "RF and Microwave Microelectronic Packaging", Springer Science+Business Media, New York 2009
15. Dr. Thomas Zetterer, "Zukunftstechnologie Keramische Leiterplatte", oral presentation Cluster Mikrosystemtechnik, Irlbach, 2009
16. C.R.Needs, D.I.Amey and S. J.Horowitz, "Cost Effective Solutions for High Density Interconnect and RF Modules using Low Temperature Cofired Ceramic Materials"
17. Thomas Bartnitzek e.a. "RF and Microwave Microelectronics Packaging" In: Ceramic systems in package for RF and microwave Springer 2011
18. Jri Lee, e.a. "A Fully-Integrated 77-GHz FMCW Radar Transceiver in 65-nm CMOS Technology" EEE JOURNAL OF SOLID-STATE CIRCUITS, VOL. 45, NO. 12, DECEMBER 2010
19. Andriy Yatsenko, e.a.: "System-in-Package solutions for WiMAX applications based on LTCC technology"
20. Pressemitteilung Januar 2008: Weltweit kleinstes Frontend-Modul für WLAN und Bluetooth, © EPCOS AG 2012 • www.epcos.com

21. J. Sachs e.a.: Digital Ultra-Wideband-Sensor Electronics integrated in SiGe-Technology, The Fifth European Microwave Week (EUMC) 23 - 27 September 2002, Milan, Italy
22. Dr. Siegbert Martin, "High Integrated Microwave Transceiver Modules in LTCC for High Capacity Radios" Kolloquium MakroNano, Ilmenau 2006
23. R. Stark, B. Schuch: Innovative Technologien für Getriebesteuerungen Continental AG, Nürnberg 2010
24. W. Röthlingshöfer: Low Temperature Cofired Ceramics (LTCC), eine Technologie für elektronische Steuergeräte unter extremen Belastungen, Gedenkkolloquium Prof. Öl, Erlangen, 2006
25. W. Missal e.a.: Calorimetric Sensitivity and Thermal Resolution of a Novel Miniaturized Ceramic DSC Chip in LTCC Technology, Thermochemical acta, 2012

Arrived: 26. 08. 2012

Accepted: 23. 10. 2012

# LTCC fluidic microsystems

Leszek J. Golonka and Karol Malecha

Faculty of Microsystem Electronics and Photonics, Wrocław University of Technology,  
Wrocław, Poland

**Abstract:** In this paper, potential of the low temperature co-fired ceramics (LTCC) technology for fluidic microsystems fabrication is discussed. The authors give a brief overview of fluidic structures fabrication process in LTCC modules. The presented micro-fabrication techniques utilize sacrificial volume materials combined with multi-step isostatic lamination. Moreover, the design and construction of the few exemplary LTCC-based microfluidic systems developed at Faculty of Microsystem Electronics and Photonics at Wrocław University of Technology are presented.

**Key words:** Low temperature co-fired ceramics (LTCC), sacrificial volume material (SVM), microfluidic, microsystem

## Tekočinski LTCC mikrosistemi

**Povzetek:** V članku je opisan potencial keramičnih tehnologij z nizko temperaturo žganja (LTCC) za proizvodnjo tekočinskih mikrosistemov. Avtorji podajo kratek pregled proizvodnih procesov tekočih struktur v LTCC modulih. Predstavljene tehnike mikroproizvodnje uporabljajo žrtveni material v kombinaciji z večstopenjsko izostatično laminacijo. Poleg tega so predstavljene oblike in zgradbe primerov mikrotekočinskih sistemov na osnovi LTCC, ki so bili izdelani na Fakulteti za mikrosistemsko elektroniko in fotoniko na univerzi v Wrocławu.

**Ključne besede:** keramične tehnologije z nizko temperaturo žganja (LTCC), žrtveni material, mikro tekočina, mikro sistem

\*Corresponding Author's e-mail: leszek.golonka@pwr.wroc.pl

### 1. Introduction

We can observe increased interest in the field of fluidic microsystems in the last two decades [1,2]. The fluidic microsystems are used in medicine, biology and analytical chemistry, as well in application in which fluid is used as a coolant. The main reason of this interest is rapid development of the microengineering techniques. Progress in microengineering enabled fabrication of miniature and precise fluidic structures (e.g. channels, cavities, chambers etc.) with characteristic dimensions from single millimeters to hundreds of nanometers. In a consequence it is possible to fabricate microsystems which are capable to handle with fluid in micro- or nanoliter volume range. Thanks to such significant reduction of the specimen volume the fluidic microsystems produce less wastes and are cheaper to use in comparison to classical laboratory apparatuses. Another aspect is the number of possible areas of the fluidic microsystem applications: analytical chemistry, medical diagnosis, DNA sequencing, cell separation, microbiological analysis, high-throughput synthesis, environmental monitoring and others [3-6].

Nowadays fluidic microsystems are fabricated using silicon/glass [7], polymer [8], PCB (Printed Circuit Board) [9] and LTCC (Low Temperature Co-fired Ceramics) [10-12] technologies. The main advantages of the LTCC in comparison to silicon, polymers and PCB are chemical inactivity, chemical resistance and high temperature stability [13,14]. Moreover, the LTCC technology enables to accomplish both mechanical and electrical functions in a single ceramic module. The possibility of integration of fluidic structures, active and passive electronic components, optoelectronic devices, sensors, actuators, MEMS (micro electro-mechanical system) and package into one multilayer module is the main advantage of the LTCC over other mentioned technologies [15,16]. Moreover, the LTCC can be bonded with other materials using anodic bonding (LTCC-Si) [17], microwave plasma (LTCC-polymer) [18] or low temperature melting glass (LTCC-ceramic). Due to all above-mentioned advantages the LTCC can be a potential alternative for fluidic microsystems fabrication.

In this paper, the main aspects of the LTCC technology for fluidic microsystems fabrication are briefly discussed. Subsequently, an overview of the techniques for fabrication of precise 3D fluidic structures in the

LTCC material using sacrificial volume materials (SVMs) is given. Finally, few exemplary LTCC-based fluidic microsystems are presented.

## 2. Fluidic structures fabrication

The section presents the SVM-based methods of three-dimensional (3D) structuration of the LTCC module for the applications in fluidics. A typical LTCC module is built of several glass-ceramic tape layers, connecting vias, surface and buried conductors and passive components. The network of conductive lines and passives are deposited using screen-printing method. After printing various shapes (channels, cavities etc.) can be cut in green LTCC tapes using laser or milling machine. In the next step all LTCC tapes are stacked together and laminated. Typically the thermo-compression lamination process is performed at high pressure (up to 20 MPa), elevated temperature (up to 90 °C) for time of 5-30 minutes. After lamination the LTCC module is co-fired according to two step thermal profile with a maximum temperature of 850-900 °C. The thermo-compressive lamination and co-firing processes provides very good bonding between individual LTCC tape layers, however, the conventional high pressure lamination methods pose some problems. High pressure and temperature of the process strongly affect the quality of the final fluidic structure and preclude realization of the complex 3D features such as: channels, cavities etc. In particular, the key challenge is the ability to form surface and buried fluidic structures without sagging during the technological process. Recently several techniques for fluidic structures fabrication have been discussed in the literature. The most common technologies for 3D processing of the LTCC tape are hot embossing [19], low pressure lamination methods [20,21] and techniques basing on sacrificial volume materials [22-24]. The SVM is a temporary insert which supports and defines fluidic structure during high pressure lamination process. Various types of materials are used as the SVMs e.g. wax, graphite, polymers, mineral materials [25,26]. Depending on the applied sacrificial volume material its elimination from LTCC module takes place either by dissociation during co-firing (polymers, graphite) or by etching or pouring out after firing (mineral materials). Commercial available SVMs are made of graphite because of its inherent features. It does not react with the LTCC material and can be easily applied as a paste or tape. Moreover, graphite burns away in air above 600 °C which is intermediate between debinding and sintering temperatures of the LTCC. The exemplary thermo-gravimetric curve of the graphite-based SVM paste is presented in Fig. 1.

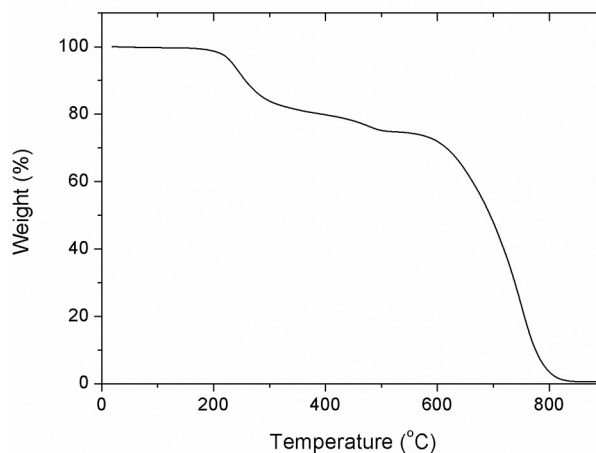


**Figure 1:** TG analysis results of the graphite-based SVM paste.

Ideally a graphite-based sacrificial volume material should be completely removed below the temperature where the open porosity of the LTCC is closed by densification (about 800 °C). Therefore, it is recommended to modify co-firing profile by applying a slower ramp rate up to 850-900 °C or additional isothermal heating stage to assure complete graphite burnout. Unsuitable thermal profile may lead to swelling or contamination of the LTCC material.

There are two common techniques of the fluidic structures fabrication which are based on the applying of graphite-based SVM paste or tape. The LTCC-based fluidic structures can be fabricated using either “define and fill” or “collate and laminate” techniques. Fabrication of the fluidic structures with the feature size from 100 µm to single centimeters is possible.

### 2.1. Define and fill

Scheme of the fluidic structure fabrication process in the LTCC using “define and fill” technique is presented in Fig. 2. In the first step of this technique a fluidic structure is cut in a green LTCC tape using laser system or milling machine. The cutting process is followed by thermo-compressive lamination of the middle and bottom LTCC tape layers. The first lamination is performed at relatively low pressure (about 1 MPa) and room temperature using isostatic or uniaxial press. After initial lamination the created fluidic structure is filled with a sacrificial volume material. The fluidic structure is filled in using screen-printing method. The SVM paste is printed through openings made in the backing polymer of the LTCC tape. The openings in the backing polymer are matched with openings in the middle LTCC tape layer. Application of the carrier film decreases number of the process steps because there is no need to make a stencil or specific pattern on the screen.

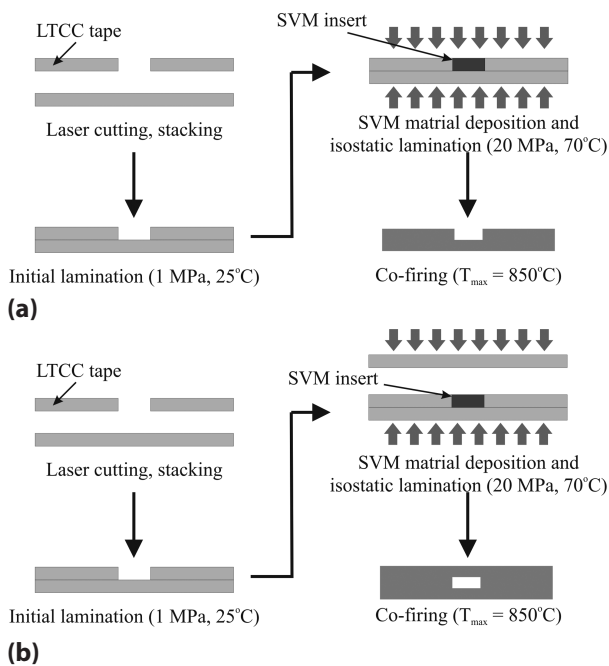


**Figure 2:** Fabrication of (a) open and (b) buried channel in LTCC module using “define and fill” technique.

Moreover, the SVM paste shrinks after drying and carrier film ensures proper thickness of dried SVM. The SVM deposition process is called “screeding” in the literature [25]. In the next step the fluidic structure is sealed with a top LTCC tape layer. Second lamination is performed at pressure of 10-20 MPa and at elevated temperature (40-70°C) in a isostatic or uniaxial press. The LTCC laminate is co-fired in air with a modified thermal profile. The additional heating stage and temperature slow ramp rate assure complete burnout of the applied SVM. The “define and fill” technique can be used for fabrication of open and buried fluidic structures in the LTCC modules. Exemplary scanning electron microscope (SEM) image of the microchannel made in the LTCC using mentioned technique is presented in Fig. 3.

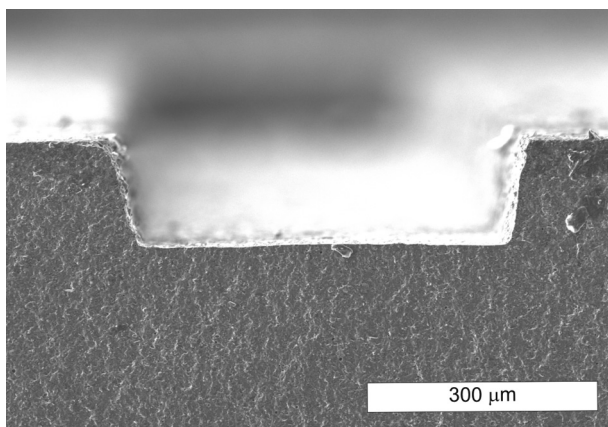


**Figure 3:** SEM image of the open channel made in the LTCC module using “define and fill” technique.

## 2.2. Collate and laminate

Alternative method which is used for fluidic structures fabrication in the LTCC modules is called “collate and laminate”. A flow-chart of this technique is presented in Fig. 4. The process starts from deposition of the pattern of the fluidic structure made of the SVM paste on green LTCC tape. In the next step the LTCC tape layer with deposited SVM is collated with another LTCC tape. The lamination process is performed at elevated pressure (5-20 MPa) and temperature (40-70 °C) using isostatic or uniaxial lamination press. In this technique there is no pre-existing fluidic structure. The fluidic structure is formed by pressure of the lamination process which deforms green LTCC material around the SVM paste and bonds compatible areas [27]. After lamination the LTCC module is co-fired with a maximum temperature of 850-900 °C. During co-firing process the SVM material is removed leaving empty volume. This technique enables to fabricate fluidic structures with characteristic dimension from 100 μm to few centimeters. SEM image of the exemplary fluidic structure made in LTCC using “collate and laminate” technique is presented in Fig. 5. The “collate and laminate” technique can also be used to fabricate tensile bars, conductor posts, membranes and suspended thick-film features [28].

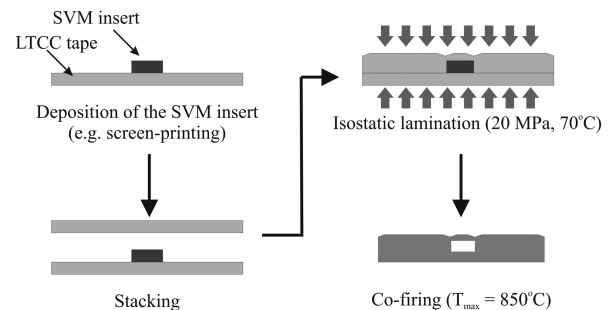


**Figure 4:** Fabrication process of the fluidic structure using “collate and laminate” technique.

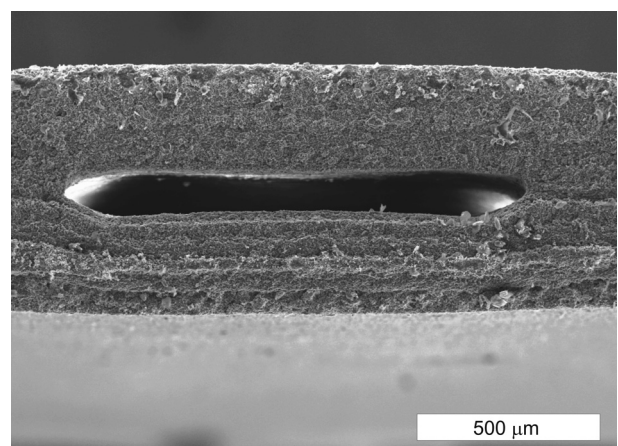


**Figure 5:** SEM image of the open channel made in the LTCC module using “collate and laminate” technique.

### 3. LTCC-based microfluidic systems

Modern microfluidic system is build of several functional blocks. These sub-systems are responsible for various functions: sample transport (micropumps and microvalves), preliminary preparation of the sample (micromixers), carrying out appropriate (bio)chemical reaction, product separation and detection. Each of sub-systems can work as separate device or can be integrated into one monolithic structure. All functional blocks can be fabricated using LTCC or hybrid LTCC-Si, LTCC-PDMS technologies.

#### 3.1. Microvalves

Microvalves are usually fabricated as a hybrid structures. They consist of moving part, usually flexible membrane, made of steel, silicon or polymer. Actuation of the membrane is provided by piezoelectric or electromagnetic principle. Construction of the initially open valve made in the LTCC is described in [29]. It consists of fluidic channels, cavity, valve seat and a steel membrane. The piezoelectric layer deposited on the steel membrane forms a unimorph piezoactuator. When electric field is applied transverse expansion and contraction of the piezoelectric layer occur. These deformation creates an internal bending moment and deflection of the structure. The unimorph piezoactuator generates approximately  $1.3 \mu\text{m}$  displacement, which closes the valve. For valves based on electromagnetic principle vertical actuation is generated by interaction between magnetic field and a permanent magnet which is placed on flexible membrane. Gongora-Rubio et al. [30] presented a LTCC-based hybrid microvalve with electromagnetic actuation. It consists of fluidic channels and a silicon membrane with bonded permanent magnet. The fluidic channels and multilayer coil are made inside the LTCC module. Using  $\text{SmCo}$  magnet with 1 mm diameter it was possible to obtain  $200 \mu\text{m}$  deflection of the  $\text{Si}$  membrane. Similar construction of the microvalve was developed at Faculty of Microsystem Electronics and Photonics at Wrocław University of Technology [31]. The valve was built of twelve LTCC tape layers and PDMS membrane with immersed permanent neodymium magnet. Scheme of the valve is presented in Fig. 6. Inlet and outlet fluidic channels and valve seat were cut in green LTCC tapes using Nd-YAG laser system. The PDMS membrane was bonded to fired LTCC structure using argon plasma. Fabricated valve is presented in Fig. 7. The presented valve is normally open. It can be closed by deflection of the PDMS membrane. The deflection is caused by magnetic force generated by current flowing through the multilayer coil.

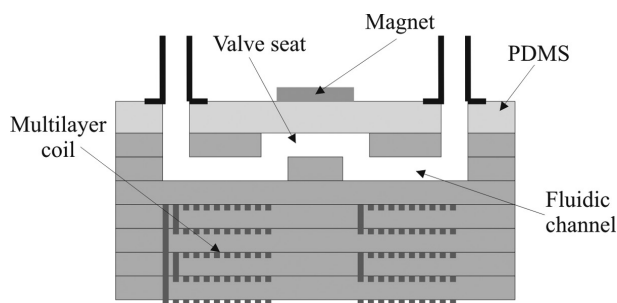


**Figure 6:** Scheme of the PDMS/LTCC-based electromagnetic valve (not to scale).

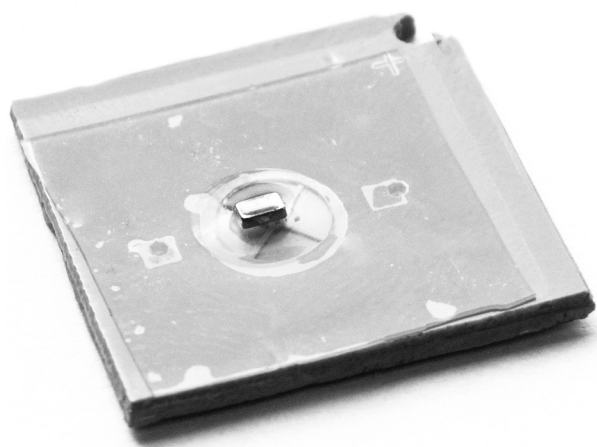


**Figure 7:** PDMS/LTCC-based valve with electromagnetic actuation [31].

#### 3.2. Micromixers

The rapid mixing between two (or more) initially segregated fluids is often crucial to the effective functioning of a modern microfluidic system. Majority of (bio)chemical processes such as enzymatic reactions require intermix of all reagents for initiations. An efficient micromixer should mix very small volumes of fluids without taking much space in acceptable time-scales. However, it is very difficult to mix microvolumes of fluid, because the flow is in a laminar regime. As a consequence mixing process is based mainly on relatively slow molecular diffusion. Diffusive mixing time is given by equation (1):

$$t_{diff} \propto \frac{D_h^2}{D} \quad (1)$$

where  $D_h$  is a characteristic dimension of the mixer (m) and  $D$  is a coefficient of molecular diffusion ( $\text{m}^2/\text{s}$ ). The micromixers are classified as either active or passive. As can be noticed from equation (1) fluids which flow with a mean velocity of  $U$  have to pass through distance equal to  $U(D_h^2/D)$  to be completely mixed. Therefore, the mixing time and distance required to effective mixing can be very high. The magnitude of the mass flux

of the fluid particles due to the molecular diffusion is described by equation (2):

$$J = -D\nabla c \quad (2)$$

where  $c$  is particles concentration ( $\text{m}^{-3}$ ). Using equation (2) it can be noticed that the key to efficient mixing relies mainly on amount of interface area between mixing fluids and ability to create high concentration gradients between fluids. Large interface area results in larger area for mass transfer and concentration gradients accelerate diffusion. Elongation of interface area and supporting concentration gradients can be obtained in microscale by stretching and folding phenomena which are characteristic for chaotic mixing. In order to provide effective mixing active and passive micromixers are used. In general, active micromixers require external energy (e.g. temperature, pressure, acoustics etc.) to disturb fluid flow pattern. Passive micromixers do not require external energy. Effective mixing is provided by micromixer's channel geometry. Spatial changes along the mixing channel axes result in frequent changes of fluid flow direction. The main advantage of the passive micromixers over active ones are easiness of fabrication and integration with other microfluidic devices. Active micromixer made with LTCC technology was presented by Bau and co-workers [32]. They shown design, realization and functioning of the magneto-hydro-dynamic (MHD) micromixer. The presented micromixer utilizes electro-magnetic (Lorentz) force to improve mixing phenomenon in micro-channel. The Lorentz force is induced by coupling between magnetic and electric fields which are generated in the micromixer. The MHD mixer consisted of the LTCC structure and a permanent Neodymium magnet. Mixing channel with electrodes on the bottom was made inside the LTCC structure. Mixing channel was filled with electrolyte solution. When the electrical potential was applied to the pairs of electrode, currents were induced in the solution. Currents and magnetic force induced by permanent magnet generate the Lorentz force in a perpendicular direction to the magnetic and electric fields.

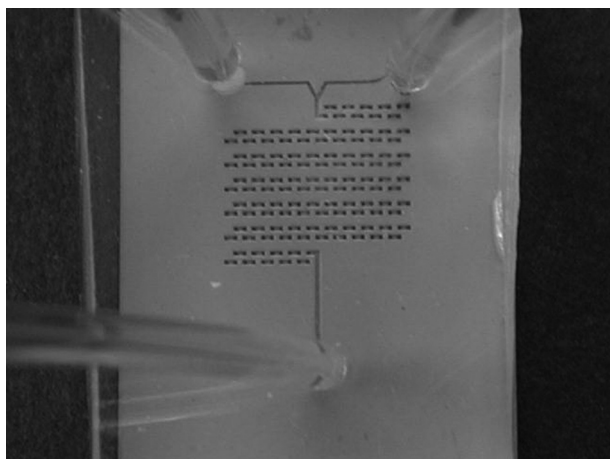


**Figure 8:** LTCC-based serpentine micromixer.

Direction of the force depends on positive and negative poles of a DC power supply. Rapid changes of the poles causes stretching and folding of the electrolyte solution in the mixing channel. The high efficient passive micromixer was developed at Faculty of Microsystem Electronics and Photonics at Wrocław University of Technology [33]. The micromixer was composed of sequence of bends arranged in I-shape serpentine. The serpentine micromixer is presented in Fig. 8.

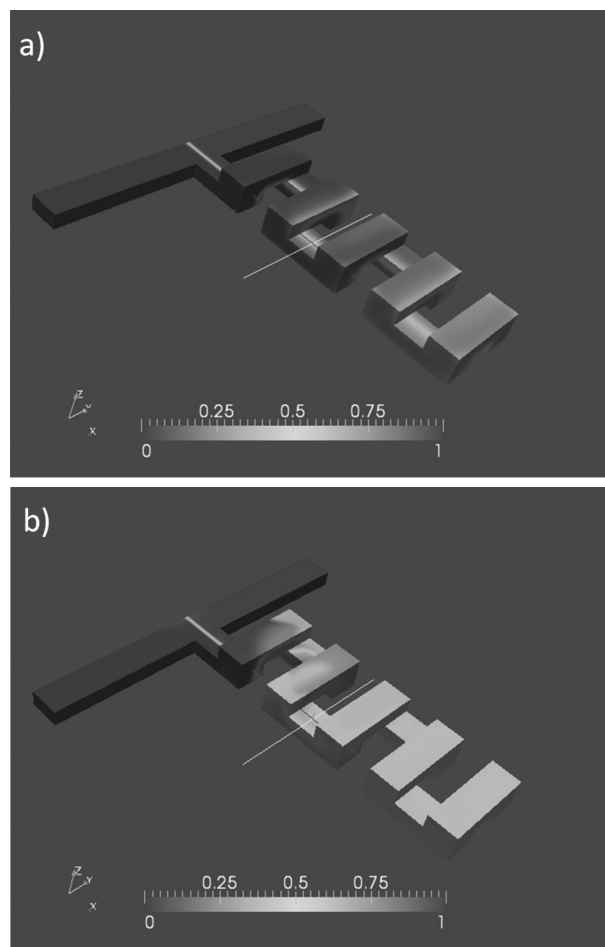


**Figure 9:** Concentration distribution in a serpentine passive micromixer for (a) low and (b) high flow rates.

The efficiency of the presented micromixer relies on inertial effects. For relatively low flow rates the mixing is poor, but for higher flow rates the mixing efficiency increases. Results of mixing modeling for low and high flow rates are shown in Fig. 9. According to numerical simulations for low flow rates viscous effects dominate, therefore, bend-induced fluid recirculation and flow pattern disturbances decay rapidly. However, for higher flow rates the mixing process is more efficient. As can be seen from Fig. 9b both fluids remain separated only in the vicinity of the junction and are well mixed after passing few bends of the serpentine. For relatively high flow rates the interface area between mixing fluids enlarges

due to the stretch and fold phenomena. Large interface area between fluids creates more space for the fluid particles for diffusion and enhances mixing process.

### 3.3. Microreactors

Microreactor technology has become very promising in the fields of chemistry, biotechnology and process engineering. A microreactor is a miniature device where appropriate (bio)chemical reaction occurs. The microreactor needs very small amounts of reagents for operation. The microreactors work either as a stand-alone devices or as a part of more sophisticated analytical system. The stand-alone microreactors are mainly used for evaluation of the influence of different chemical compounds and drugs on enzyme activity and high throughput chemical synthesis. In general, they can be classified as a batch type or flow-through microreactors. The batch type microreactors are filled with a catalytic bed made of porous material. The catalyst (e.g. enzyme) is immobilized on the surface of the porous carrier. For flow-through microreactors the catalyst is immobilized on its channels walls. Exemplary batch type microreactor made of LTCC is presented in Fig. 10. It consists of two chambers separated with a threshold and integrated heater and temperature sensor. Heater provides uniform temperature distribution in the whole area of the reaction chamber. The catalytic bed in the form of porous glass or polymeric beads with immobilized enzyme (urease) is placed in a larger chamber of the microreactor. The threshold precludes catalytic bed to move to the chamber for reaction products. A LTCC-based flow-through microreactor is presented in Fig. 11. It is composed of inlet and outlet chambers connected with sixteen parallel microchannels and integrated heater. Enzyme is immobilized on the surface of the microchannel walls.

The presented microreactors were used for urea determination in biological fluids [34]. The principle of their operation is based on hydrolysis of urea catalyzed by urease. One of the reaction products are hydroxyl ions which are used for indirect determination of urea in the sample.

### 3.4. Detection unit

Detector is one of the most important part of the substantial number of fluidic systems. It is responsible for qualitative or quantitative detection of the analyte in the liquid sample. A very small volumes of the fluid can be analyzed using either electrochemical or optical methods. The optical methods are characterized by very good sensitivity and repeatability. The LTCC-based optical detection module for absorbance measurement is presented in Fig. 12.

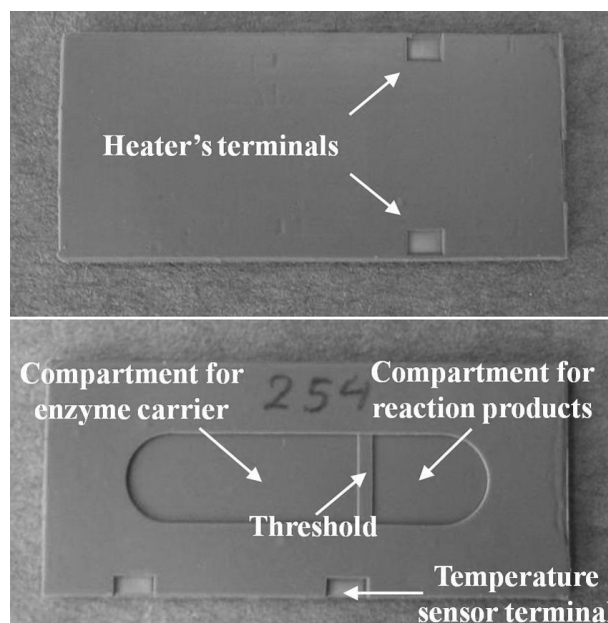


**Figure 10:** Batch type microreactor made with LTCC technology.

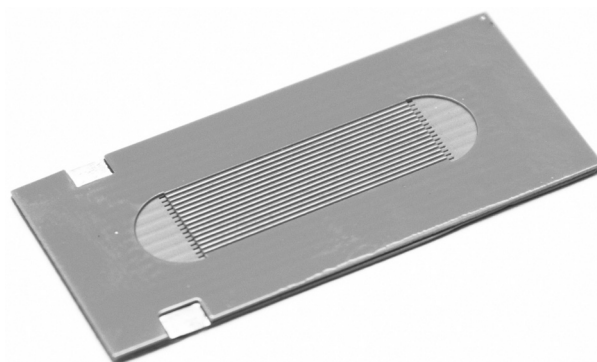
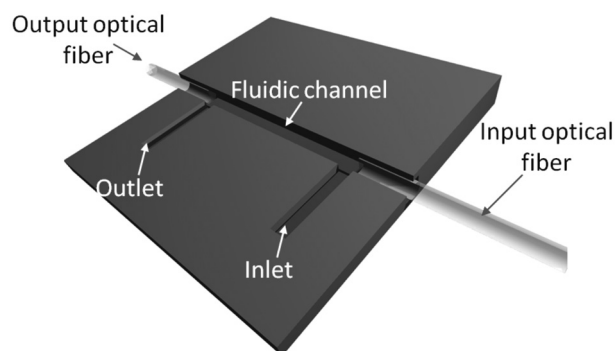
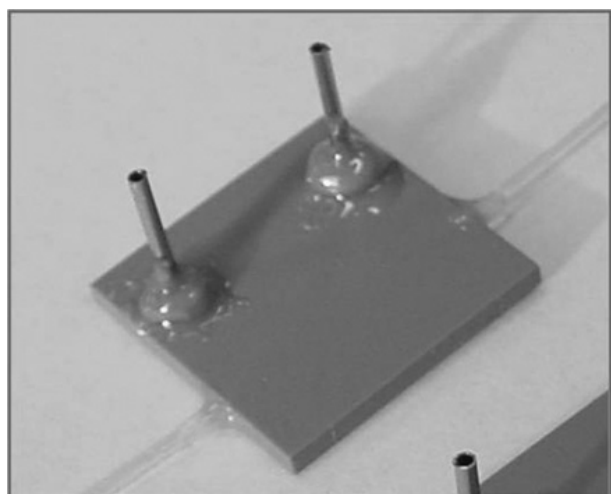


**Figure 11:** Flow-through microreactor made with LTCC technology.

It consists of U-shaped microfluidic channel and two polymeric optical fibers [35]. Space between optical fibers creates 10 mm long absorption cell. The input optical fiber is connected with light emitting diode and the output optical fiber is connected to light-to-voltage converter. Principle of operation is based on selective light absorption by the analyte. A green light ( $\lambda_{\text{max}} = 565 \text{ nm}$ ) from LED is transmitted via input optical fiber to the absorption cell. The analyte which flows between two optical fibers absorbs a portion of light. The rest of the light is transmitted via output optical fiber to the light-to-voltage converter. The changes of the light intensity on the light-to-voltage converter are proportional to the changes of the analyte concentrations. According to the Beer's law magnitude of the absorbed light  $A$  is proportional to concentration of the analyte:



(a)



(b)

**Figure 12:** LTCC-based detection unit for absorbance measurements: (a) schematic view and (b) photograph.

$$A \equiv \log \frac{I_0}{I} = \epsilon c l \quad (3)$$

where  $I_0$  and  $I$  are intensities of the light before and after absorption,  $c$  is the molar concentration of the analyte (M),  $\epsilon$  is the molar absorptivity ( $\text{cm}^{-1} \text{M}^{-1}$ ) and  $l$  is the absorption cell length (cm). It can be seen that for fixed length of absorption cell and the same molar absorptivity of the analyte the absorbance is proportional to the concentration of the analyte. Utilizing the light-to-voltage converter as a light detector it is possible to measure the optical absorbance using following formula:

$$A \equiv \log \frac{I_0}{I(c)} = \log \frac{U_0}{U(c)} \quad (4)$$

where  $U_0$  is the output voltage for distilled water and  $U(c)$  is the output voltage for analyte with concentration  $c$ . Exemplary dynamic response of the presented LTCC detection module for various concentrations of potassium permanganate ( $\text{KMnO}_4$ ) is presented in Fig. 13. As can be seen from Fig. 13 the presented LTCC detection module is characterized by high signal-to-noise ratio and good repeatability of the output signal.

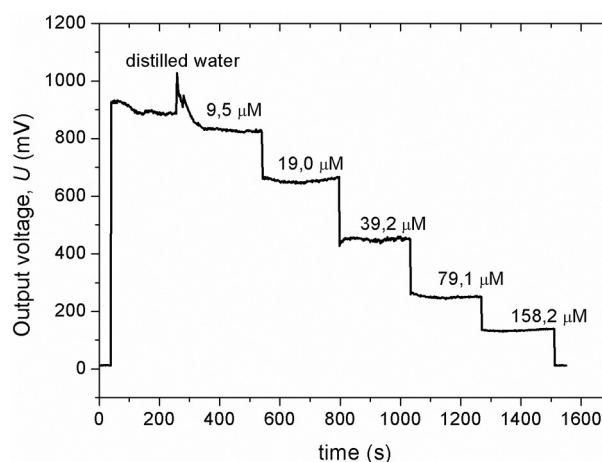


**Figure 13:** Dynamic response of the LTCC detection module for various concentrations of  $\text{KMnO}_4$  test solution ( $\lambda_{\text{max}} = 565 \text{ nm}$ )

#### 4. Conclusions

Short overview of the fluidic structures fabrication methods in LTCC has been discussed in the paper. The presented methods are based on application of the sacrificial volume materials. Using SVM it is possible to fabricate various fluidic structures with a characteristic dimensions from hundreds microns to single centimeters. By applying appropriate technological procedure it is possible to fabricate open or buried fluidic structures in the LTCC multilayer module.

The exemplary LTCC-based fluidic microsystems (valve, micromixer, microreactor and optical detection module) developed and fabricated at Faculty of Microsystem Electronics and Photonics at Wrocław University of Technology has been presented. The presented fluidic microsystems has been fabricated using SVM-based fabrication methods.

The performed research has shown the LTCC technology potential to fabricate fluidic microsystems. The presented technology can be successfully applied for fabrication of all functional blocks of the integrated micro-total analysis systems or lab-on-chip devices.

#### Acknowledgments

The financial support of the European Union through the MULTILAYER project (FP7-NMP4-2007-214122) is gratefully acknowledged.

## References

1. A. Manz, N. Graber, M.H. Widem, "Miniaturized total chemical analysis systems: a novel concept for chemical sensing", *Sens. Actuators B: Chem.*, vol. 1, pp. 244-248, 1990.
2. P. Gravesen, J. Branebjerg, O. Søndergård, "Microfluidic – a review", *J. Micromech. Microeng.*, vol. 3, pp. 168-182, 1993.
3. A. Daridon, V. Fascio, J. Lichtenberg, R. Wutrich, H. Langen, E. Verpoote, N. Rooij, "Multi-layer microfluidic glass chips for microanalytical applications", *Fresenius J. Anal. Chem.*, vol. 371, pp. 261-269, 2001.
4. C.F. Chou, R. Changrani, P. Roberts, D. Sadler, J. Burdon, F. Zenhausern, S. Lin, A. Mulholland, N. Swami, R. Terbrugge, "A miniaturized cyclic PCR device – modeling and experiments", *Microelectronic Engineering*, vol. 61-62, pp. 921-925, 2002.
5. P. Norblin, O. Ohman, B. Ekstrom, L. Forssen, "A chemical micro analysis system for the measurement of pressure, flow rate, temperature, UV-absorption and fluorescence", *Sens. Actuators B: Chem.*, vol. 49, pp. 34 – 39, 1998.
6. Y. Yonemori, E. Takahashi, H. Ren, T. Hayashi, H. Endo, "Biosensor system for continuous glucose monitoring in fish", *Anal. Chim. Acta*, vol. 633, pp. 90-96, 2009.
7. D.G. Pijanowska, A.J. Sprenkles, W. Olthuis, P. Bergveld, "A flow-through amperometric sensor for micro-analytical systems", *Sens. Actuators B: Chem.*, vol. 91, pp. 98-102, 2003.
8. T. Fuji, "PDMS-based microfluidic devices for biomedical applications", *Microelectronic Engineering*, vol. 61-62, pp. 907-914, 2002.
9. T. Merkel, M. Graeber, L. Pagel, "A new technology for fluidic microsystems based on PCB technology", *Sens. Actuators A: Phys.*, vol. 77, pp. 98-105, 1999.
10. L.J. Golonka, "Technology and applications of low temperature cofired ceramic (LTCC) based sensors and microsystems", *Bull. Pol. Acad. Sci. Tech. Sci.*, vol. 54, no. 2, pp. 221-231, 2006.
11. K. Malecha, M. Dawgul, D.G. Pijanowska, L.J. Golonka, "LTCC microfluidic systems for biochemical diagnosis", *Biocybernetics and Biomedical Engineering*, vol. 31, no. 4, pp. 31-41, 2011.
12. N. Ibanez-Garcia, C.S. Martinez-Cisoneros, F. Valdes, J. Alonso, "Green-tape ceramics. New technological approach for integrating electronics and fluidics in microsystems", *Trends in Analytical Chemistry*, vol. 27, pp. 24-33, 2008.
13. T. Thelemann, M. Fisher, A. Groß, J. Müller, "LTCC-based fluidic components for chemical applications", *Journal of Microelectronics and Electronic Packaging*, vol. 4, no. 4, pp. 167-172, 2007.
14. D. Nowak, D. Kulczak, M. Januszkiewicz, A. Dziedzic, "High temperature LTCC package for SiC-based gas sensor", *Opt. Appl.*, vol. 39, no. 4, pp. 701-704, 2009.
15. R. Tadaszak, A. Łukowiak, L.J. Golonka, S. Patela, "Hybrid sol-gel-glaze planar optical waveguides on LTCC substrate – preliminary works", *Opt. Appl.*, vol. 41, no. 2, pp. 493-500, 2010.
16. P. Markowski, "Thick-film photoimageable and laser-shaped arms for thermoelectric micro-generators", *Microelectronics International*, vol. 28, pp. 43-50, 2011.
17. M.F. Khan, F.A. Ghavanini, S. Haasl, L. Löfgren, K. Persson, C. Rusu, K. Schjøllberg-Henriksen, P. Enoksson, "Methods for characterization of wafer-level encapsulation applied on silicon to LTCC anodic bonding", *J. Micromech. Microeng.*, vol. 20, pp. 064020.1-10, 2010.
18. K. Malecha, I. Gancarz, L.J. Golonka, "A PDMS/LTCC bonding technique for microfluidic application", *J. Micromech. Microeng.*, vol. 19, pp. 105016.1-8, 2009.
19. T. Rabe, P. Kuchenbecker, B. Schulz, "Hot embossing: an alternative method to produce cavities in ceramic multilayer", *Int. J. Appl. Ceram. Technol.*, vol. 4, no. 1, pp. 38-46, 2007.
20. K. Schindler, A. Roosen, "Manufacture of 3D structures by cold low pressure lamination of ceramic green tapes", *Journal of the European Ceramic Society*, vol. 29, pp. 899-904, 2009.
21. D. Jurków, H. Roguszczyk, L.J. Golonka, "Cold chemical lamination of ceramic Green tapes", *Journal of the European Ceramic Society* vol. 29, pp. 703-709, 2009.
22. H. Birol, T. Maeder, C. Jacq, S. Straessler, P. Ryser, "Fabrication of low-temperature co-fired ceramics micro-fluidic devices using sacrificial carbon layers", *Int. J. Appl. Ceram. Technol.*, vol. 2, no. 5, pp. 364-373, 2005.
23. K. Malecha, L.J. Golonka, "Microchannel fabrication process in LTCC ceramics", *Microelectronics Reliability*, vol. 48, pp. 866-871, 2008.
24. K. Malecha, T. Maeder, C. Jacq, "Fabrication of membranes and microchannels in low-temperature co-fired ceramic (LTCC) substrate using novel water-based sacrificial carbon pastes", *Journal of the European Ceramic Society*, vol. 32, pp. 3277-3286, 2012.
25. C. Lucat, P. Ginet, C. Castille, H. Debeda, F. Menil, "Microsystem elements based on free-standing thick-films made with a new sacrificial layer process", *Microelectronics Reliability*, vol. 48, pp. 872-875, 2008.
26. W. Kinzy Jones, Y. Liu, M. Gao, "Micro heat pipes in low temperature cofire ceramic (LTCC) substrate",

- IEEE Trans. Compon. Packag. Technol., vol. 26, no. 1, pp. 110-115, 2003.
27. K.A. Peterson, R.T. Knudson, E.J. Garcia, K.D. Patel, M. Okandan, C.K. Ho, C.D. James, S.B. Rohde, B.R. Rohrer, F. Smith, L.R. Zawicki, B.D. Wroblewski, "LTCC microelectronics, microsystems, and sensors", Proc. 15th IEEE Int. Conf. MIXDES, 19-21 June 2008, Poznań (Poland), pp. 23-37.
  28. K.A. Peterson, K.D. Patel, C.K. Ho, S.B. Rohde, C.D. Nordquist, C.A. Walker, B.D. Wroblewski, M. Okandan, "Novel microsystem applications with new techniques in low-temperature co-fired ceramics", Int. J. Appl. Ceram. Technol., vol. 2, no. 5, pp. 345-363, 2005.
  29. M. Sobociński, J. Juuti, H. Jantunen, L.J. Golonka, "Piezoelectric unimorph valve assembled on an LTCC substrate", Sens. Actuators A: Phys., vol. 149, pp. 315-319, 2009.
  30. M.R. Gongora-Rubio, P. Espinoza-Vallejos, L. Sola-Laguna, J.J. Santiago-Avilés, "Overview of low temperature co-fired ceramics tape technology for meso-system technology (MsST)", Sens. Actuators A: Phys., vol. 89, pp. 222-241, 2001.
  31. K. Czajkowska, "Design and manufacturing of microvalve in fluidic LTCC module", MSc Thesis, Wrocław University of Technology, Wrocław, 2012.
  32. H.H. Bau, J. Zhong, M. Yi, "A minute magneto hydro dynamic (MHD) mixer", Sens. Actuators B: Chem., vol. 79, pp. 207-215, 2001.
  33. K. Malecha, L.J. Golonka, J. Bałdyga, M. Jasińska, P. Sobieszuk, "Serpentine microfluidic mixer made in LTCC", Sens. Actuators B: Chem., vol. 143, pp. 400-413, 2009.
  34. K. Malecha, D.G. Pijanowska, L.J. Golonka, W. Torbicz, "LTCC microreactor for urea determination in biological fluids", Sens. Actuators B: Chem., vol. 141, pp. 301-308, 2009.
  35. K. Malecha, T. Zawada, L.J. Golonka, "LTCC based microfluidic optical detector", Proc. 28th IEEE Int. Spring Seminar on Electronic Technology, May 19-22 2005, Wiener Neustadt (Austria), pp. 347-351.

Arrived: 10. 08. 2012

Accepted: 25. 10. 2012.

# *3D structuration of LTCC and related technologies for thermal management and microfluidic structures*

*Thomas Maeder, Conor Slater, Bo Jiang, Fabrizio Vecchio, Caroline Jacq and Peter Ryser*

*Laboratoire de Production Microtechnique (LPM), École Polytechnique Fédérale de Lausanne (EPFL), Lausanne, Switzerland*

**Abstract:** Ceramic technologies such as LTCC (Low Temperature Co-fired Ceramic) and thick-film are used widely in electronic circuits exposed to harsh environments, for applications in fields such as aerospace, automotive and energy exploration, where, owing to their thermal and chemical stability, they have an extensive and successful track record. Recently, the extensive structuration possibilities afforded by LTCC have led to its use in sensors, microfluidics and thermal management (hotplates). In the first part of this work, we present both new and classical techniques for structuring ceramic devices for thermal management, microfluidics or both. Critical aspects for achieving successful structuration and reliable device operation are discussed, such as lamination and sealing techniques, materials formulation and selection, as well as thermomechanical design. These considerations are illustrated in the second part of this work with several examples: micro-hotplates for various applications, microfluidic coolers, chemical reactors and solid-oxide fuel cell (SOFC) components.

**Key words:** Thick-film technology, LTCC, 3D structuration, microfluidics, thermal management.

## *3D strukturiranje LTCC in sorodnih tehnologij za termično upravljanje in mikro tekočinske strukture*

**Povzetek:** Keramične tehnologije, kot je LTCC (keramika z nizko temperaturo žganja) in debeli sloji, se pogosto uporabljajo v elektronskih vezjih, ki so izpostavljena neugodnemu okolju, za aplikacije v vesolju, avtomobilskih in energetskih raziskavah, kjer imajo s svojo termično in kemijsko stabilnostjo uspešno in dolgo zgodovino. Velike možnosti strukturiranja, ki jih nudi LTCC so omogočile njihovo uporabo v senzorjih, mikro tekočinah in termičnem upravljanju (hotplate – vroča plošča). V prvem delu članka predstavljamo klasično metodo strukturiranja keramičnih elementov za termično upravljanje, za mikro tekočine ali oboje. Opisani so kritični vidiki za doseganje uspešnega strukturiranja in zanesljivega delovanja, kot je laminacija, tehnike pečatenja, formuliranja in izbora materialov, kakor tudi termomehantična oblika. Te odločitve so v drugem delu članka predstavljene s pomočjo naslednjih primerov: mikro vroča plošča za različne aplikacije, mikro tekočinski hladilniki, kemični reaktorji in deli gorivnih celic s trdnim elektrolitom (SOFC).

**Ključne besede:** debeloplastna tehnologija, LTCC, 3D strukturiranost, mikro tekočine, termično upravljanje.

\* Corresponding Author's e-mail: [thomas.maeder@epfl.ch](mailto:thomas.maeder@epfl.ch)

### *1. Introduction*

Originally introduced as a chip / multichip module packaging and high-reliability circuit technology [1-4], LTCC has found important additional applications in the field of advanced packaging, sensors and microfluidics. This requires more advanced 3D structuration techniques, required to form features such as thin bridges, cavities, membranes, channels and hotplates [5-16].

In the green state, LTCC tape is easily shapeable, and may be cut and further processed by a wide variety of methods (Table 1), which in principle easily allows features such as channels, bridges and membranes (Figure 1). An overview of the resulting LTCC applications is given in Table 2 (see also other paper at this conference [17] for mechanical sensors). The very wide range of devices and applications attest for the excellent 3D structurability of LTCC.

However, problems that appear at the different stages of processing (handling, lamination and firing, Table 1) in practice severely hamper many applications. Moreover, the properties and limitations of LTCC as a material must also be taken into account, such as mechanical strength (short- and long-term), chemical durability and thermal stability. Also, physical properties such as the coefficient of thermal expansion (CTE) and elastic modulus are important for device performance.

The purpose of the present work is therefore to give an overview of the applications of LTCC structuration, centred on microfluidics and thermal management, with the associated themes:

- Processing issues and how they are resolved
- Properties and limitations of LTCC as a material
- Implications on device design

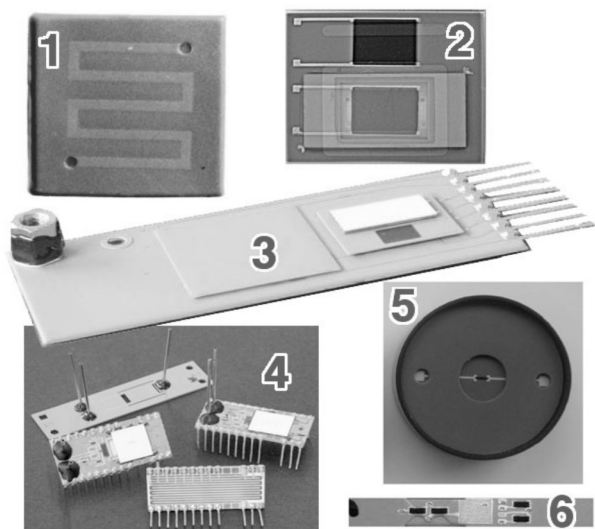


**Figure 1:** Example LTCC structures (see table 2) (1-3) Meander channel (1) and heater module (2) for gas viscosity sensor (3, with membrane) [18-20]; 4) chemical microreactor with complex fluidic circuit [16, 20]; 5) thermal bubble inclinometer (with membrane) [9]; 6) cantilever sensor for low forces [9, 16, 21, 22].

**Table 1:** Methods and operations used in 3D structuration of LTCC. † SVM = sacrificial volume material. # MSM / FSM = mineral / fugitive sacrificial (volume) material.

Operation	Methods
Cutting / drilling / shaping	<ul style="list-style-type: none"> <li>- Mechanical microdrilling / end milling [7, 23]</li> <li>- Punching / stamping [24]</li> <li>- Laser cutting of LTCC [24-26]; of conductors [27, 28]</li> <li>- Embossing [24, 29, 30]</li> <li>- Controlled laser ablation [31]</li> <li>- Solvent vapour jet cutting [32]</li> <li>- None (lamination directly around SVM†) [7, 33, 34]</li> </ul>

Lamination methods and conditions (LP/HP = low-/high-pressure)	No sacrificial material <ul style="list-style-type: none"> <li>- Uniaxial, HP, cold [13, 35]</li> <li>- Uniaxial, minimal-pressure, cold [36] or warm [37]</li> <li>- Adhesive tape, LP [38, 39]</li> <li>- Solvent / adhesive paste / adhesive solution, LP [12, 40-44]</li> <li>- Hot-melt adhesive layer, LP [45]</li> </ul> With sacrificial material <ul style="list-style-type: none"> <li>- Warm, HP, uniaxial or isostatic (standard methods)</li> </ul>
Lamination order	<ul style="list-style-type: none"> <li>- All at once (standard procedure)</li> <li>- Sequence of partial laminations, often with different methods/parameters [13, 44, 46, 47]</li> </ul>
Firing	No sacrificial material or MSM# <ul style="list-style-type: none"> <li>- Standard, in air (usually)</li> </ul> With FSM# <ul style="list-style-type: none"> <li>- Air (match sintering and burnout kinetics) [10, 48-51]</li> <li>- Air-N2-air (sinter in N2, then oxidise FSM) [17, 52]</li> </ul>
Post-firing operations (depending on device)	<ul style="list-style-type: none"> <li>- MSM† removal by chemical dissolution [52-57] or mechanical blowing [8]</li> <li>- Screen-printing of materials incompatible with co-firing</li> <li>- Cutting of temporary supports [58 2012]</li> <li>- Singulation by dicing or breaking</li> </ul>

**Table 2:** Applications of LTCC structuration techniques beyond purely electrical ones. † M(O)EMS: micro (opto) electromechanical system. # μ-SOFC: micro solid-oxide fuel cells.

Field	Applications
Advanced & high-reliability hermetic packaging	<ul style="list-style-type: none"> <li>- MOEMS† package [59]</li> <li>- Package + quality control [60, 61]</li> <li>- MEMS pressure sensor package for medical applications [62]</li> <li>- Active getter module [63]</li> </ul>
Pressure sensing	<ul style="list-style-type: none"> <li>- Piezoresistive (membrane) [64, 65]</li> <li>- Piezoresistive high-pressure cell (direct compression) [20, 66]</li> <li>- Piezoelectric (resonance) [67]</li> <li>- Capacitive (membrane) [68, 69]</li> <li>- Complete piezoresistive pressure sensor (+electronics) [15, 17, 70, 71]</li> </ul>
Force & accel. sensing	<ul style="list-style-type: none"> <li>- Low forces [9, 16, 21, 22]; applied to low pressures (indirect) [72]</li> <li>- Acceleration [17]</li> </ul>
Optical sensors	<ul style="list-style-type: none"> <li>- pH [73]</li> <li>- Absorbance [74] &amp; fluorescence [75]</li> </ul>
Flow & liquid sensing	<ul style="list-style-type: none"> <li>- Fuel injection (thermal) [76]</li> <li>- Flow sensor, thermal [17, 71, 77, 78] or mechanical [79]</li> <li>- Thermal bubble inclinometer [9]</li> </ul>
Flow control	<ul style="list-style-type: none"> <li>- Valve [80]</li> <li>- Substrate for electrovalves [13]</li> </ul>

Liquid micro-reactors	<ul style="list-style-type: none"> <li>- Emulsifier [81], dilution device [82]</li> <li>- Mixer [83, 84]</li> <li>- Particle synthesis [85]</li> <li>- Electrochemical [86]</li> <li>- Polymerase chain reaction [87]</li> <li>- Photocatalysis [88]</li> <li>- Integrated, + flow sensing &amp; calorimetry [11, 20, 89] / flow &amp; pressure &amp; liquid sensing [90]</li> </ul>
Gas micro-reactors	<ul style="list-style-type: none"> <li>- H<sub>2</sub>-O<sub>2</sub> combustor [91]</li> <li>- Gas burner with window [41]</li> <li>- Fuel cell reformer [92, 93]</li> <li>- Micro-plasma generator [94]</li> </ul>
Hotplates	<ul style="list-style-type: none"> <li>- For gas sensing [27, 95-97]</li> <li>- Scanning microcalorimeter [98]</li> <li>- Atomic clock module [99, 100]</li> <li>- Fluidic &amp; thermal package for MEMS† μ-SOFC# [101, 102] and μ-thrusters [103]</li> </ul>
Multi-sensors /-physics	<ul style="list-style-type: none"> <li>- Flow / pressure / temperature sensor for compressed air [46, 104]</li> <li>- Gas viscosity &amp; thermal conductivity sensor [18-20]</li> </ul>
Micro-thrusters	<ul style="list-style-type: none"> <li>- Liquid fuel [44, 105, 106]</li> <li>- Solid propellant [107]</li> </ul>

## 2. Processing techniques

The present section reviews the different techniques and issues at each stage of processing. Processing issues are usually exacerbated when using fine structures, such as required for sensitive device.

### 2.1. Basic processing routes

The most straightforward processing route is the “cut-and-laminate” one, whereby each LTCC laser is simply cut (usually by laser), with the resulting stack then being uniaxially laminated and fired (Figure 2). This simple route is feasible for applications involving relatively robust structures, where crushing and sagging of layers are not a big issue, such as the chemical microreactor shown on Figures 5 & 6.

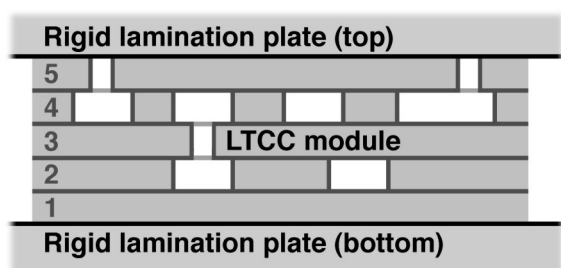


**Figure 2:** “Cut-and-laminate” structuration of LTCC: uniaxial lamination of previously processed sheets between rigid metal plates.

If slender membranes or bridges are used, sacrificial volume materials (SVMs) may be used to avoid crushing / sagging (Figure 3), using uniaxial or (pseudo-)isostatic lamination.

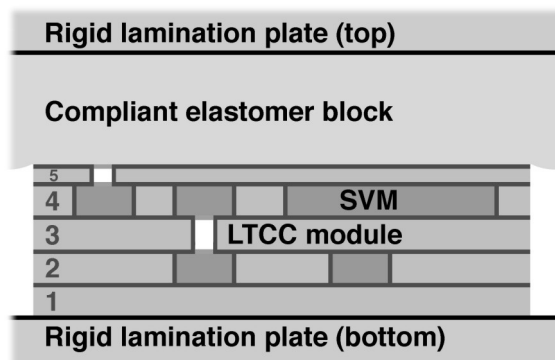


**Figure 3:** Filling crushable cavities with SVM, with pseudo-isostatic lamination (isostatic or uniaxial also possible).

Finally, cavities may be directly created by printing SVM onto LTCC, without removing the corresponding volume from the tape (Figure 4), which requires (pseudo-)isostatic lamination.

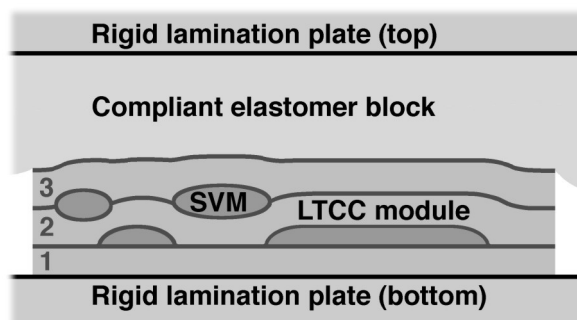


**Figure 4:** Pseudo-isostatic (similar to isostatic, where the bottom face is also deformed) lamination of LTCC modules, with printed SVM to create cavities.

### 2.2. Handling during screen-printing

Structural features such as intricate channels and thin bridges exacerbate the usual difficulties of handling fine LTCC tapes. Especially, simply cutting out complex channel networks (Figure 6) in one layer is difficult or even impossible, as this would structurally separate the tape, or weaken it excessively. To get around this issue, two techniques are commonly used:

- **“Stitching”** the fluidic circuit across several layers allows fabrication of complex and strongly meandering structures, as often seen in fluidic process devices such as microreactors (Table 2, corresponding section; Figure 6), using the classical “cut-and-laminate” route. This requires an additional layer (or two, if crossovers are desired),

and creates some additional dead volumes due to alignment tolerances.

- **Sacrificial volume materials** (SVMs) allow “printing” of channels without requiring the tape to be cut out: the channel is then formed during or after firing by removal of the SVM (Figure 4). However, this technique does have restrictions: it requires “standard”, high-pressure isostatic or pseudo-isostatic lamination to deform the LTCC tapes around the printed SVM, and results in significant deformation of the tapes and of the surface of the device [8, 11, 13, 59], which may not be the most convenient method for shaping other structures such as large cavities. Also, there are practical limits to the achievable aspect ratios, stemming from the screen printing process and restricted deformability of the LTCC tapes [14]. Finally, printing large amounts of sacrificial material can destroy the tape through attack from the SVM paste solvent. However, recent developments in screen-printing vehicle formulation show progress in formulating SVM inks that have low aggressivity towards LTCC tapes, and even allow removal of misprints by rinsing in water [33, 34, 108].

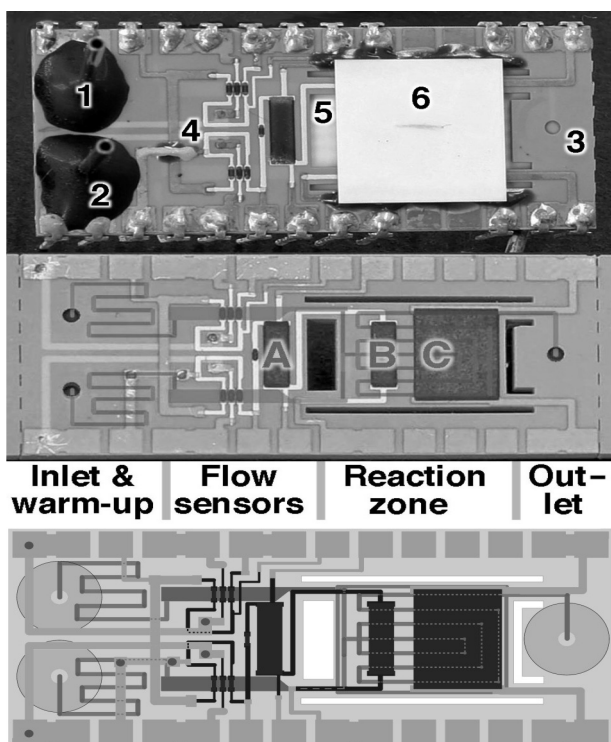


**Figure 5:** Chemical microreactor: device (top), LTCC module with superposed fluidic layout (middle) and complete electrical & fluidic layout (bottom). 1) Inlets & heat-up meanders; 2) outlet; 3) flow sensors; 4) bottom alumina heat spreader, below LTCC; 5) alumina heat shield for reaction zone. A) Thermistor for body temperature; B) thermistor for reaction zone temperature; C) resistor for heat output calibration.

### 2.3. Lamination and firing

Optimal lamination is often a compromise: applying excessive pressure and temperature can result in deformation and crushing of cavities, while the reverse yields poor bonding (Figure 7). Several techniques, described in section 3, have therefore been developed to alleviate this issue in difficult cases: SVMs to protect cavities, and “glues” to facilitate lamination.

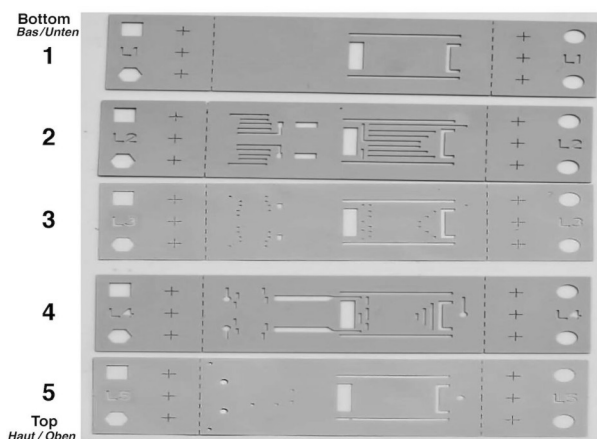


**Figure 6:** Chemical microreactor: LTCC layers, in unfired state, showing cut-outs for fluidic channels and thermal decoupling of calorimetric reaction zone. 1) Bottom wall; 2) bottom fluidic layer; 3) fluidic separation layer; 4) top fluidic layer; 5) top lid.

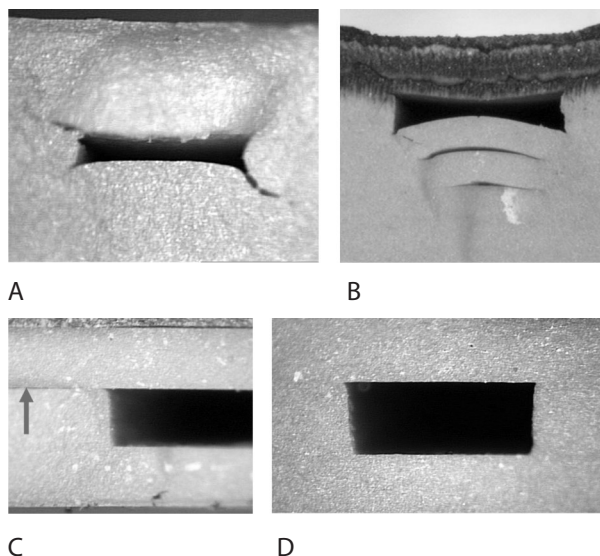


**Figure 7:** Lamination problems in fluidic structures: A) crushing of cavities; B) deformations combined with poor interlayer lamination below cavity due to absence of pressure; C) poor lamination, at arrow; D) good lamination with low deformation, with correct parameters [13].

Firing of slender structures also may lead to deformations, stemming from shrinkage mismatch between LTCC, functional materials and SVM, or simply from sag-

ging of structures under their own weight. This may again be counteracted by SVMs, which however must be correctly formulated to avoid imparting deformations themselves during LTCC sintering [10, 13, 46, 52, 57].

### 3. SVM & Adhesive formulations

In addition to the LTCC tape itself and the assorted functional materials (conductors, resistors, etc.), 3D structuration may use two types of “auxiliary” materials, which are eventually removed during processing: 1) SVMs and 2) adhesives for low-pressure lamination.

#### 3.1. Sacrificial volume materials (SVMs)

SVMs support the 3D LTCC structure during lamination, avoiding crushing, or may even be used to create cavities by themselves (see 2.1 / Figure 4). If just used to fill existing cavities, they tend to add complexity to the manufacturing process, but careful design, e.g. limiting SVM deposition to just one layer, or special processes such as filling with liquid wax [43], reduce this inconvenient.

A wide variety of SVMs have been investigated (Table 3), with carbon-based pastes or tape inserts being by far the most common.

Carbon / wax / polymer-based compositions are labelled fugitive sacrificial materials (FSMs), as they escape during firing, by evaporation, pyrolysis or oxidation to CO/CO<sub>2</sub>, which may lead to sagging during sintering through loss of support. To avoid this issue, carbon-based (mostly graphite) materials may be used; graphite is “semi-fugitive”, as it is stable to very high temperatures in inert atmospheres, and only begins to oxidise rapidly above 600-650°C in oxygen-containing ones. This allows two strategies (see Table 1, firing):

- 1 **Firing in air**, carefully matching sintering of LTCC with graphite oxidation kinetics by varying temperature rise rate and graphite particle size [8, 10, 48-51]
- 2 **Sintering in inert atmosphere**: burnout in air, up to ca. 600°C, followed by sintering in nitrogen (which preserves the graphite), and final oxidation of the graphite by switching back to air [17, 52].

Firing in air may be carried out also without restrictions, using mineral sacrificial materials (MSMs), which however requires an additional post-firing chemical or mechanical removal step (Table 1). This restricts in practice MSMs to open structures such as cantilevers or bridges on the surface of substrates [53-57, 109]. Further issues lie shrinkage mismatch, chemical interactions and limited chemical stability of some fired LTCC materials [57].

**Table 3:** Parameters and their values. † Applied to classical thick-film technology on Al<sub>2</sub>O<sub>3</sub>.

Type	Sacrificial volume material (SVM)
FSM (fugitive)	<ul style="list-style-type: none"> <li>- Carbon paste (printed) [10, 33, 34, 49-52, 108] or tape insert [8, 43]</li> <li>- Wax, screen-printed [7] or filled as liquid [43]</li> <li>- Kapton foil, laser-ablated [7]</li> </ul>
MSM (mineral)	<ul style="list-style-type: none"> <li>- Al<sub>2</sub>O<sub>3</sub> setter tape [8]</li> <li>- PbO-2SiO<sub>2</sub> glass [52]</li> <li>- CaO-B<sub>2</sub>O<sub>3</sub> [109]; CaO-borax [53]</li> <li>- Au [110]</li> <li>- CaCO<sub>3</sub> + C [55]</li> <li>- MgO-CaB<sub>2</sub>O<sub>4</sub> [57]</li> <li>- SrCO<sub>3</sub>† [54]</li> <li>- MgO-B<sub>2</sub>O<sub>3</sub>† [56]</li> </ul>

#### 3.2. Lamination adhesives

In many cases, deformations mainly stem from the high pressures required to achieve good lamination. Moreover, simple uniaxial lamination of multilayer structures intrinsically faces the issues of low stresses above cavities (Figure 7B). Therefore, many techniques have been investigated to achieve satisfactory lamination quality at moderate pressures and temperatures (see Table 1, lamination), the most common being 1) application of adhesive tapes, and 2) printing of liquid / paste adhesives or solvents. There are however some drawbacks to these methods, as they require careful application of the adhesive, and handling of the resulting sticky LTCC tape can be quite cumbersome. Therefore, in order to facilitate handling, we recently proposed an alternative method using hot-melt adhesive layers [45], which are first generically deposited onto the LTCC tape. The adhesive is formulated to be tack-free or low-tack in ambient conditions, facilitating handling and minimising dust pickup, and then melt at moderate (≤60°C) temperatures, allowing low-pressure lamination at moderate temperatures.

During lamination, adhesives interact with the tape, and assist binding at low temperatures. The additional amount of organic material must be accounted for by somewhat lengthening the debinding step.

## 4. Materials limitations of LTCC

Fired LTCC material properties are typical of glass-ceramic materials (brittleness, relatively good thermal stability), and may be compared to thick-film multilayer dielectrics, from which they are derived.

#### 4.1. Mechanical strength

LTCC has somewhat lower short-term strength than alumina, of the order of 300 MPa, depending on the grade [111-114]. In sensitive mechanical structures such as low-range force and pressure sensors, this is offset by a much lower elastic modulus [113, 115], of the order of 100 GPa, yielding a comparable strain, i.e. resulting signal.

However, ceramics may be susceptible to stress corrosion in the presence of humidity, which must be accounted for in device design. This ageing behaviour is more severe in glassy ceramics such as LTCC than in standard 96% thick-film grade alumina, with glass-free materials such as yttria-stabilised zirconia (YSZ) and zirconia-toughened alumina (ZTA) essentially unaffected at ambient temperatures. To complicate matters, short- and especially long-term strength is affected by overlying thick-film materials, an effect that has yet to be studied on LTCC [112, 116, 117].

#### 4.2. Chemical durability

Whereas fired LTCC may be expected to be resistant to organic solvents, chemical durability in aqueous environments shows very strong variations: on the one hand, some materials (such as Du Pont 951) allow short-term operation ( $\approx 1$  day) of microreactors with aggressive chemicals such as HCl and NaOH at concentrations  $>1$  M. On the other hand, 3D structuration of LTCC using MSM was found to be hindered by degradation of LTCC in the relatively weak acetic acid used to dissolve the MSM [57]. Other studies also yielded very contrasting results, depending the LTCC material [118-120].

#### 4.3. Thermal stability & expansion

Essentially all common LTCC grades exhibit reasonable thermal stability up to ca. 500°C. Above this temperature, performance depends on the phase assemblage and chemical composition, with the more crystalline, essentially alkali-free materials exhibiting good mechanical stability and high resistivity at temperatures in excess of 600°C [115, 121]. This, together with the moderate thermal conductivity and CTE [113-115], allows creation of a wide range of hotplate structures (Table 2).

## 5. Conclusions

Due to its advantageous properties and relative ease of 3D structuration, LTCC has recently found wide appli-

cation in fluidic and/or heater structures. This trend is expected to intensify, due by advances in process technology and materials characterisation.

## References

1. R. Tummala, "Ceramics in microelectronic packaging", *Am. Ceram. Soc. Bull.* 67 (4), 752-758, 1988.
2. S. Nishigaki & J. Fukuta, "Low-temperature, cofirable, multilayered ceramics bearing pure-Ag conductors and their sintering behavior", *Advances in Ceramics : Ceramic Substrates and Packages for Electronic Applications* 26, 199-215, 1989.
3. C. J. Sabo, W. A. Vitriol, C. L. Slaton & D. L. Rychlick, "The use of low-temperature, cofired ceramic technology for the fabrication of high-density, hermetic, multicavity modules", *Advances in Ceramics : Ceramic Substrates and Packages for Electronic Applications* 26, 217-228, 1989.
4. M. Fukaya, T. Matsuo, S. Nishigaki & C. Higuchi, "Highly reliable and lead (Pb) free thick film resistor paste system for low thermal expansion LTCC application," 1997 International Symposium on Microelectronics, Philadelphia (USA), 1997.
5. R. Bauer, L. Rebenklau, M. Luniak & K. J. Wolter, "Mikrotechnische Applikationen mit der Dickfilmtechnik [Microtechnological applications with thick-film technology]," ISHM Deutschland Konferenz, München (DE), 1998.
6. J. J. Santiago-Avilès, M. R. Gongora-Rubio, P. Espinoza-Vallejos & L. Sola-Laguna, "Sensors, actuators and other non-packaging applications of LTCC tapes," IMAPS Conference, Ceramic Interconnect Technology, Denver (USA), 2004.
7. W. K. Jones, S. Kappagantula & J. Wang, "Micro channel fabrication in LTCC substrate," 1st International Conference on Ceramic Interconnect and Ceramic Microsystems Technologies (CICMT), Baltimore (USA), 2005.
8. K. A. Peterson, K. D. Patel, C. K. Ho, S. B. Rohde, C. D. Nordquist, C. A. Walker, B. D. Wroblewski & M. Okandan, "Novel microsystem applications with new techniques in low-temperature co-fired ceramics", *Int. J. Appl. Ceram. Tech.* 2 (5), 345-363, 2005.
9. H. Birol, T. Maeder, C. Jacq, G. Corradini, M. Boers, S. Straessler & P. Ryser, "Structuration and fabrication of sensors based on LTCC (low temperature co-fired ceramic) technology", *Key Engineering Materials, High Performance Ceramics IV* 336-338, 1849-1852, 2007.
10. H. Birol, "Fabrication of low temperature co-fired ceramic (LTCC) - based sensor and micro-fluidic structures," PhD, EPFL, Switzerland, 2007.

11. T. Maeder, Y. Fournier, S. Wiedmer, H. Birol, C. Jacq & P. Ryser, "3D structuration of LTCC / thick-film sensors and fluidic devices," 3<sup>rd</sup> International Conference on Ceramic Interconnect and Ceramic Microsystems Technologies (CICMT), Denver (USA), 2007.
12. W. Smetana, B. Balluch, G. Stangl, S. Lüftl & S. Seidler, "Fine structured channel arrays and bridging elements for LTCC - technology applications," *Microelectron. Reliab.* 49 (6), 592-599, 2009.
13. Y. Fournier, "3D structuration techniques of LTCC for microsystems applications," PhD, Laboratoire de Production Microtechnique, EPFL, Lausanne (CH), 2010.
14. L. E. Khoong, Y. M. Tan & Y. C. Lam, "Overview on fabrication of three-dimensional structures in multi-layer ceramic substrate," *J. Eur. Ceram. Soc.* 30 (10), 1973-1987, 2010.
15. U. Partsch, "Multilayertechnik für keramische MEMS [Multilayer technology for ceramic MEMS]," *Mikroproduktion* (6), 38-41, 2011.
16. T. Maeder, "Ceramic modules for sensors, fluidics & packages in harsh environments," *MEMS Technology Review* (8), 10-13, 2011.
17. U. Partsch, C. Lenz, S. Ziesche, C. Lohrberg, H. Neubert & T. Maeder, "LTCC-based sensors for mechanical quantities," *Journal of Microelectronics, Electronic Components and Materials* 42(4), 260-271, 2012.
18. T. Maeder, C. Jacq, I. Saglini, G. Corradini, S. Strässler, H. Birol & P. Ryser, "LTCC thermal gas viscometer – heater module," 4<sup>th</sup> European Microelectronics and Packaging Symposium (EMPS), Terme Čatež (SI), 2006.
19. T. Maeder, N. Dumontier, C. Jacq, G. Corradini & P. Ryser, "LTCC Gas-Viskositätssensor," IMAPS Deutschland Konferenz, München (DE), 2007.
20. C. Jacq, T. Maeder & P. Ryser, "Sensors and packages based on LTCC and thick-film technology for severe conditions," *SĀDHANĀ - Acad. Proc. Eng. Sci.* 34 (4), 677-687, 2009.
21. H. Birol, T. Maeder, I. Nadzeyka, M. Boers & P. Ryser, "Fabrication of a millinewton force sensor using low temperature co-fired ceramic (LTCC) technology," *Sens. Actuat. A* 134, 334-338, 2007.
22. C. Jacq, T. Maeder & P. Ryser, "Signal stability of LTCC cantilever force sensors," *Procedia Eng.* 25, 551-554, 2011.
23. D. Jurków & L. Golonka, "Application of design of the experiment in preliminary investigations on the end milling of low temperature co-fired ceramics," *Int. J. Appl. Ceram. Tech.*, in press, 2012.
24. G. Hagen, T. Kopp, S. Ziesche, U. Partsch & E. Ruprecht, "Combined 3D micro structuring of ceramic green tape using punching, embossing and laser processing," 8<sup>th</sup> International Conference on Ceramic Interconnect and Ceramic Microsystems Technologies (CICMT), Erfurt (DE), 2012.
25. K. H. Drüe & J. Müller, "UV-laser drilled  $\mu$ -vias in dielectric layers on LTCC as part of a build-up technology for high density interconnection," 5<sup>rd</sup> IMAPS / ACerS International Conference on Ceramic Interconnect and Ceramic Microsystems Technologies (CICMT), Denver (USA), 2009.
26. D. Jurków, K. Malecha, L. Golonka, G. Hagen, P. Petkov, J. Stiernstedt & M. Cristea, "Laser patterning of green ceramic tapes for 3D structures," XXXIII International Conference of IMAPS Poland Chapter, Gliwice – Pszczyna (PL), 2009.
27. J. Kita, A. Dziedzic, L. Golonka & A. Bochenek, "Properties of laser cut LTCC heaters," *Microelectron. Reliab.* 40 (6), 1005-1010, 2000.
28. K. Zaraska, B. Gröger, A. Bienkowski, P. Guzdek, M. Cież & W. Zaraska, "Investigation of machining parameters for laser patterning of LTCC conductive layers," XXXIII International Conference of IMAPS Poland Chapter, Gliwice – Pszczyna (PL), 2009.
29. X. Shan, K. M. Chua, Y. C. Soh & C. W. Lu, "Determining the optimal process conditions of micro roller embossing for large-area patterning of green ceramic substrates," *J. Micromech. Microeng.* 19 (1), 017001, 2009.
30. O. Shorina & J. Müller, "Improvement of ampacity of LTCC conductors," 8<sup>th</sup> International Conference on Ceramic Interconnect and Ceramic Microsystems Technologies (CICMT), Erfurt (DE), 2012.
31. K. Nowak, H. Baker & D. Hall, "Cold processing of green state LTCC with a CO<sub>2</sub> laser," *Appl. Phys. A* 84, 267-270, 2006.
32. R. E. B. Leminski, E. W. Simões, R. Furlan, M. R. Gongora-Rubio, Z. M. da Rocha, M. R. da Cunha, I. Ramos, N. I. Morimoto & J. J. Santiago-Aviles, "Development of microfluidic devices using LTCC substrates," 1<sup>st</sup> International Conference on Ceramic Interconnect and Ceramic Microsystems Technologies (CICMT), Baltimore (USA), 2005.
33. K. Malecha, T. Maeder, C. Jacq & P. Ryser, "Structuration of the low temperature co-fired ceramics (LTCC) using novel sacrificial graphite paste with PVA-propylene glycol-glycerol-water vehicle," *Microelectron. Reliab.* 51 (4), 805-811, 2011.
34. K. Malecha, T. Maeder & C. Jacq, "Fabrication of membranes and microchannels in low-temperature co-fired ceramic (LTCC) substrate using novel water-based sacrificial carbon pastes," *J. Eur. Ceram. Soc.* 32 (12), 3277-3286, 2012.
35. Y. Fournier, L.-S. Bieri, T. Maeder & P. Ryser, "Influence of lamination parameters on LTCC shrinkage under unconstrained sintering," 4<sup>th</sup> European Microelectronics and Packaging Symposium (EMPS), Terme Čatež (SI), 2006.

36. K. Malecha, D. Jurków, J. Stiernstedt & L. J. Golonka, "Influence of the latex binder type on alumina tapes lamination process," 8<sup>th</sup> International Conference on Ceramic Interconnect and Ceramic Microsystems Technologies (CICMT), Erfurt (DE), 2012.
37. D. Jurków & L. Golonka, "Low-pressure, thermo-compressive lamination," *J. Eur. Ceram. Soc.* 32 (10), 2431–2441, 2012.
38. A. Roosen, "New lamination technique to join ceramic green tapes for the manufacturing of multi-layer devices," *J. Eur. Ceram. Soc.* 21 (10-11), 1993-1996, 2001.
39. K. Schindler & A. Roosen, "Manufacture of 3D structures by cold low pressure lamination of ceramic green tapes," *J. Eur. Ceram. Soc.* 20 (5), 899-904, 2009.
40. N. Suppakarn, H. Ishida & J. D. Cawley, "Roles of poly(propylene glycol) during solvent-based lamination of ceramic green tapes," *J. Am. Ceram. Soc.* 84 (2), 289-294, 2001.
41. M. H. Wu, R. A. Yeller & V. Yang, "A low temperature co-fired ceramic burner for studying micro flames," 3<sup>rd</sup> International Conference on Ceramic Interconnect and Ceramic Microsystems Technologies (CICMT), Denver (USA), 2007.
42. D. Jurków & L. Golonka, "Novel cold chemical lamination bonding technique - a simple LTCC thermistor-based flow sensor," *J. Eur. Ceram. Soc.* 29 (10), 1971-1976, 2009.
43. K. Malecha, D. Jurków & L. J. Golonka, "Comparison of solvent and sacrificial volume-material-based lamination processes of low-temperature co-fired ceramics tapes," *J. Micromech. Microeng.* 19 (6), 065022, 2009.
44. M. H. Wu & P. S. Lin, "Design, fabrication and characterization of a low temperature co-fired ceramic gaseous bi-propellant microthruster," *J. Micromech. Microeng.* 20 (8), 085026, 2010.
45. T. Maeder, B. Jiang, F. Vecchio, C. Jacq, P. Ryser & P. Mural, "Lamination of LTCC at low pressure and moderate temperature using screen-printed adhesives," 8<sup>th</sup> International Conference on Ceramic Interconnect and Ceramic Microsystems Technologies (CICMT), Erfurt (DE), 2012.
46. Y. Fournier, T. Maeder, G. Boutinard-Rouelle, A. Barras, N. Craquelin & P. Ryser, "Integrated LTCC pressure / flow / temperature multisensor for compressed air diagnostics," *Sensors* 10 (12), 11156-11173, 2010.
47. M. F. Farhan Shafique, A. Laister, M. Clark, R. E. Miles & I. D. Robertson, "Fabrication of embedded microfluidic channels in low temperature co-fired ceramic technology using laser machining and progressive lamination," *J. Eur. Ceram. Soc.* 31 (13), 2199–2204, 2011.
48. H. Birol, T. Maeder, J. Jacq, S. Straessler & P. Ryser, "Fabrication of low-temperature co-fired ceramics micro-fluidic devices using sacrificial carbon layers," *Int. J. Appl. Ceram. Tech.* 2 (5), 364-373, 2005.
49. H. Birol, T. Maeder & P. Ryser, "Processing of graphite-based sacrificial layer for microfabrication of low temperature co-fired ceramics (LTCC)," *Sens. Actuat. A* 130-131, 560-567, 2006.
50. H. Birol, T. Maeder & P. Ryser, "Application of graphite-based sacrificial layers for fabrication of LTCC (low temperature co-fired ceramic) membranes and micro-channels," *J. Micromech. Microeng.* 17 (1), 50-60, 2007.
51. L. E. Khoong, Y. M. Tan & Y. C. Lam, "Carbon burn-out and densification of self-constrained LTCC for fabrication of embedded structures in a multi-layer platform," *J. Eur. Ceram. Soc.* 29 (3), 457-463, 2009.
52. P. Espinoza-Vallejos, J. Zhong, M. R. Gongora-Rubio, L. Sola-Laguna & J. J. Santiago-Aviles, "Meso (intermediate) - scale electromechanical systems for the measurement and control of sagging in LTCC structures," *Mater. Res. Soc. Symp. Proc.* 518, 73-79, 1998.
53. Y. Fournier, S. Wiedmer, T. Maeder & P. Ryser, "Capacitive micro force sensors manufactured with mineral sacrificial layers," 16<sup>th</sup> IMAPS European Microelectronics & Packaging Conference (EMPC), Oulu (FI), 2007.
54. C. Lucat, P. Ginet & F. Ménil, "New sacrificial layer based screen-printing process for free-standing thick-films applied to MEMS," *J. Microelectron. Electron. Pack.* 4 (3), 86-92, 2007.
55. Y. Fournier, O. Triverio, T. Maeder & P. Ryser, "LTCC free-standing structures with mineral sacrificial paste," 4<sup>th</sup> International Conference on Ceramic Interconnect and Ceramic Microsystems Technologies (CICMT), Munich (DE), 2008.
56. T. Maeder, C. Jacq, Y. Fournier, W. Hraiz & P. Ryser, "Structuration of thin bridge and cantilever structures in thick-film technology using mineral sacrificial materials," 5<sup>th</sup> International Conference on Ceramic Interconnect and Ceramic Microsystems Technologies (CICMT), Denver (USA), 2009.
57. T. Maeder, C. Jacq, Y. Fournier, W. Hraiz & P. Ryser, "Structuration of zero-shrinkage LTCC using mineral sacrificial materials," 17<sup>th</sup> IMAPS European Microelectronics & Packaging Conference (EMPC), Rimini (IT), 2009.
58. F. Vecchio, V. Venkatraman, H. R. Shea, T. Maeder & P. Ryser, "Dispensing and hermetic sealing Rb in a miniature reference cell for integrated atomic clocks," *Sens. Actuat. A* 172 (1), 330-335, 2011.

59. F. Seigneur, Y. Fournier, T. Maeder, P. Ryser & J. Jacot, "Hermetic package for optical MEMS", *J. Microelectron. Electron. Pack.* 6 (1), 32-37, 2009.
- [60. F. Seigneur, T. Maeder & J. Jacot, "Laser soldered packaging hermeticity measurement using metallic conductor resistance", *Electron Tech.* 37-38 (8), 1-4, 2006.
61. J. Leschik, A. Harasim & J. Müller, "Intelligent hermetically sealed LTCC Package with an integrated sensor system for avionics," 8<sup>th</sup> International Conference on Ceramic Interconnect and Ceramic Microsystems Technologies (CICMT), Erfurt (DE), 2012.
62. R. Blechschmidt, U. Lörcher, O. Hohlfeld, R. Müller & R. Werthschützki, "Piezoresistive sensors for medical applications," Tunisian-German Conference on Smart Systems, Hammamet, Tunisia, 2001.
63. T. Maeder, N. Dumontier, T. Haller, Y. Fournier, F. Seigneur & P. Ryser, "LTCC active oxygen getter module for hermetic packaging applications," 4<sup>th</sup> International Conference on Ceramic Interconnect and Ceramic Microsystems Technologies (CICMT), Munich (DE), 2008.
64. H. Lynch, J. Park, V. Espinoza, PA, A. Santiago, JJ & L. Solá, LM, "Meso-scale pressure transducers utilizing low temperature co-fired ceramic tapes", *Mater. Res. Soc. Symp. Proc.* 546, 177-182, 1999.
65. M. Santo Zarnik & D. Belavič, "Stability of a piezoresistive ceramic pressure sensor made with LTCC technology," 8<sup>th</sup> International Conference on Ceramic Interconnect and Ceramic Microsystems Technologies (CICMT), Erfurt (DE), 2012.
66. T. Maeder, B. Afra, Y. Fournier, N. Johner & P. Ryser, "LTCC ultra high isostatic pressure sensors," 16<sup>th</sup> IMAPS European Microelectronics & Packaging Conference (EMPC), Oulu (FI), 2007.
67. U. Partsch, D. Arndt, U. Keitel & P. Otschik, "Piezoelectric pressure sensors in LTCC-technology," 14<sup>th</sup> European Microelectronics and Packaging Conference, Friedrichshafen (DE), 2003.
68. D. Belavič, M. Santo Zarnik, M. Hrovat, M. Jerlah & S. Maček, "3D LTCC structure designed for the capacitive pressure sensors," XXXII International Conference of IMAPS Poland Chapter, Pułtusk (PL), 2008.
69. M. Santo Zarnik, D. Belavič & S. Maček, "Investigation of a thick-film capacitive pressure sensor in a three-dimensional LTCC structure," XXXIII International Conference of IMAPS Poland Chapter, Gliwice – Pszczyna (PL), 2009.
70. U. Partsch, D. Arndt & H. Georgi, "A new concept for LTCC-based pressure sensors," 3<sup>rd</sup> International Conference on Ceramic Interconnect and Ceramic Microsystems Technologies (CICMT), Denver (USA), 2007.
71. Y. Fournier, G. Boutinard-Rouelle, N. Craquelin, T. Maeder & P. Ryser, "SMD pressure and flow sensor for compressed air in LTCC technology with integrated electronics", *Procedia Chem.* 1, 1471-1474, 2009.
72. C. Jacq, T. Maeder, E. Haemmerle, N. Craquelin & P. Ryser, "Ultra-low pressure sensor for neonatal resuscitator", *Sens. Actuat. A* 172 (1), 135-139, 2011.
73. R. J. Tadaszak, A. Łukowiak & L. J. Golonka, "Optical pH sensor based on LTCC and sol-gel technologies," IMAPS - IEEE CPMT Poland Conference, Gdańsk-Sobieszewo (PL), 2011.
74. M. Czok, P. Bemnowicz & L. J. Golonka, "LTCC system for light absorbance measurement," 8<sup>th</sup> International Conference on Ceramic Interconnect and Ceramic Microsystems Technologies (CICMT), Erfurt (DE), 2012.
75. M. Czok, K. Malecha, M. Malawski & L. J. Golonka, "LTCC microfluidic chip with fluorescence based detection," IMAPS - IEEE CPMT Poland Conference, Gdańsk-Sobieszewo (PL), 2011.
76. U. Schmid, "A robust flow sensor for high pressure automotive applications", *Sens. Actuat. A* 97-98, 253-263, 2002.
77. Y. Fournier, R. Willigens, T. Maeder & P. Ryser, "Integrated LTCC micro-fluidic modules - an SMT flow sensor," 15<sup>th</sup> European Microelectronics and Packaging Conference (EMPC), Brugge (BE), 2005.
78. D. Jurków, K. Malecha & L. Golonka, "Three element gas flow sensor integrated with low temperature cofired ceramic (LTCC) module," 16<sup>th</sup> Mixed Design of Integrated Circuits and Systems (MIXDES), Łódź (PL), 2009.
79. D. Jurków, L. Golonka & H. Roguszczyk, "LTCC gas flow detector," 16<sup>th</sup> European Microelectronics & Packaging Conference (EMPC), Oulu (FI), 2007.
80. M. R. Gongora-Rubio, L. Solá-Laguna, P. J. Moffett & J. J. Santiago-Avilés, "The utilization of low temperature co-fired ceramics (LTCC-ML) technology for meso-scale EMS, a simple thermistor based flow sensor", *Sensors and Actuators* 73 (3), 215-221, 1999.
81. M. R. Gongora-Rubio, M. R. da Cunha, A. P. de Oliveira-Costa & M. I. Ré, "Preparation of polymeric microspheres by an emulsification / solvent diffusion process employing LTCC microfluidic structures," 1<sup>st</sup> International Conference on Ceramic Interconnect and Ceramic Microsystems Technologies (CICMT), Baltimore (USA), 2005.
82. M. R. da Cunha, M. R. Gongora Rubio, I. D. Alvim & M. I. Ré, "Fabrication and testing of a LTCC microfluidic serial dilution device," 4<sup>th</sup> International Conference on Ceramic Interconnect and Ceramic Microsystems Technologies (CICMT), Munich (DE), 2008.

83. T. Thelemann, M. Fischer, M. Groß & J. Müller, "LTCC-based fluidic components for chemical applications", *J. Microelectron. Electron. Pack.* 4 (4), 167-172, 2007.
84. M. R. da Cunha, A. C. Seabra & M. R. Gongora-Rubio, "LTCC 3D micromixer optimization for process intensification," 8<sup>th</sup> International Conference on Ceramic Interconnect and Ceramic Microsystems Technologies (CICMT), Erfurt (DE), 2012.
85. M. R. Gongora-Rubio, K. H. G. Freitas, J. de Novais-Schianti, A. M. de Oliveira, N. N. Pereira-Cerize & M. H. Ambrosio-Zanin, "Fab in a package: LTCC microfluidic devices for micro and nanoparticle fabrication," 8<sup>th</sup> International Conference on Ceramic Interconnect and Ceramic Microsystems Technologies (CICMT), Erfurt (DE), 2012.
86. V. Mengeaud, O. Bagel, R. Ferrigno, H. H. Girault & A. Halder, "A ceramic electrochemical microreactor for the methoxylation of methyl-2-furoate with direct mass spectrometry coupling", *Lab On A Chip* 1 (2), 9-44, 2002.
87. A. J. Vissotski, A. J. Moll & D. G. Plumlee, "Development of a continuous flow polymerase chain reaction device in low temperature co-fired ceramics," 5<sup>th</sup> IMAPS / ACerS International Conference on Ceramic Interconnect and Ceramic Microsystems Technologies (CICMT), Denver (USA), 2009.
88. R. Gorges, S. Meyer & G. Kreisel, "Photocatalysis in microreactors", *J. Photochem. Photobiol. A* 167, 95-99, 2004.
89. R. Willigens, "Microréacteur calorimétrique intégré en technologie céramique co-cuite à basse température (LTCC)," Masters, Université de Liège / EPFL, Liège (BE) / Lausanne (CH), 2005.
90. M. Schirmer, J. Uhlemann, L. Rebenklau, T. Bauer & K. J. Wolter, "3D-microfluidic reactor in LTCC," 31<sup>st</sup> International Spring Seminar on Electronics Technology - ISSE, Budapest (H), 2008.
91. M. McCrink & D. G. Plumlee, "Design and analysis of a low temperature co-fired ceramic micro-combustor," 5<sup>th</sup> International Conference on Ceramic Interconnect and Ceramic Microsystems Technologies (CICMT), Denver (USA), 2009.
92. Y. Shin, O. Kim, J. C. Hong, J. H. Oh, W. J. Kim, S. Haam & C. H. Chung, "The development of micro-fuel processor using low temperature co-fired ceramic (LTCC)", *Int. J. Hydrogen Ener.* 31 (13), 1925-1933, 2006.
93. D. Belavič, M. Hrovat, G. Dolanc, S. Hočevar, I. Stegel, M. Santo Zarnik, J. Holc, K. Makarovič, J. Batista & P. Fajdiga, "Design and fabrication of a complex LTCC-based reactor for the production of hydrogen for portable PEM fuel cells," 7<sup>th</sup> International Conference on Ceramic Interconnect and Ceramic Microsystems Technologies (CICMT), San Diego (USA), 2011.
94. R. K. Yamamoto, P. B. Verdonck & M. R. Gongora-Rubio, "Meso-scale remote plasma generator using LTCC technology," 1<sup>st</sup> International Conference on Ceramic Interconnect and Ceramic Microsystems Technologies (CICMT), Baltimore (USA), 2005.
95. H. Teterycz, J. Kita, R. Bauer, L. J. Golonka, B. W. Licznernski, K. Nitsch & K. Wisniewski, "New design of an SnO<sub>2</sub> gas sensor on low temperature cofiring ceramics", *Sens. Actuat. B* 47 (1-3), 100-103, 1998.
96. R. Moos & J. Kita, "Ceramic multilayer gas sensors - an overview," XXXI International Conference of IMAPS Poland Chapter, Krasiczyn (PL), 2007.
97. S. N. Reddy, J. Wang & W. K. Jones, "Development of a low-power 700°C micro heater in low temperature cofire ceramics," 15<sup>th</sup> European Microelectronics and Packaging Conference (EMPC), Brugge (BE), 2005.
98. W. Missal, J. Kita, E. Wappler, F. Gora, A. Kipka, T. Bartnitzek, F. Bechtold, D. Schabbel, B. Pawlowski & R. Moos, "Miniaturized ceramic differential scanning calorimeter with integrated oven and crucible in LTCC technology", *Sens. Actuat. A* 172 (1), 21-26, 2011.
99. F. Vecchio, T. Maeder, C. Slater & P. Ryser, "Effects of thermal losses on the heating of a multifunctional LTCC module for atomic clock packaging", *Solid State Phenom.* 188, 244-249, 2012.
100. R. K. Chutani, S. Galliou, N. Passilly, C. Gorecki, A. Sitomaniemi, M. Heikkinen, K. Kautio, A. Keränen & A. Jornod, "Thermal management of fully LTCC-packaged Cs vapour cell for MEMS atomic clock", *Sens. Actuat. A* 174, 58-68, 2012.
101. B. Jiang, P. Mural, T. Maeder, P. Heeb, A. J. S. Alvarez, M. Nabavi, D. Poulikakos & P. Niedermann, "Design, fabrication and characterization of a gas processing unit testing platform for micro-solid oxide fuel cells", *Procedia Eng.* 25, 811-814, 2011.
102. T. Maeder, B. Jiang, Y. Yan, P. Ryser & P. Mural, "Ceramic modules for micro solid-oxide fuel cells," 7<sup>th</sup> International Conference on Ceramic Interconnect and Ceramic Microsystems Technologies (CICMT), San Diego (USA), 2011.
103. R. Krpoun, "Micromachined electro-spray thrusters for spacecraft propulsion," PhD, EPFL, Lausanne (CH), 2009.
104. T. Maeder, Y. Fournier, J. B. Coma, N. Craquelin & P. Ryser, "Integrated SMD pressure/flow/temperature multisensor for compressed air in LTCC technology: Thermal flow and temperature sensing", *Microelectron. Reliab.* 51 (7), 1245-1249, 2011.
105. D. Kellis, A. Moll & D. Plumlee, "Effects of silver paste application on embedded channels in low temperature co-fired ceramics", *J. Microelectron. Electron. Pack.* 6 (1), 54-58, 2009.

106. T. W. Towner & D. G. Plumlee, "Design and fabrication of LTCC catalyst chambers," 7<sup>th</sup> International Conference on Ceramic Interconnect and Ceramic Microsystems Technologies (CICMT), San Diego (USA), 2011.
107. J. Thakur, R. Pratap, Y. Fournier, T. Maeder & P. Ryser, "Realization of a solid-propellant based micro-thruster using low temperature co-fired ceramics", *Sens. Transduc.* 117 (6), 29-40, 2010.
108. T. Maeder, C. Jacq, Y. Fournier & P. Ryser, "Formulation and processing of screen-printing vehicles for sacrificial layers on thick-film and LTCC substrates," XXXII International Conference of IMAPS Poland Chapter, Pułtusk (PL), 2008.
109. H. Birol, T. Maeder & P. Ryser, "Preparation and application of minerals-based sacrificial pastes for fabrication of LTCC structures," 4<sup>th</sup> European Microelectronics and Packaging Symposium (EMPS), Terme Čatež (SI), 2006.
110. C. B. Sippola & C. H. Ahn, "A thick film screen-printed ceramic capacitive pressure microsensor for high temperature applications", *J. Micromech. Microeng.* 16 (5), 1086-1091, 2006.
111. W. K. Jones, Y. Liu, B. Larsen, P. Wang & M. Zampino, "Chemical, structural and mechanical properties of the LTCC tapes", *J. Microelectron. Electron. Pack.* 23 (4), 469-473, 2000.
112. T. Maeder, H. Birol, C. Jacq & P. Ryser, "Strength of ceramic substrates for piezoresistive thick-film sensor applications," European Microelectronics and Packaging Symposium, Prague (CZ), 2004.
113. D. Belavič, M. Hrovat, M. Santo Zarnik, J. Cilenšek, J. Kita, L. J. Golonka, A. Dziedzic, W. Smetana, H. Homolka & R. Reicher, "Benchmarking different substrates for thick-film sensors of mechanical quantities," 15<sup>th</sup> European Microelectronics and Packaging Conference (EMPC), Brugge (BE), 2005.
114. K. Makarovič, A. Meden, M. Hrovat, J. Holc, A. Benčan & A. Dakskobler, "The effect of phase composition on the mechanical and thermal properties of LTCC material", *J. Am. Ceram. Soc.* 95 (2), 760-767, 2012.
115. M. Unger, W. Smetana, T. Koch & G. Radosavljevic, "High temperature characteristics of various LTCC-tapes," XXXIII International Conference of IMAPS Poland Chapter, Gliwice – Pszczyna, Poland, 2009.
116. T. Maeder, C. Jacq, G. Corradini & P. Ryser, "Effect of thick-film materials on the mechanical integrity of high-strength ceramic substrates," 15<sup>th</sup> European Microelectronics and Packaging Conference (EMPC), Brugge (BE), 2005.
117. T. Maeder, C. Jacq & P. Ryser, "Long-term mechanical reliability of ceramic thick-film circuits and mechanical sensors under static load", *Sens. Actuat. A*, in press, DOI 10.1016/j.sna.2012.05.031, 2012.
118. L. Rebenklaus, J. Uhlemann, M. Thummler & K. J. Wolter, "Biological characteristics of commercial low temperature cofiring ceramics," 14<sup>th</sup> European Microelectronics and Packaging Conference, Friedrichshafen (DE), 2003.
119. A. Bittner & U. Schmid, "Permittivity of LTCC substrates porousified with a wet chemical etching process", *Procedia Eng.*, 2010.
120. W. Zhang & R. E. Eitel, "Biostability of LTCC materials for microfluidics and biomedical devices", *Int. J. Appl. Ceram. Tech.* 9 (1), 60-66, 2012.
121. C. Bienert & A. Roosen, "Characterization of material behavior of low temperature cofired ceramics at elevated temperatures", *J. Eur. Ceram. Soc.* 30 (2), 369-374, 2010.

Arrived: 14. 08. 2012

Accepted: 06. 11. 2012

# Cofired Platinum /Alumina Microsystems for Implantable Medical Applications

Ali Karbasi, W. Kinzy Jones

Department of Mechanical and Material Engineering, Florida International University,  
 Miami, FL, USA

**Abstract:** With the desire for reduction in size and increased requirements for higher input/output (I/O) for implantable microsystems, cofired platinum/ high temperature alumina cofire ceramic (HTCC) is emerging as a technology of choice due to the long reliable history of Pt wire /alumina ceramics use as feedthrough structures in pacemakers. The new developments require the development of brazing processes to attach a titanium seal ring to develop a hermetic enclosure and feedthrough requirements into the hundreds of I/Os for neurostimulator applications. This work evaluates the development of a cofired Pt/Alumina materials system, including interconnects and high density via structures. Reactions previously unreported have been investigated, including the catalytic reaction with organic binders, the reduction of alumina with platinum into PtAl<sub>3</sub> and the reduction of the melting point of platinum 3000 C below its melting point, independent of the particle size (nano to micron size particles) or particle morphology. Firing atmosphere (air, hydrogen, inert), firing profiles and additives to control thermal expansion was evaluated to minimize exothermic reaction using high temperature X-ray diffraction, FIB nano-machining, SEM with EDS analysis and TEM for each of these conditions.

**Key words:** High density feedthrough, HTCC, cofired platinum- alumina

## Žgani mikrosistemi platina/aluminijev oksid za implantacijske medicinske naprave

**Povzetek:** Z zahtevami po zmanjševanju velikosti in povečevanju vhodno/izhodnih (I/O) zahtev implantacijskih naprav se je, zaradi že dolgo uporabljene keramike z žico iz platine / aluminijevim oksidom v vzpodbujevalcih srca, pojavila možnost uporabe žgane platine / žgane keramike z visokotemperaturnim aluminijevim oksidom. Nov razvoj zahteva uporabo procesa spajkanja titanovega tesnilnega obroča za izdelavo hermetičnega sistema s številnimi I/O prehodi za uporabo v nevrostimulatorjih. Delo ovrednoti razvoj žganih Pt/aluminijev oksid materialov skupaj s povezavami in veznimi strukturami visoke gostote. Še neobjavljene reakcije so raziskane skupaj s katalitično reakcijo organskih vezi, redukcijo Al oksida s platino v PtAl<sub>3</sub> in znižanjem točke taljenja platine 300°C pod njegovo točko talitve neodvisno od velikosti delcev (nano do mikro velikosti) ali morfologije delcev. Atmosfera žganja (zrak, vodik, inertni plin), profil žganja in aditivi za kontroliranje termičnega raztezanja so obravnavani v smislu minimiziranja eksotermične reakcije z uporabo visokotemperaturne difrakcije x-žarkov, FIB nano strojno obdelavo, SEM skupaj z EDS analizo in TEM za vsako od opisanih okoliščin.

**Ključne besede:** pretok visoke gostote, HTCC, žgana platina/aluminijev oksid

\* Corresponding Author's e-mail: jones@fiu.edu

### 1. Introduction

Platinum metallization is finding increases applications in implantable systems, especially in neural stimulator. Platinum has a long history as a conductor wire feedthrough materials for low input/output devices like pacemakers and implantable defibrillators or as feedthroughs and leads [1, 2] in higher output neural stimulator devices such as implantable cochlea, retinal implants and deep brain and muscle stimulators. Platinum is readily weldable and solderable, leading to easily second level assembly processes for micro-

electronic modules within the hermetic enclosure or attachment of micro lead structures. With the development of medical devices such as the implantable retina, the possibility of having I/O structures in the 300 to 1000 range is becoming a possibility. Additionally, neurological implants often require a much smaller device configuration footprint to minimize physiological interaction and external, RF coupled power coupling configurations to minimize the size of the device. As an example, the housing for one implantable retina under development is small enough to be attached to the eye to allow the microelectronics assembly to rotate with

eye movement. The combined demands of small size, high I/O count, hermeticity and biocompatibility has pushed the development of a new class of cofired platinum / alumina feedthrough, leads [3] and microcircuit structures with I/Os in excess of 40/mm<sup>2</sup>, gold brazed to a titanium housing which is welded to provide a hermetic enclosure capable of meeting the hermeticity requirement of  $1 \times 10^{-9}$  cc He/sec/atm, currently found in FDA approved medical devices [4, 5].

The bonding mechanism between platinum and alumina is believed to be by solid-state ceramic-metal diffusion bonding. However, despite different reaction mechanisms and products that have already been reported for the Pt/Al<sub>2</sub>O<sub>3</sub> system, the exact bonding mechanism between them is not clear [6-9].

The glass phase of the alumina-glass ceramic plays several important roles in ceramic/metal bonding. It anchors the metal to the ceramic by a combination of mechanical interlocking and chemical bonding and ensuring the hermeticity by filling the porosity in the metal [10]. During sintering of the substrate, a silica based liquid is formed between the alumina grains and penetrates the porous, fine-grained metallization layers. This occurs because of the capillary pressure difference between the porous alumina layer and the porous metal layer due to the smaller grain size of the latter and difference between their surface tension [11]. The contact angle of glass/ceramic is almost constant over the range of temperature and is about 30°. However, with refractory metals such as Mo and W, the contact angle of the glass/ metal interface decreases with increasing firing temperature in a hydrogen atmosphere [10-12]. The contact angle of glass/platinum does not change uniformly with temperature. It decreases with increasing the temperature up to about 1150° C and then increases. This change of behavior can be due to the change of surface properties of platinum with temperature [13]. This change of behavior can change the effect of the glass in metal/ ceramic binding.

Recently, Lu et al. [14] and Suppel et al. [15] showed that the strength of direct bonding Pt/Al<sub>2</sub>O<sub>3</sub> depends basically on the crystal orientation of platinum and alumina. When the orientation is suitable for semi-coherency, the interface has a strong driving force to adopt direct metal-ceramic bonding; when the orientation is not suitable for coherency, then a weaker metal-glass-ceramic bond is favored since the covalent bonds in the glass and alumina are more conducive to mutual bonding.

In the current paper, the effect of glass migration mechanism and effect of the via diameter are studied initially, then the evaluation of the pt/alumina reation

and effect of temperature on the microstructure and diffusion processes.

## 2. Experiments

Conventional high temperature cofired ceramics (HTCC) processing was used to develop the feedthrough [16]. 92% ceramic alumina tape (AdTech Ceramics Co.) and two different platinum powder, a spray dried and sintered Pt black platinum (Heraeus Inc. PM-100-10) and a spherical Pt (2 μm) from Alfa Asar were used as the primary materials. The inks were mixed on a Hoover Color Muller parallel plate mixer. The ceramic tape was punched with a Keko PAM mechanical punch machine and punched vias were filled with platinum ink by the means of a PTC vacuum assisted bladder filler. Filled tapes were stacked, isostatically laminated and fired up to the temperature range of 1050-1550° C in different atmosphere.

Shrinkage of platinum powder and ceramic alumina tape was measured by the Horizontal optical dilatometer Misura® ODLT. TA Q600 SDT machine was used to measure the colorimetric behavior of the platinum in high temperature. JEOL JSM-6330F FE/SEM was used to capture the secondary electron image of the samples. Siemens x-ray system with MoKa ( $\lambda = 0.71073\text{Å}$ ) radiation was used to measure the crystal structure of the samples. High temperature *in-situ* X-ray diffraction experimnts were conducted on the beam line B-2 ( $\lambda = 0.485946\text{Å}$ ) of the Cornell High Energy Synchrotron Source (CHESS). Diffracted x-rays were collected between Bragg angles of  $2\theta=5^\circ$  and  $2\theta=25^\circ$  using a MAR3450 imaging detector.

## 3. Results and Discussion

### 3.1. Effect of Heating Rate

Figure 1 showed the densification behavior of nano platinum and alumina tape with temperature with the heating rate of 5°C/min up to the temperature 1500 °C.

As it can be seen in about 1500 C the density of nano platinum increased about 35%, while alumina's was increased only about 17%. The high difference in densification and sintering kinetics of platinum and alumina could create defect like cracks and camber in the final multilayer assembly. However, densification behavior of the platinum and ceramic could be controlled by the heating rate. Basically higher densification can achieve by lowering the heating rate [17].

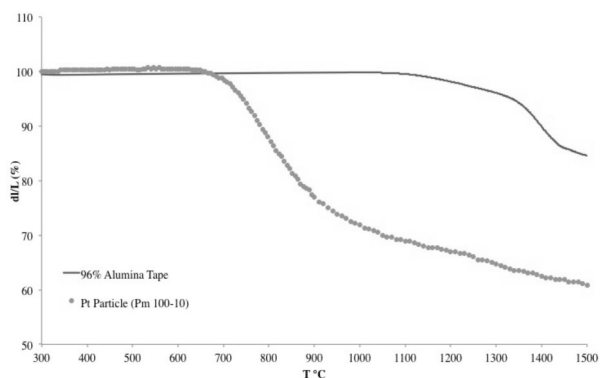


**Figure 1:** The nonisothermal densification behavior of platinum powder and alumina tape.

SEM images of feedthrough assembly fired in four different heating rates are showed in figure 2 and a summary of their densification results are also showed in table 1. Each measurement in the table 1 is the average of the 5 – 10 platinum via in one sample.

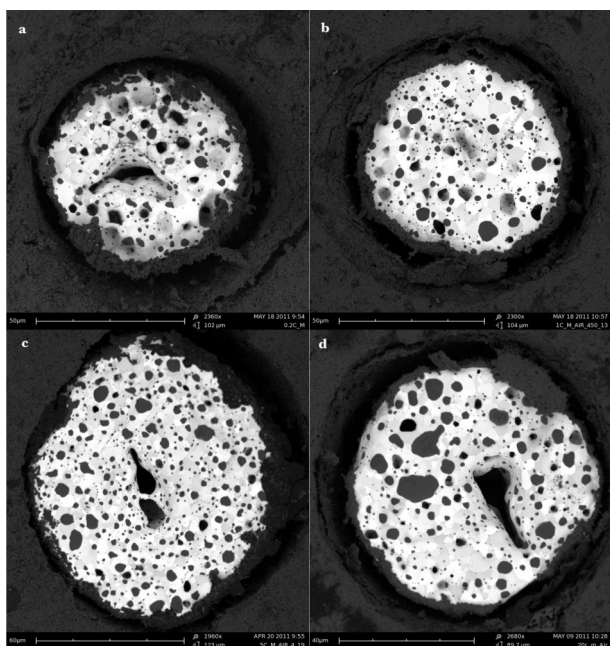


**Figure 2:** Backscatter SEM image of the platinum via fired in different heating rate. a) 0.2 °C/min, b) 1 °C/min, c) 5 °C/min and d) 20 °C/min.

As it can be seen in the pictures all of the four samples showed delamination of metal from ceramic and camber generation. Still, the results in table 1 showed that the minimum difference between platinum and alumina archived with the heating rate around 5 °C/min.

**Table 1:** Densification behavior of platinum and alumina in different heating rate.

Heating rate (°C/min)	Platinum (µm)	Alumina (µm)	Difference (µm)
<b>0.2</b>	64.068	86.891	22.822
<b>1</b>	66.287	87.707	21.42
<b>5</b>	68.36	82.37	14.01
<b>20</b>	69.775	88.043	18.268

Diameter of platinum via metallization is decreased by decreasing the heating, while we cannot see such behavior for alumina. Decreasing the heating rate increases the shrinkage of the alumina. On the other hand the interaction of platinum and alumina can increase the adhesion force between them. The strong metal support interaction that was observed several times in the platinum supported catalyst, could describe this interaction. Hwang et. al. [18] and Luo et. al. [19] showed that platinum aluminate (i.e.  $Pt_xAl_yO_z$ ) structure could be formed in the process of sintering Pt/Alumina mixture; in addition to that low heating rate can increase the diffusion of platinum to alumina and alumina to platinum and increase their physical adhesion. In result of such interaction, platinum tries to pull in alumina with itself. However the interaction force is not enough, which makes ceramic to tear apart in the interface area as it can be seen in the figure 2.

It should be noted, that the hole which can be seen in almost all of the samples could be attributed to the formation of volatile platinum oxide which is usually formed in temperatures above 650 °C [20].

### 3.2. Glass migration behaviour

As shown previously, camber developed in the via and the platinum delaminated from the ceramic wall due to the difference in densification behavior of metal and ceramic tape. In the sintering process of alumina-glass ceramic, the melting of glass enhances the sintering of alumina at lower temperatures due to liquid phase sintering. The flux of glass from the alumina to refractory metals increases the adhesion of the metal/ceramic joint. In contrast to refractory metals, in the Pt/glass system, due to the complex surface tension behavior, increasing the temperature increases the flow of glass at first but the decrease in the Pt/glass surface tension decreases the flow and causes the separation of the glass from the Pt as shown in figure 2.

Point 3 in figure 3 shows the average composition of the via. It is mostly occupied with platinum and has aluminum, carbon and oxygen as impurity. Presence of carbon could be attributed to an incomplete burn-out

process. Aluminum and oxygen could be from the diffusion of alumina in the platinum in high temperature. However, the presence of all three elements could also be due environmental contamination and experimental error.

The elemental analyses of point 1 and 2 indicated the presence of Si, Mg and Ca in addition to Pt, Al, C and O. This elemental composition implies the formation of the glass on the surface of platinum via. Glass particles usually have the flake-like structure with the average size of 10-20  $\mu\text{m}$ , but the glass particles shown in figure 3 have spherical shape with size of 5  $\mu\text{m}$ . This indicates the melting of glass at high temperatures. At high temperatures, melted glass failed to wet the platinum and floated to the surface of the via, and solidified into the spherical shape in the cooling process. In the cool down process, the temperature of the surface of platinum is less than the bulk. This temperature gradient could differentiate the glass/metal surface tension and produces capillary force to push the molten glass out of the metal. This mechanism can explain the formation of glass on the top surface of platinum via.

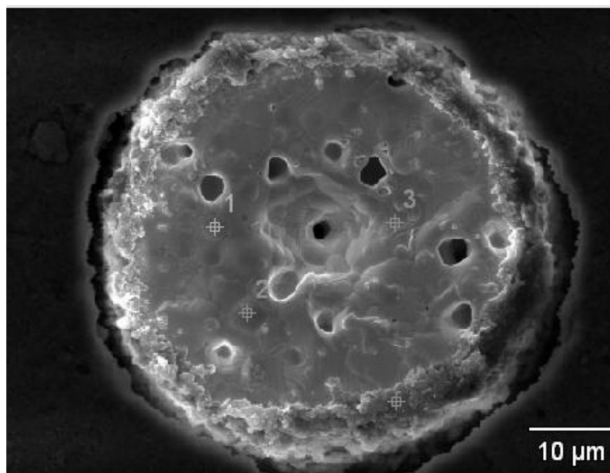


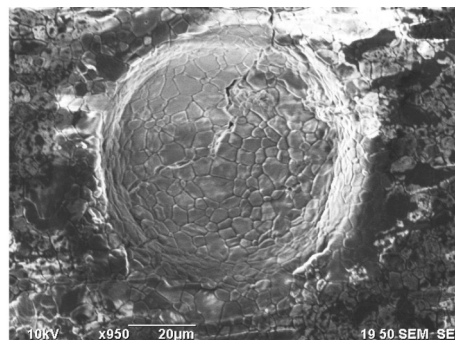
**Figure 3:** Backscatter image of Platinum Feedthrough fired in Air

### 3.3. Via diameter

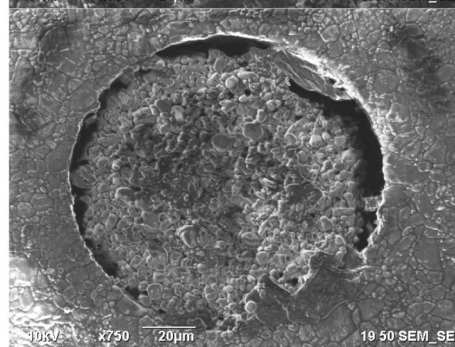
Similar to glass particles, metal oxide materials, such as alumina powder, which are used to decrease the shrinkage of the ink, could also migrate to the surface of the via due to the capillary force. This migration increases by increasing the aspect ratio of the via. Via diameter could control the migration of the light oxide material to the surface since increasing the via diameter decreases aspect ratio. Results of the application of 20% volume fraction of  $\text{Al}_2\text{O}_3$  in the platinum ink, for the vias with different diameters fired in air atmosphere, are shown in figure 4.

As depicted in the figure 4, increasing the via diameter decreases the migration of the oxide to the surface. The surface of the 100  $\mu\text{m}$  via diameter completely covered with recrystallized ceramic. The EDS results show that the ceramic has the composition of the alumina.

100  $\mu\text{m}$



150  $\mu\text{m}$



250  $\mu\text{m}$

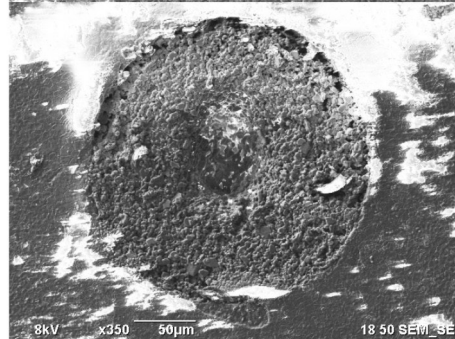


**Figure 4:** Microstructures of Platinum via with, 20%  $\text{Al}_2\text{O}_3$  in different via size

### 3.4. Effect of Atmosphere

Atmosphere condition is the most important factor to control the interface of platinum and alumina. In addition to that replacing air with neutral atmosphere, such as argon, could eliminate evaporation of platinum. SEM image of sample fired in the air and Ar atmosphere with heating rate of 5  $^\circ\text{C}/\text{min}$  are showed in figure 5.

As it can be seen that platinum densified in Ar more than air. This behavior of platinum could be attributed to the decomposition of platinum dioxide and desorption of oxygen from the bulk of platinum. This oxygen layer is adsorbed on the layer of platinum below the surface and it is almost inert in temperature below 800

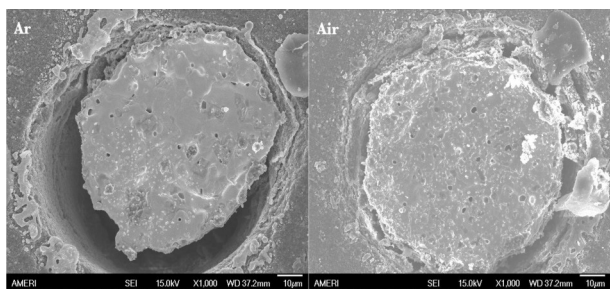


**Figure 5:** Secondary electron SEM image of feedthrough fired in air and argon atmosphere.

°C [21]. The results of DSC experiments of sintering of platinum are shown in figure 6. The colorimetric experiment followed the same condition was used in firing of feedthrough. As it can be seen, the exothermic reaction of decomposition occurred around 1000 – 1200°C. Heat generation in neutral atmosphere is more than air, which could result in local super heating in sample and increase the shrinkage of the platinum.

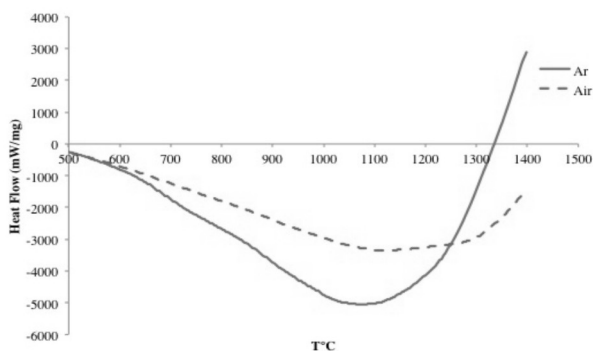


**Figure 6:** DSC analyses of the platinum powder in air and argon.

### 3.5. Pt/Alumina reaction

The reaction of Pt/Al<sub>2</sub>O<sub>3</sub> could be enhanced in a reduced atmosphere due to Pt-Al alloy formation [15, 22]. Hydrogen can reduce alumina and the major product of this reaction is Pt<sub>3</sub>Al. The X-ray diffraction pattern

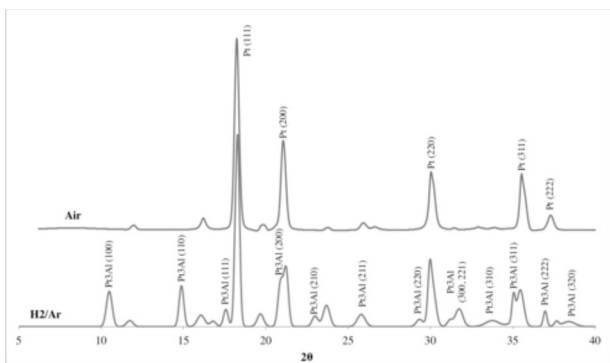


**Figure 7:** X-ray diffraction pattern of Platinum/ Alumina combination heated in two different environments in 1400°C

of reaction of the 25% Vol. powder mixture of alumina/platinum in the hydrogen and air atmosphere in 1400°C is shown in figure 7.

As is seen from figure 7, the first peak of Pt<sub>3</sub>Al appeared in 2θ=10.40° in a hydrogen atmosphere, which indicates the reaction between platinum and alumina. To better understand the reaction of Pt/Alumina, a high temperature X-ray diffraction technique was utilized, using carbon as reducing agent. The result of the reaction of Pt/Alumina in the presence of carbon is shown in figure 8.

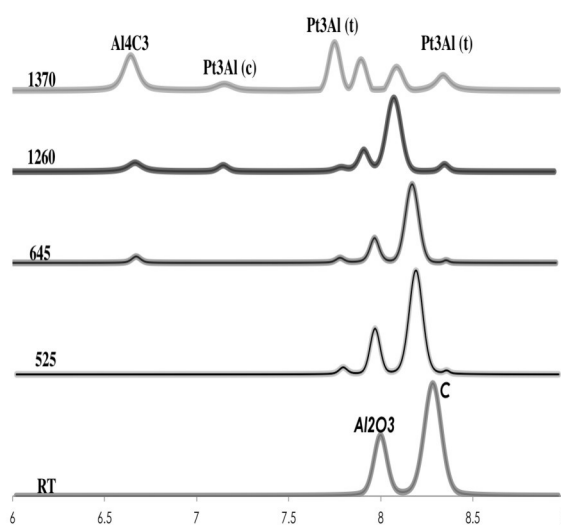


**Figure 8:** High temperature diffraction data of Pt/Alumina system

The first two peaks in 2θ=7.77° and 8.35° appeared at the temperature about 530 °C. Those peaks are related to tetragonal Ir<sub>3</sub>Si structure. Pt<sub>3</sub>Al in temperatures lower than 400 °C exhibit a tetragonal crystal structure [23]. By increasing the temperature up to 650 °C, another peak appeared at 2θ=6.65°. That peak is attributed to the formation of rhombohedral structure of aluminum carbide [24]. In the temperature above 1250 °C, a new peak appeared at 2θ=7.15°, which corresponds to the cubic Pt<sub>3</sub>Al structure. The Ir<sub>3</sub>Si tetragonal structure could transform to cubic Cu<sub>3</sub>Al easily. The Pt<sub>3</sub>Al was formed with the tetragonal structure at low temperature and the crystal structure transformed to the cubic structure at high temperatures. From the results showed in figure 7, the equilibrium structure of the Pt<sub>3</sub>Al is cubic, with sufficient amount of time and hydrogen concentration, the tetragonal structure transforms completely to the cubic structure.

A common firing profile consists of heating and soaking in temperature below 450 °C to burn-out the organic. During this portion of the profile, polymeric binder produces a fair amount carbon, which could

evaporate from the sample. Different burn-out process could change the carbon evaporation behavior and subsequently change the possibility of the reaction in platinum/carbon/alumina system. The results of firing of platinum feedthrough with two different burn-out process is shown in figure 9.

It could be seen that the thickness of ceramic layer around platinum decreases with increasing the time of burn-out process. Fast burn-out process could decrease the evaporation of the carbon from the system and increase the reaction between platinum and alumina.

TEM image of the platinum/alumina interface showed in figure 10. The interface shows strong bonding between platinum and alumina, which is due to the reduction reaction of alumina and formation of  $PtAl_3$ .

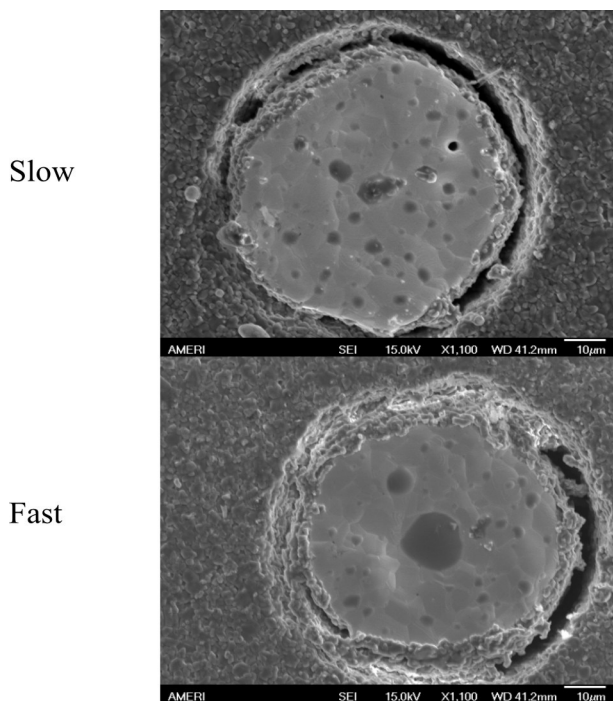


**Figure 9:** SEM image of the platinum particle via fired in different burn-out processes

### 3.6. Firing temperature

In addition to the reaction products, temperature could control the final microstructure of the feedthrough sample as well. The effect of firing temperature on the properties of the Pt-100-10 nano platinum powder feedthrough in a reduced atmosphere is given in figures 11. After the burn-out process, each feedthrough was heated up to the desired temperature at the heating rate of 10 °C/min, maintained at that temperature for an hour and was rapidly cooled down. Firing was done in the  $H_2 - Ar$  (25-75) atmosphere.

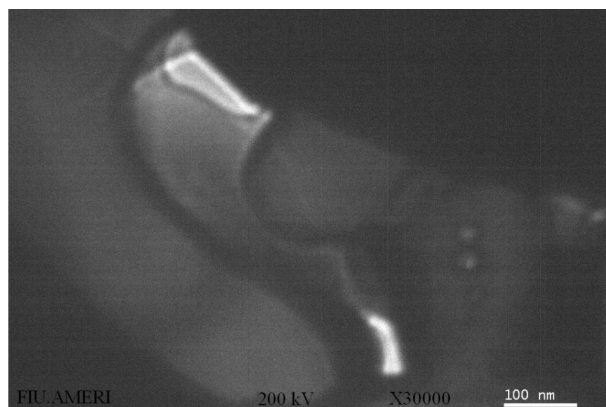


**Figure 10:** TEM image of the interface between platinum and alumina via fired ceramic particle.

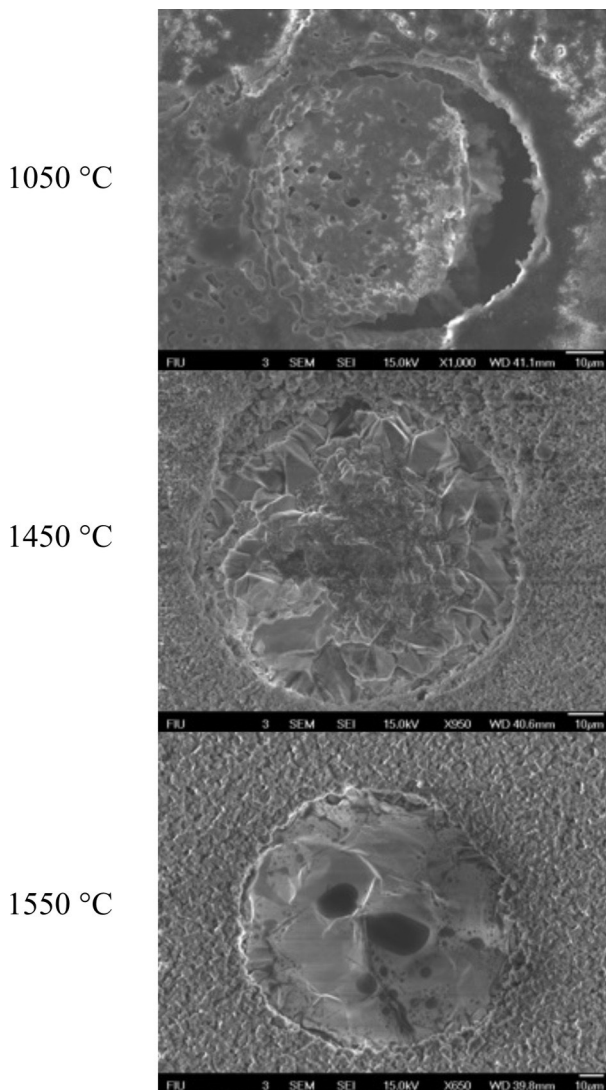


**Figure 11:** SEM image of the platinum particle via fired in different temperature

The behavior of platinum powders starts to change after the temperature reaches 1350 °C. In the range of 1350 – 1550 °C, by increasing the temperature, platinum starts

to expand and fill the via. In the temperature range of 1350 – 1450 °C, a coating of alumina covers the surface. In this temperature range, platinum dissolves some of the ceramic from the sidewalls and the alumina is transported to the top surface. At 1450 °C, the alumina covers the surface completely with a large grain structure. At the highest temperature, platinum completely dissolves the ceramic and there is no sign of it on the surface. A large droplet shape ceramic also appears on top of the platinum via, but it does not have a grain structure. The ceramic structure is more like a solidified glass, which was confirmed from the EDS results.

The results of the micro-sized platinum powder feedthrough fired in 1550 °C in the same condition is showed in figure 12 for comparison.

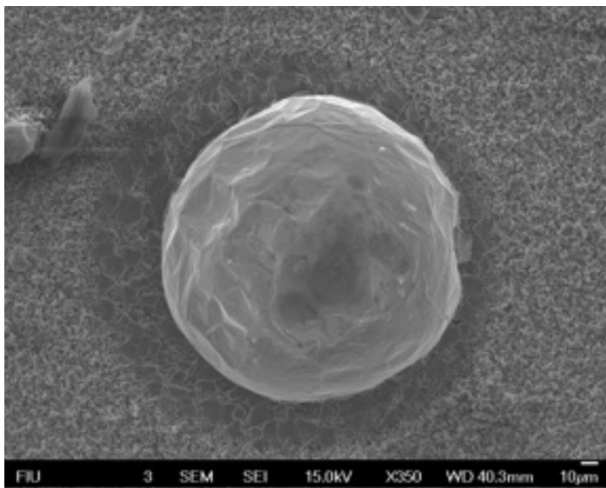


**Figure 12:** SEM image of the micron-sized platinum particle feedthrough via fired in 1550°C

By increasing the platinum particle size, platinum starts to expand and ultimately makes a dome-like structure above the via. As is seen from figure 12, the ceramic around the platinum disappears and creates a recessed structure. At 1550 °C, the platinum via is 150 µm in diameter and the recessed area around the platinum increased up to 200 µm. Platinum dissolves alumina and glass from the surrounding area and expands. By the introduction of alumina and glass particles into platinum, platinum starts to expand up to 150 µm and creates a dome structure. Platinum powder dissolves alumina at high temperatures, however, different final microstructure of the two platinum particles could suggest that smaller size particles wicks the alumina and push it to the top surface by capillary action.

Figure 13 shown the concentration gradient of different elements in platinum for the micron-sized platinum powder via fired at 1550 °C, determined by EDS analyses. It is obvious that silicon diffuse through the entire width of the via. The weight concentration of the

silicon is almost constant and is about 3.5%. Pt-Si phase diagram [25] does not show any solid solution of silicon in platinum. Therefore, the 3.5% concentration of silicon in platinum suggests the reaction of SiO<sub>2</sub> with platinum and the creation of a Pt<sub>3</sub>Si phase. Silicate compounds, which are used mostly as the glass phase in HTCC ceramic tape formulation, could be the source of SiO<sub>2</sub> for reaction. Aluminum is found in the first few microns from the interface. The concentration of aluminum in platinum is about 1.5 Wt.%, which is equal to the solubility of aluminum into platinum [26]. After about 8 microns from the interface, the concentration of the alumina dropped drastically and it is almost negligible. This behavior could suggest that silicon prevents diffusion of aluminum into platinum.

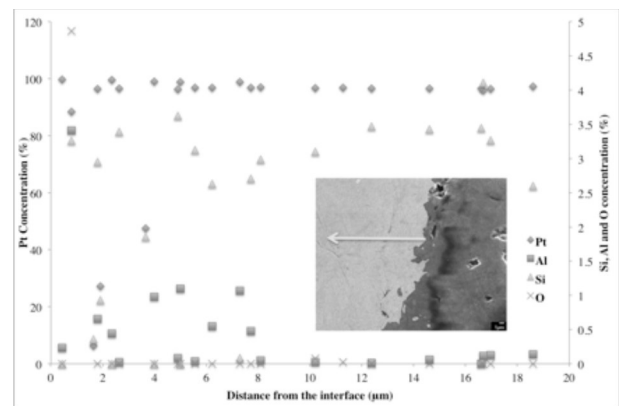


**Figure 13:** Concentrations gradient of different elements in platinum for the micron-sized platinum powder. Feedthrough fired in the H<sub>2</sub> – Ar (25-75) atmosphere at 1550 °C

To minimize the effect of silicon on the diffusion of the aluminum, the 99.9% HTCC ceramic tape were use to develop a feedthrough and the concentration gradient of different elements are shown in figure 14.

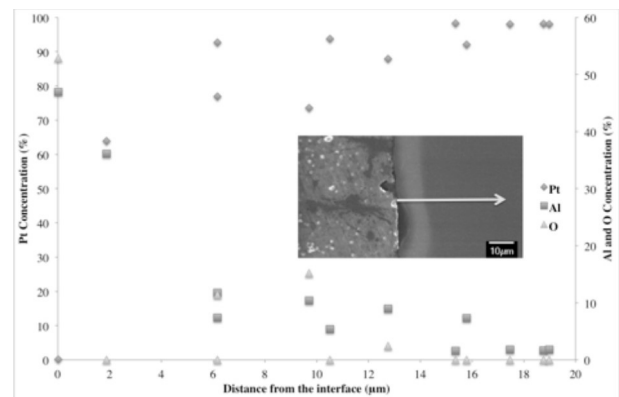


**Figure 14:** Concentration gradient of different element in platinum for the micron-sized platinum powder and 99.9% HTCC ceramic tape. Feedthrough fired in the H<sub>2</sub> – Ar (25-75) atmosphere at 1550 °C

It is clear that the concentration of the aluminum gradually decrease, however the final concentration is about 5 Wt%, which is more than the solubility limit of the aluminum in platinum. This behavior promotes the formation of Pt<sub>3</sub>Al phase. The concentration of oxygen shown in Figure 7 and 8 is almost zero in all cases, which is due to the reduction of alumina and silica in the reduced atmosphere. It should be noted that the EDS does not show any trace of platinum in alumina, which indicates that diffusion only occurs from the alumina side to the platinum.

At high temperatures, platinum absorbs the ceramic grains and glass from the sidewalls and that expands the structure. Platinum dissolves silicon and cannot maintain the solubility of the aluminum, thus the aluminum moves to the surface as alumina. Based on the temperature, alumina could recrystallize to large grains or small grain size. However, at temperatures above 1500 °C, it dissolves into the platinum and remains as a reaction product. This could be due to the formation of a Pt-Al compound as a second phase in the platinum-alumina interface.

#### 4. Conclusion

The results of firing of feedthrough assembly in different conditions showed that glass migration mechanism is complicated in Pt/Al<sub>2</sub>O<sub>3</sub> system and glass is not very useful in improving the metal/ceramic joint. Introducing some metal oxide powder as a shrinkage control agent to the formulation of the platinum ink also could improve the sintering kinetics of platinum and improve the properties of feedthrough assembly. However, the oxide material could float to the surface of the via. Decreasing the via diameter increases the migration of the ceramic powder to the top surface of the via. Mixture of hydrogen and argon is the best possible environment for firing the feedthrough. In addition to that, Pt/alumina mixture starts to react in temperature as low as 550 °C. The tetragonal Pt<sub>3</sub>Al forms in low temperature and transforms to the stable cubic structure in high temperature. In reduced atmospheres, the firing temperature could be adjusted by the size of platinum particle. Larger platinum particles could be fired in temperatures lower than 1550 °C.

#### Acknowledgements

The authors acknowledge the Advanced Materials Engineering Research Institute (AMERI) at FIU for SEM and DSC analysis. Funding is acknowledged from MIT subaward 5710002662 and Florida International Uni-

versity Graduate School, Dissertation Evidence Acquisition Fellowship (DEA). Part of this work is based upon research conducted at the Cornell High Energy Synchrotron Source (CHESS), which is supported, by the National Science Foundation and the National Institutes of Health/National Institute of General Medical Sciences under NSF award DMR-0936384.

#### References

1. Brummer S, Turner M. Electrochemical considerations for safe electrical stimulation of the nervous system with platinum electrodes. *Biomedical Engineering, IEEE Transactions on.* 1977(1):59-63.
2. Schuettler M, editor. *Electrochemical properties of platinum electrodes in vitro: comparison of six different surface qualities* 2007: IEEE.
3. Suaning G, Lavoie P, Forrester J, Armitage T, Lovell N, editors. *Microelectronic retinal prosthesis: III. A new method for fabrication of high-density hermetic feedthroughs* 2006: IEEE.
4. Guenther T, Dodds C, Lovell N, Suaning G, editors. *Chip-scale hermetic feedthroughs for implantable bionics* 2011: IEEE.
5. Karbasi A, Kinzy Jones W, editors. *Evaluation of cofired platinum/alumina high density feedthrough for implantable neurostimulator applications. 18th European Microelectronics and Packaging Conference (EMPC); 2011 12-15 Sept. 2011; Brighton, UK: IEEE.*
6. Becher PF, Murday JS. Thick film adherence fracture energy: influence of alumina substrates. *Journal of Materials Science.* 1977;12(6):1088-94.
7. Allen RV, Borbidge WE. Solid state metal-ceramic bonding of platinum to alumina. *Journal of Materials Science* 1983;18:2835-43.
8. Panfilov P, Bochegov A, Yermakov A. The Transition Layer in Platinum-Alumina. *Platinum Metals Review.* 2004;48(2):47-55.
9. Ivanova AS, Slavinskaya EM, Gulyaev RV, Zaikovskii VI, Stonkus V, Danilova IG, et al. Metal-support interactions in Pt/Al<sub>2</sub>O<sub>3</sub> and Pd/Al<sub>2</sub>O<sub>3</sub> catalysts for CO oxidation. *Applied Catalysis B: Environmental.* 2010;97(1-2):57-71.
10. Lazaroff JE, Ownby PD, Weirauch DA. Wetting in an Electronic Packaging Ceramic System: 1, Wetting of Tungsten by Glass in Controlled Oxygen Partial Pressure Atmospheres. *Journal of the American Ceramic Society.* 1995;78(3):539-44.
11. Twentyman ME. High-temperature metallizing, Part 1. The mechanism of glass migration in the production of metal-ceramic seals. *Journal of Materials Science.* 1975;10(5):765-76.

12. Behrens G, Heuer AH. Microstructural Characterization of Cofired Tungsten-Metallized High-Alumina Electronic Substrates. *Journal of the American Ceramic Society*. 1992;75(10):2815-24.
13. Selman GL, Spender MR, Darling AS. The Wetting of Platinum and Its Alloys By Glass I, Contact Angle Determination Between Glass and Pure Platinum. *Platinum Metals Review*. 1965;9(3):92-9.
14. Lu H, Svehla MJ, Skalsky M, Kong C, Sorrell CC. Pt-Al<sub>2</sub>O<sub>3</sub> interfacial bonding in implantable hermetic feedthroughs: Morphology and orientation. *Journal of Biomedical Materials Research Part B: Applied Biomaterials*. 2011:n/a-n/a.
15. Suppel KP, Forrester JS, Suaning GJ, Kisi EH. A Study of the Platinum/Alumina Interface. *Advances in Science and Technology*. 2006;45:1417-22.
16. Gangqiang W, Folk EC, Barlow F, Elshabini A. Fabrication of microvias for multilayer LTCC substrates. *Electronics Packaging Manufacturing, IEEE Transactions on*. 2006;29(1):32-41.
17. Bernard-Granger G, Guizard C, Addad A. Sintering of an ultra pure  $\alpha$ -alumina powder: I. Densification, grain growth and sintering path. *Journal of Materials Science*. 2007;42(15):6316-24.
18. Hwang CP, Yeh CT. Platinum-oxide species formed by oxidation of platinum crystallites supported on alumina. *Journal of Molecular Catalysis A: Chemical*. 1996;112(2):295-302.
19. Luo M-F, Ten M-H, Wang C-C, Lin W-R, Ho C-Y, Chang B-W, et al. Temperature-Dependent Oxidation of Pt Nanoclusters on a Thin Film of Al<sub>2</sub>O<sub>3</sub> on NiAl(100). *The Journal of Physical Chemistry C*. 2009;113(28):12419-26.
20. Jehn H. High temperature behaviour of platinum group metals in oxidizing atmospheres. *Journal of the Less Common Metals*. 1984;100(Journal Article):321-39.
21. Gland JL, Sexton BA, Fisher GB. Oxygen interactions with the Pt(111) surface. *Surface Science*. 1980;95(2-3):587-602.
22. Klomp J. Ceramic-metal reactions and their effect on the interface microstructure. *Ceramic microstructures '86: Role of interfaces; Proceedings of the International Materials Symposium; 28-31 July 1986; Berkeley, CA; UNITED STATES 1987*. p. 307-17.
23. Chauke HR, Minisini B, Drautz R, Nguyen-Manh D, Ngoepe PE, Pettifor DG. Theoretical investigation of the Pt<sub>3</sub>Al ground state. *Intermetallics*. 2010;18(4):417-21.
24. Foster LM, Long G, Hunter MS. Reactions Between Aluminum Oxide and Carbon The Al<sub>2</sub>O<sub>3</sub>—Al<sub>4</sub>C<sub>3</sub> Phase Diagram. *Journal of the American Ceramic Society*. 1956;39(1):1-11.
25. Tanner LE, Okamoto H. The Pt-Si (Platinum-Silicon) system. *Journal of Phase Equilibria*. 1991;12(5):571-4.
26. McAlister A, Kahan D. The Al-Pt (Aluminum-Platinum) system. *Journal of Phase Equilibria*. 1986;7(1):47-51.

Arrived: 21. 08. 2012

Accepted: 13. 11. 2012

# *Mechanical Properties of Low Temperature Co-fired Ceramics: Testing Methodologies for Strength Characterization*

*Raul Bermejo*

*Montanuniversität Leoben, Institut für Struktur- und Funktionskeramik, Leoben, Austria*

**Abstract:** Functional components such as multilayer Low Temperature Co-fired Ceramics (LTCC) are examples of combination of a ceramic-based substrate with internal electrodes as well as surface features (e.g. metallization, contacting pads, cylindrical vias, etc) employed to provide the component with a given functionality. Due to miniaturization and design complexity, no standard methods for mechanical testing can be applied for component characterization. An experimental approach is here presented using the Ball-on-three-Balls (B3B) method, based on localized biaxial testing of metalized LTCC samples, at several locations under different environments, to quantify the effect of surface features or metallization (e.g. contacting pads or cylindrical vias) on the material strength distribution. Experimental findings show that the strength distribution of LTCC can be negatively affected by environmental degradation, where Subcritical Crack Growth (SCCG) phenomena can be enhanced in conditions of high relative humidity. In addition, metallization at the surface subjected to tensile stresses can even raise the strength of the component acting as a protective layer against environmental degradation, whereas cylindrical vias can become weak points in the design.

**Key words:** Functional ceramic components, Biaxial Strength, Fracture, Weibull Statistics, Environmental brittleness.

## *Mehanske lastnosti keramike z nizko temperaturo žganja: metodologije testiranja trdnosti*

**Povzetek:** Funkcionalne sestavine, kot je večplastna keramika z nizko temperaturo žganja (LTCC), so primeri kombinacij substratov na osnovi keramike in internih elektrod, kot tudi površinskih lastnosti (metalizacija, kontaktne blazinice, cilindrične povezave itd.), ki dajejo komponenti željeno funkcionalnost. Standardne metode testiranja mehanskih lastnosti, zaradi miniaturizacije in kompleksnosti oblik, niso primerne za karakterizacijo elementa. V članku je predstavljen je eksperimentalen postopek na osnovi Ball-on-three-Balls (B3B) metode, ki temelji na lokaliziranem dvoosnem testiranju metaliziranih LTCC vzorcev na različnih lokacijah in okoljih in je namenjen kvalifikaciji vpliva površinskih lastnosti ali metalizacije (kontaktne blazinice, cilindrične povezave) na porazdelitev sil v materialu. Rezultati poskusov so pokazali, da ima lahko degradacija zaradi okolja negativen vpliv na razporeditev sil LTCC. Pri visoki relativni vlažnosti se lahko pospeši rast razpok (Subcritical Crack Growth – SCCG). Dodatno lahko površinske natezne sile zaradi metalizacije izboljšajo čvrstost in delujejo kot zaščitni sloj pred vplivi okolja, pri čemer pa cilindrične povezave predstavljajo šibke točke v konstrukciji.

**Ključne besede:** funkcionalne keramične komponente, dvoosna sila, frakcije, Weibullova statistika, okoljska občutljivost.

\*Corresponding Author's e-mail: raul.bermejo@unileoben.ac.at

### *1. Introduction*

Many applications in microelectronics involve combinations of ceramic and metal constituents. Due to the different properties of the materials involved (e.g. thermal expansion coefficients, elastic constants, yield strength) components can be subject to internal stresses during fab-

rication, which may induce cracks that truncate the electrical performance of the device [1-4]. Other processes after fabrication (e.g. packaging) can also involve high tensile stresses which may damage the component. In addition, mechanical stresses occurring during service conditions (e.g. rapid temperature changes, mechanical vibration, bending) can affect the structural integrity of the device.

Functional components such as multilayer varistors (MLV), piezoelectric actuators (MPA), Low Temperature Co-fired Ceramics (LTCC) or semiconductors, among others, are examples of combination of a ceramic-based (or Si-based) substrate with internal electrodes as well as surface features (e.g. metallization, contacting pads, cylindrical vias, etc) employed to provide the component with a given functionality. For instance, LTCC consist of a complex three-dimensional micro-network of metal structures embedded within a ceramic substrate with a large content of glass. The low sintering temperature of the ceramics in LTCC (i.e. below 900 °C) can be achieved by using a glass matrix with a low melting point, allowing a vitrification of the glass ceramic composite material [5, 6]. This makes feasible the use of excellent electronic conductors such as silver, gold or mixtures of silver–palladium, arranged within and/or on the surfaces of the ceramic substrate, forming complex multi-layered structures. Today, they can be found in electronic devices (e.g. for mobile and automotive technologies) which have to operate under harsh conditions such as relatively high temperatures and mechanical shock under different environments.

A limiting factor for the lifetime of glass- and ceramic-based components is associated with the subcritical crack growth (SCCG) phenomenon, especially in environments with high moisture content [7-9]. The lifetime is thus related to their mechanical strength and crack growth resistance during service conditions. It is also known that metallization as well as surface features (such as contact pads or metal cavities) can affect the strength of components (see for instance [10-13]). In summary, a combined effect of environmental degradation and geometry features can decrease the strength of brittle functional components.

In this paper, a testing method (the Ball-on-three-balls) is employed to measure the mechanical biaxial strength of commercial and sample LTCCs. Different loading conditions and environments are selected aiming to reproduce possible loading scenarios during service. In addition, an experimental approach combining both humid and relatively dry environments (i.e. water and silicone oil) is presented to assess the effect of different surface metallization on the strength of sample LTCC components.

## 2. Experimental

### 2.1. Material of study

The substrate (glass-ceramic) employed to fabricate the LTCC specimens of study is made of approx. 50%

of  $\text{Al}_2\text{O}_3$  as filler and 50% of several glasses containing Ca, Na, Si, K, B and Al, where the crystallisation degree after sintering exceeds 90%. Figure 1 shows a SEM micrograph of a typical polished area on a LTCC of study. The bright phase corresponds to  $\text{Al}_2\text{O}_3$  particles which are embedded in a glassy matrix (grey phase). Microstructural characterisation of the bulk material can be found elsewhere [14].

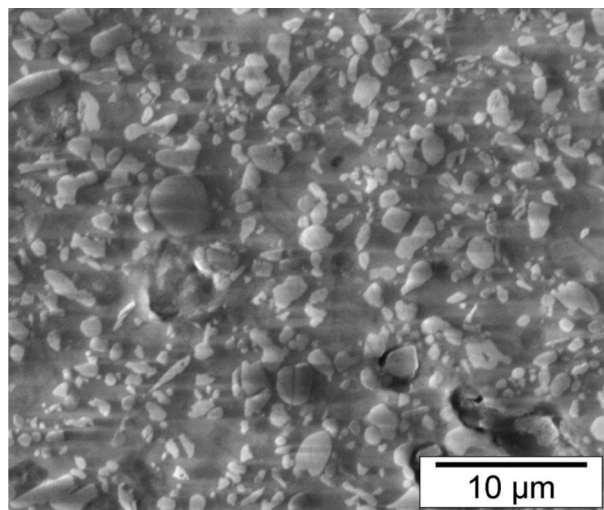


**Figure 1:** SEM micrograph of a LTCC microstructure showing alumina phase (bright) in a glassy matrix (dark).

#### 2.1.1. Commercial LTCC components

The specimens used for the biaxial strength tests were cut from commercial LTCC-Tapes (panels of ca. 100 x 100 x 0.45 mm<sup>3</sup>), provided by the company TDK-EPC, Deutschlandsberg, Austria (Fig. 2).

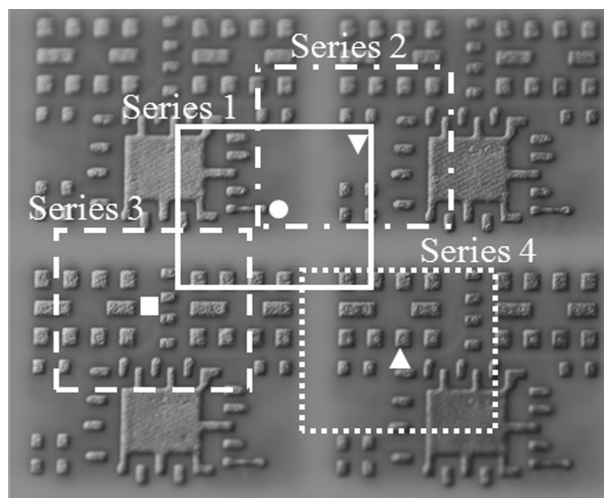


**Figure 2:** Scheme of a panel where the samples are cut out in such a way that the position to be tested lies in the centre of the specimen.

For the inner metallisation only Ag is used, whereas for the outer metallisation the silver pads are covered with a nanometric Ni/Au layer, which is employed to avoid corrosion and further guarantee good adhesion of possible soldered components. The thickness of the metal pads is approx. 7  $\mu\text{m}$ . The processing route employed was tape casting and the co-sintering was performed in a furnace at 850  $^{\circ}\text{C}$ . After sintering, four different samples of rectangular plates of ca. 11.0 x 9.7 x 0.45  $\text{mm}^3$  were cut from each panel, as indicated in Fig. 2. In each case, the centre of the plate contains a different region of the LTCC-unit. Bulk specimens of the same dimension were also tested as reference material.

### 2.1.2. Sample LTCC

In order to distinguish the effect of inner structures and surface metallization on the biaxial strength, sample structures were fabricated using the same process as for commercial LTCC components. Rectangular testing plates of ca. 11.0 x 9.7 x 0.45  $\text{mm}^3$  were diced from each panel with a diamond saw. In addition to bulk material without metallization as reference material (Fig. 3a), three LTCC samples with different surface metallization were fabricated:

- (i) MT: Bulk LTCC with a full metallization layer of ca. 10 $\mu\text{m}$  on top of the substrate (Fig. 3b).
- (ii) CP: Bulk LTCC with contact pads of 1.5 x 1.8 mm and ca. 10 $\mu\text{m}$  thickness, covering the 75% of the top surface (Fig. 3c).
- (iii) CV: Bulk LTCC with cylindrical vias on the top with a diameter of 100 $\mu\text{m}$  and a pitch of 300 $\mu\text{m}$ , with a depth into the material of ca. 50 $\mu\text{m}$  (Fig. 3d).

### 2.2. Mechanical testing: Ball-on-three-balls

The biaxial strength of the LTCC specimens was determined using a miniaturised Ball-on-three-Balls (B3B) fixture (Fig. 4a) especially built in-house to match the dimensions of the supplied components. In the B3B method, a rectangular plate (or a disc) is symmetrically supported by three balls on one face and loaded by a fourth ball in the centre of the opposite face (see Fig. 4b), which produces a very well defined biaxial stress field [15, 16]. The four balls had a diameter of 8 mm. A pre-load of 7 N was applied to hold the specimen between the four balls. The load is increased until fracture occurs, and the fracture load can be used to calculate the maximum tensile biaxial stress in the specimen at the moment of fracture.

For a bulk plate of an elastically isotropic material the equivalent maximum stress  $\sigma_{\text{max}}$  corresponding to the fracture load  $P$  can be calculated as follows:

$$\sigma_{\text{max}} = f \cdot P/t^2 \quad (1)$$

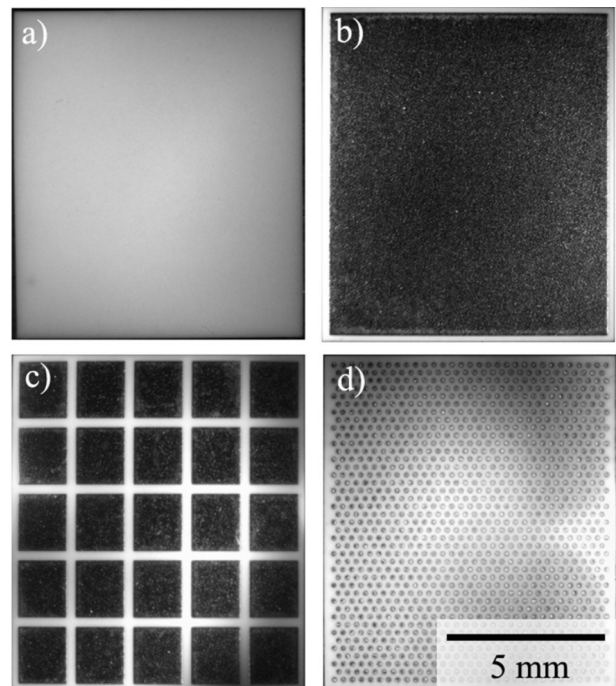


**Figure 3:** Samples with different metallization at the top surface of the substrate: a) bulk without metallization, b) bulk with full metallization layer, c) bulk with contact pads, and d) bulk with cylindrical vias of 100 $\mu\text{m}$  diameter and 50 $\mu\text{m}$  depth.

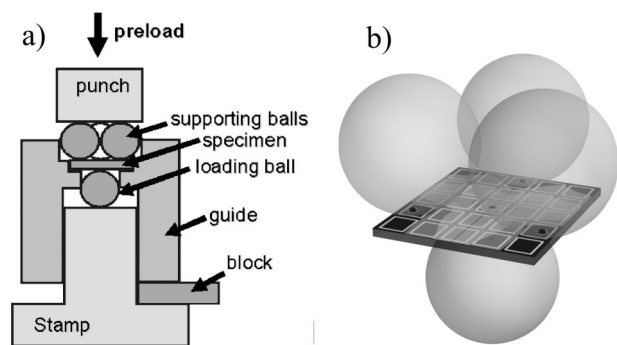


**Figure 4:** a) Schematic of the ball-on-three-balls test for biaxial testing and b) FE simulation of the stress distribution in the plate during loading.

where  $t$  is the specimen thickness, and  $f$  is a dimensionless factor which depends on the geometry of the specimen, on the Poisson's ratio of the tested material, and on the details of the load transfer from the jig into the specimen. Elastic properties were determined by means of the Resonant Beam Method [17] in a bulk LTCC sample, resulting in a Young's modulus of  $E = 113 \pm 1$  GPa and a Poisson's ratio of  $\nu = 0.2 \pm 0.01$ . The factor  $f$  was calculated for the given geometry and Poisson's ratio as function of the thickness of the specimens. The resulting geometric factors corresponding to commercial LTCC and sample structures investigated here are reported elsewhere [13, 18].

### 2.2.1. Testing of commercial LTCC

The tests on commercial LTCC were conducted under displacement control at a rate of 0.5 mm/min and a relative humidity (RH) of  $23 \pm 2\%$  at  $21 \pm 1\text{ }^\circ\text{C}$  (i.e.  $H_{\text{abs}} \approx 4.3 \pm 0.4 \text{ g}_{\text{H}_2\text{O}}/\text{m}^3$ ), using a universal testing machine (Zwick Z010, Zwick/Roell, Ulm, Germany) with a load cell of 200 N. The load was increased until fracture occurred and the fracture load was used to calculate the maximum tensile biaxial stress in the specimen at the moment of fracture using Eq. (1). A total of 30 specimens were tested for each series.

### 2.2.2. Testing of sample structures

In order to discern the effect of surface metallization (e.g. contacting pads or cylindrical vias) and the effect of the environment on the strength of components, a novel experimental approach has been proposed. Biaxial strength tests were performed within two different environmental conditions: a) in water and b) in silicone oil bath, in order to reproduce high and low relative humidity conditions, respectively. In both cases, the samples (as described in Fig. 3), were placed in the B3B fixture and the corresponding fluid (i.e. water or silicone oil) was pumped into the specimen holder to fully cover the specimen during the entire loading. The temperature was maintained constant for all tests, i.e.  $22 \pm 2\text{ }^\circ\text{C}$ . The number of specimens tested for each sample ranged between 15 and 30, for statistical significance. The tests were conducted under displacement control at a constant cross-head speed (i.e. 0.1 mm/min) using a universal testing machine, (Zwick Z010, Zwick/Roell, Ulm, Germany).

## 3. Results and discussion

### 3.1. Strength of commercial components

Fig. 5 shows a Weibull diagram of the four LTCC series corresponding to four different tested regions of the LTCC-unit. Bulk specimens of the same dimension were also tested as reference material. Each distribution was collected on a sample of 30 specimens, which ensures statistical significance for the Weibull analysis. The nominal failure load,  $P$ , is represented vs. the probability of failure,  $F$ . The corresponding equivalent failure stress,  $\sigma_f$ , calculated with Eq. (1) for every tested specimen is also represented in the plot. The strength results from the bulk specimens are also shown for comparison.

It can be inferred from Fig. 5 that all series follow a Weibull distribution. Nevertheless, the strength distribution between some of the series with metallisation and the bulk series is different. This can be associated

with stress concentrations near metallization regions and/or residual stresses developed during co-sintering of metal-ceramic parts. In addition, some of the diagrams seem to follow a typical two-parameter Weibull distribution (e.g. series 1 in Fig. 5), whereas others show a so-called “concave banana-shape” (i.e. the strength distribution in the Weibull diagram deviates from a lineal trend, pointing downwards for lower failure stress values). In such cases (see for instance series 2 and 4 in Fig. 5) a minimum failure stress level (“threshold stress”) may be defined under which the material may not fail. This can be a result of metal electrodes arresting the crack in its propagation from the surface towards the bulk. A comprehensive study of the crack propagation can be found in [11, 13].

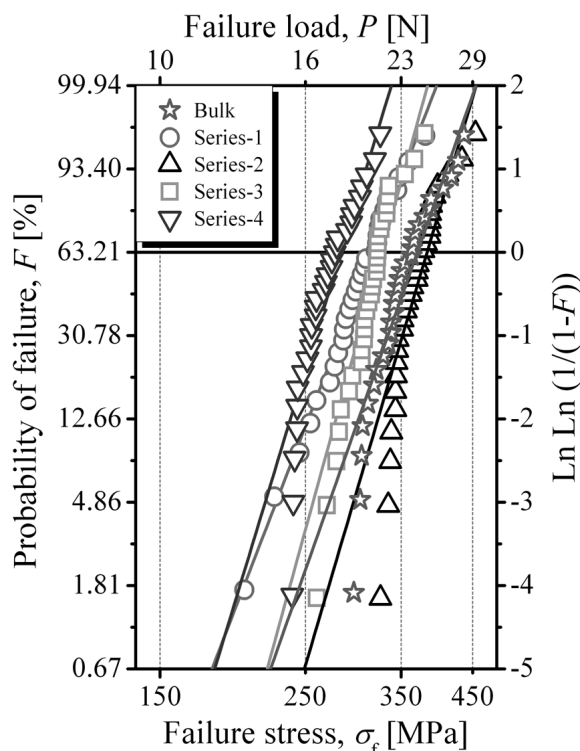


**Figure 5:** Weibull diagram of LTCC samples corresponding to four different tested regions of the LTCC-unit. A sample of bulk specimens is also shown for comparison.

### 3.2. Effect of surface metallization on strength distribution

In order to discern the effect of surface metallization (e.g. contacting pads or cylindrical vias) and the effect of the environment on the strength of components, an experimental approach has been proposed, based on localized biaxial testing of brittle samples at several locations under low and high humidity environments (i.e. silicone oil and water) respectively [18]. Figure 6 represents the corresponding Weibull diagram, where the equivalent failure stress,

$\sigma_r$  (calculated for every specimen according to Eq. (1)) is represented versus the probability of failure,  $F$ , for the bulk sample tested in water and in silicone oil. It can be observed that the failure stress values follow a Weibull distribution, which is associated with the flaw size distribution in the sample. The Weibull parameters,  $\sigma$  and  $m$  were calculated according to EN-843-5 [19]. The full line represents the best fit of the strength data using the maximum likelihood method. The 90% confidence interval for the measured values is also shown in the referred figure as broken lines. It represents the range where the true Weibull parameter can be found with a 90% probability and reflects the influence of the sampling procedure. The characteristic flexural strength and Weibull modulus for all samples tested, with the calculated 90% confidence intervals, are given in Table 1.

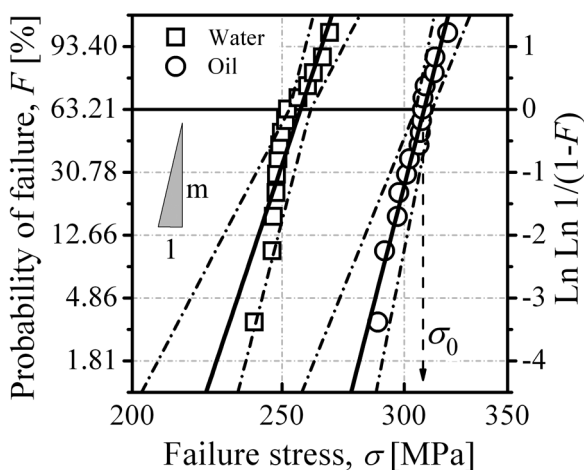


**Figure 6:** Weibull diagram of bulk LTCC samples tested in water and in oil.

**Table 1:** Characteristic strength,  $\sigma_0$ , and Weibull modulus,  $m$ , of samples with different surface metallization, tested in water and in silicone oil.

Sample	Water		Silicone Oil	
	$\sigma_0$ (MPa)	$m$	$\sigma_0$ (MPa)	$m$
Bulk	257 (253–261)	32 (20–42)	309 (305–313)	41 (26–54)
MT	303 (295–311)	20 (13–26)	305 (300–311)	27 (17–35)
CP	296 (289–303)	22 (14–29)	298 (294–302)	38 (24–50)
CV	164 (161–167)	28 (17–37)	220 (217–222)	42 (27–54)

The effect of the environment on  $\sigma_0$  can be clearly seen in Fig. 6, as has been reported elsewhere [14]. The SCCG of defects during loading in water diminishes the strength (ca. 20%) as compared to testing in dry conditions for the same loading rate. According to the results listed in Table 1, for the case of samples with a

metal layer on the top (tensile) surface (MT samples), no difference can be appreciated between both environments, yielding strength values similar to those for bulk substrate tested in oil (i.e. 309 MPa). This indicates that the metal layer “protects” the substrate from SCCG effects. The same applies for CP samples loaded both in water and in oil (see Ref. 18 for more details). A different situation is found for CV samples which reveal not only an effect of the environment (i.e.  $\sigma_0 = 165$  MPa in water vs.  $\sigma_0 = 220$  MPa in oil), but also a negative effect of the vias on the strength, compared to substrate (bulk) material (see Table 1); i.e. strength can be reduced up to 40% compared to bulk material.

#### 4. Conclusions

In summary, it has been shown that localised biaxial testing using the ball-on-three-balls method performed in different environments can be used as methodology for reliability assessment as well as to quantify the effect of surface features on the strength of functional ceramic components. Whereas surface contacts such as cylindrical vias can become weak points in the design, metallization at the surface subjected to tensile stresses can even raise the strength of the component acting as a protective layer against environmental degradation.

#### Acknowledgments

Financial support by the Austrian Federal Government (in particular from the Bundesministerium für Verkehr, Innovation und Technologie and the Bundesministerium für Wirtschaft und Arbeit) and the Styrian Provincial Government, represented by Österreichische Forschungsförderungsgesellschaft mbH and by Steirische Wirtschaftsförderungsgesellschaft mbH, within the research activities of the K2 Competence Centre on “Integrated Research in Materials, Processing and Product Engineering”, operated by the Materials Center Leoben Forschung GmbH in the framework of the Austrian COMET Competence Centre Programme, is gratefully acknowledged. The authors specially thank the company TDK-EPC for providing the specimens for this investigation.

#### References

1. Evans AG, Biswas DR, Fulrath RM. Some Effects of Cavities on the Fracture of Ceramics: I, Cylindrical Cavities. *J Am Ceram Soc.* 1979;62(1-2):95-100.

2. Evans AG, Biswas DR, Fulrath RM. Some Effects of Cavities on the Fracture of Ceramics: II, Spherical Cavities. *J Am Ceram Soc.* 1979;62(1-2):101-6.
3. Hsueh CH, Evans AG. Residual Stresses and Cracking in Metal/Ceramic Systems for Microelectronics Packaging. *J Am Ceram Soc.* 1985;68(3):120-7.
4. Hsueh CH, Evans AG. Residual Stresses in Meta/Ceramic Bonded Strips. *J Am Ceram Soc.* 1985;68(5):241-8.
5. Imanaka Y. Multilayered low temperature cofired ceramics (LTCC) technology. In: Springer Science-Business Media I, editor. New York, NY 10013, USA, 2005.
6. Makarovic K, Bermejo R, Kraveva I, Bencan A, Hrovat M, Holc J, Malic B, Kosec M. The Effect of Phase Composition on the Mechanical Properties of LTCC Material. *Int J Appl Ceram Techn.* 2013; doi: 10.1111/ijac.12030.
7. Gurney C. Delayed fracture in glass. *Proc Phys Soc London.* 1947;59:169-85.
8. Wiederhorn SM. Subcritical Crack Growth in Ceramics. In: Bradt RC, Hasselman DPH, Lange FF, editors. *Fracture mechanics of ceramics.* New York: Plenum, 1974.
9. Wiederhorn SM. Influence of water vapour on crack propagation in soda-lime glass. *J Am Ceram Soc.* 1967;50:407-14.
10. Dannheim H, Roosen A, Schmid U. Effect of metallization on the lifetime prediction of mechanically stressed low-temperature co-fired ceramics multilayers. *J Am Ceram Soc.* 2005;88(8):2188-94.
11. Bermejo R, Kraveva I, Antoni M, Supancic P, Morrell R. Influence of internal architectures on the fracture response of LTCC components. *Key Eng Mat.* 2009;409:275-8.
12. Deluca M, Bermejo R, Pletz M, Supancic P, Danzer R. Strength and fracture analysis of silicon-based components for embedding. *J Eur Ceram Soc.* 2011;31(4):549-58.
13. Bermejo R, Supancic P, Kraveva I, Morrell R, Danzer R. Strength reliability of 3D low temperature cofired multilayer ceramics under biaxial loading. *J Eur Ceram Soc.* 2011;31(5):745-53.
14. Bermejo R, Supancic P, Krautgasser C, Morrell R, Danzer R. Subcritical crack growth in low temperature cofired ceramics under biaxial loading. *Engng Fract Mech.* 2012; doi: 10.1016/j.engfracmech.2012.12.004.
15. Danzer R, Supancic P, Harrer W. Biaxial Tensile Strength Test for Brittle Rectangular Plates. *J Ceram Soc Japan.* 2006;114(11):1054-60.
16. Danzer R, Harrer W, Supancic P, Lube T, Wang Z, Börger A. The ball on three balls test – Strength and failure analysis of different materials. *J Eur Ceram Soc.* 2007;27:1481-5.
17. Lins W, Kaindl G, Peterlik H, Kromp K. A novel resonant beam technique to determine the elastic moduli in dependence on orientation and temperature up to 2000 °C. *Review of Scientific Instruments.* 1999;70(7):3052-8.
18. Bermejo R, Supancic P, Aldrian F, Danzer R. Experimental approach to assess the effect of metallization on the strength of functional ceramic components. *Scripta Mater.* 2012;66(8):546-9.
19. EN 843-5. *Advanced Technical Ceramics - Monolithic Ceramics - Mechanical Tests at Room Temperature - Part 5: Statistical Analysis.* 1997. p. 40.

Arrived: 24. 08. 2012

Accepted: 25. 11. 2012

# LTCC-Based Sensors for Mechanical Quantities

Uwe Partsch<sup>1)</sup>, Christian Lenz<sup>1)</sup>, Steffen Ziesche<sup>1)</sup>, Carolin Lohrberg<sup>1)</sup>, Holger Neubert<sup>2)</sup>, Thomas Maeder<sup>3)</sup>

<sup>1)</sup> Fraunhofer IKTS, Dresden, Germany

<sup>2)</sup> Technische Universität Dresden, Germany

<sup>3)</sup> Laboratoire de Production Microtechnique, EPFL, Lausanne, Switzerland

**Abstract:** Besides their excellent dielectric and thermo-mechanical characteristics Low Temperature Cofiring Ceramics (LTCC) are also well suited for the fabrication of 3D micromechanical components such as sensors for mechanical quantities. This paper describes the development of such sensors covering some material and technological aspects. Furthermore, the design process for mechanical sensors is discussed as well as application examples of sensors for the detection of pressure, force, acceleration and flow.

**Key words:** LTCC, Sensors, 3D-Integration.

## Senzorji mehanskih veličin na osnovi LTCC

**Povzetek:** Poleg odličnih dielektričnih in termo-mehanskih lastnosti so keramike z nizko temperaturo žganja (LTCC) primerne tudi za izdelavo 3D mikro mehanskih komponent, kot so senzorji mehanskih veličin. Članek opisuje razvoj teh senzorjev vključno z nekaterimi tehnološkimi in materialnimi vidiki. Dodatno je predstavljen postopek oblikovanja mehaničnih senzorjev in nekaj primerov senzorjev tlaka, sile, pospeška in pretoka.

**Ključne besede:** LTCC, senzorji, 3D-integracija

\* Corresponding Author's e-mail: uwe.partsch@ikts.fraunhofer.de

### 1. Introduction

Ceramic sensors are applied when specific requirements have to be fulfilled, e.g. a high reliability at elevated and cycled temperatures, harsh environment as well as in aggressive chemicals.

The ceramic multilayer technology (e.g. LTCC) enhances these advantages because of its ability (i) for a complex 3D miniaturization with embedded deformable bodies (cantilever, diaphragms), channels and cavities as well as the ability (ii) for the direct integration of electronic components for signal conditioning and processing.

One reason for the outstanding commercialization success of LTCC-based sensors is the cost level which is mainly defined by material and process costs. In order to reduce material and process costs, miniaturization is the most important leverage.

layers and different functional materials. During cofiring, in particular, intensive mechanical and chemical interactions can appear, strongly influencing the component performance.

The successful processing of multilayered multi-material based miniaturized LTCC components requires the proper control of different materials and technological aspects.

#### 2.1 LTCC

One reason that ceramic materials are advantageously used for deforming bodies in sensor applications is their linear stress vs. strain behaviour. Table 1 compares different ceramic materials in terms of their mechanical properties.

### 2. Material aspects

The manufacturing of LTCC-based 3D micro-components means the co- and post-firing of glass-ceramic

**Table 1:** Mechanical properties of different ceramics (CTE ... coefficient of thermal expansion (20... 400°C), E ... Young's modulus,  $\sigma_B$  ... bending strength).

Material	CTE	E	$\sigma_B$	$\sigma_B/E$
	ppm/ K	GPa	MPa	$10^{-3}$
96% Al <sub>2</sub> O <sub>3</sub> <sup>1)</sup>	7.6	350	310	0.9
99.8% Al <sub>2</sub> O <sub>3</sub> <sup>2)</sup>	7.5	406	630	1.6
LTCC <sup>3)</sup>	5.8	120	320	2.7
YSZ <sup>4)</sup>	11.2	210	1050	5.0
ZTA <sup>5)</sup>	8.1	357	1350	3.8

Datasheet values: <sup>1)</sup> CeramTec V38, <sup>2)</sup> CeramTec RK 87, <sup>3)</sup> Du Pont DP 951, <sup>4)</sup> CeramTec MZ 429, <sup>5)</sup> CeramTec DC 25.

The  $\sigma_B/E$  ratio determines the dimension of the deforming bodies in terms of sensitivity and overload stability. The larger the  $\sigma_B/E$  ratio the smaller the deforming bodies can be designed. It can be seen that LTCC is well suited because of a  $\sigma_B/E$  ratio of 2.7. However, YSZ ( $\sigma_B/E = 5$ ) and ZTA ( $\sigma_B/E = 3.8$ ) have a better mechanical performance, but embedding e.g. of low sintering noble metals as well as resistors can only be realized using a low temperature firing system.

Different types of LTCC show a different bending strength behavior [1]. Best values can be obtained using the Du Pont's Green Tape 951 system (Figure 1). It must however be noted that, in order to ensure long-term reliability, static [2] and cyclic fatigue [3] must also be accounted for.

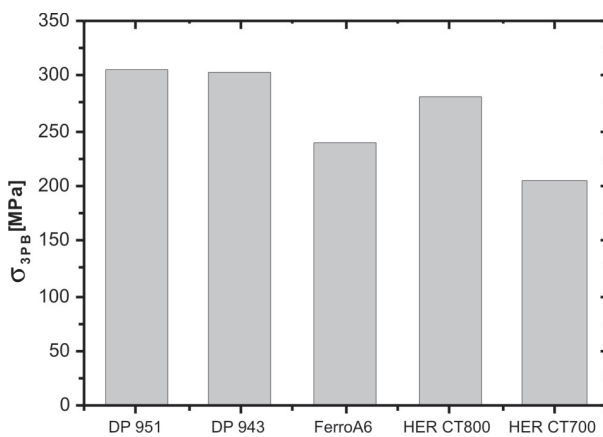


**Figure 1:** Comparison of different LTCC types regarding their fractural strength (re-calculated after [1]).

The 951 system offers different tape thicknesses (50 – 254 μm unfired) as well as a full system of the required pastes (inner/outer conductors, via, outer/inner resistors). This makes it particularly well suited for the fabrication of sensors.

The shrinkage control of LTCC multilayer components plays an important role regarding the final dimensional control e.g. for advanced electronic packages (chip sized packages, flip chip) but also in the case of mechanical sensors.

Shrinkage occurring during firing can be influenced by controlling the process factors (of lamination and firing). Figure 2 shows the influence of lamination temperature and pressure.

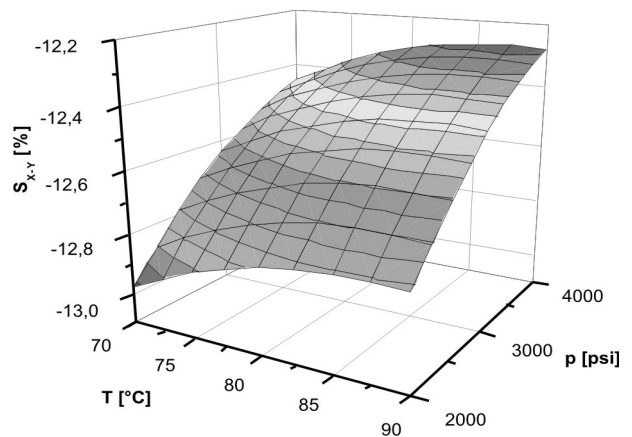


**Figure 2:** LTCC DP 951 X-Y shrinkage ( $S_{x,y}$ ) vs. lamination temperature (T) and pressure (p) [4].

## 2.2 Functional Thick Films

### 2.2.1 Metallization

In many cases, LTCC-suited inner metallization pastes are silver-based. The interaction between silver and LTCC during co-firing was described in the past by several authors e.g. [4-6], it can lead to significant warping of thin and 3D structured LTCC geometries.

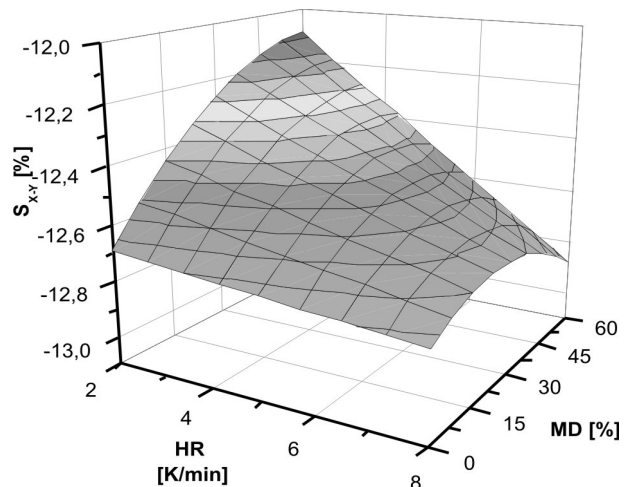


**Figure 4:** LTCC DP 951 X-Y shrinkage ( $S_{x,y}$ ) vs. heat up ramp (HR) and metallization degree (MD) [4].

Figure 4 shows that the shrinkage of a DP 951-based LTCC multilayer during firing is – in addition to the lamination parameters – also influenced by the degree of metallization and the heat up ramp. It can be seen that there is only a slight effect on the X-Y shrinkage by changing the heat up rate, when the multilayer is not metalized. In the case of an extensive metallization (60% metallization area) there is a strong dependence on the heat up ramp. The metalized multilayer shrinks in the same way as the non-metalized multilayer at higher heat up ramps (12.8% @ 8K/min). Using low heat up ramps (2 K/min), the shrinkage is reduced to 12.1%. The silver layer has a “locking” function due to the different shrinkage behavior.

Besides this pure mechanical effect there are also chemical interactions between the silver layer and the LTCC. [6] and [5] demonstrated a strong degree of silver diffusion into the LTCC, which can reach some 10 μm. [7] showed that silver influences the viscosity of the LTCC glass leading to an earlier densification and crystallization. Because silver enters the LTCC glass matrix in an oxidized status, a nitrogen sintering atmosphere can minimize the discussed effects, by shifting the chemical equilibrium between Ag<sup>+</sup>(glass) and Ag<sup>0</sup> (metal) in favour of the latter.

2.2.2 Piezo-Resistors

The transformation of a mechanical quantity into an electrical signal by piezo-resistors is one of the most common measuring principles. Using a deformable body with piezo-resistors in the areas with high mechanical strain, a mechanical input quantity (e.g. force) can be transduced into a proportional resistance/bridge voltage change (Figure 5).

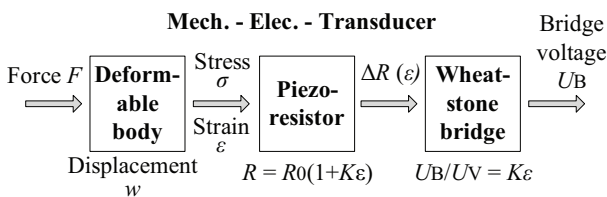


Figure 5: Sensor transmission chain [8].

Based on their microstructure and effective conducting mechanism, thick-film resistors (TFRs) always have a strain sensitive behavior.

As well as the thermal behavior, the strain sensitivity of TFRs is dominated by insulating/semi-conductive nanoscale glass layers between conducting particles, within the three-dimensional conductive chains, strain-dependent interparticle tunneling being the favoured mechanism [9, 10].

The strain sensitivity is specified using the K- or gauge factor which determines the ratio between the relative change of resistance and the applied strain.

Measured gauge factors of TFRs are between 2 and 35. They are influenced by (i) the composition of the TFR (type, grain sizes and proportion of glasses and conductive phases), (ii) the firing process (dissolution of the conductive phase into the glass), and (iii) the interactions between the TFR and the substrate as well as the terminations (diffusion of silver ions into the TFR glass matrix) [11]. The maximum signal gain of TFRs is limited by noise. Therefore, the effective signal-to-noise ratio is suitable as a normalized parameter [12]:

$$SNR_{eff} [dB] = -20 \cdot \frac{\lg U_S}{U_N} \quad (1)$$

$U_S$  and  $U_N$  are the effective signal voltage and the peak-to-peak noise voltage. Here,  $U_S$  was calculated using the measured gauge factors, a supply voltage of 5 V and a relative strain of  $\epsilon = 2.7 \cdot 10^{-4}$  (corresponds to 50% of the maximum deflection before substrate breakage).  $U_N$  was calculated by solving the definition of the noise index (NI).

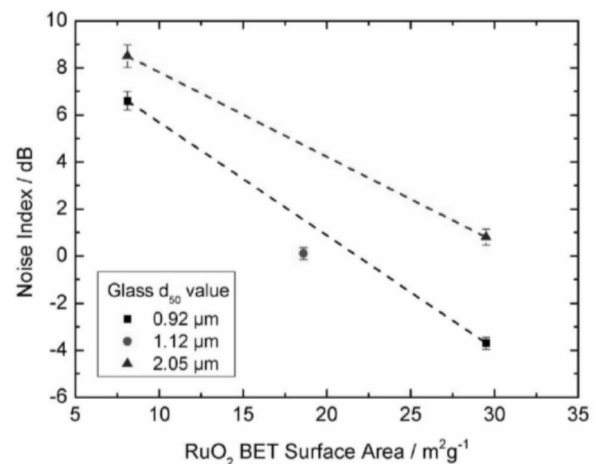
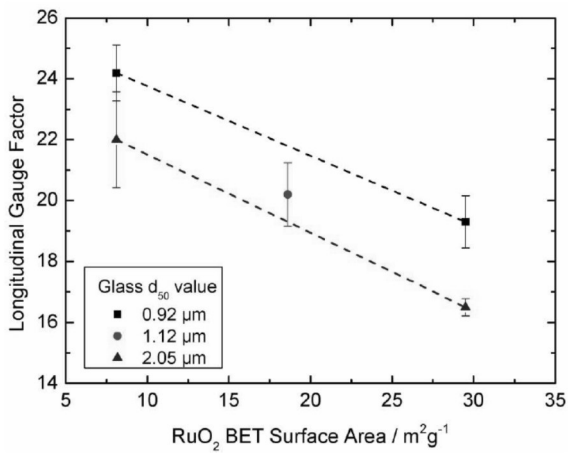


Figure 6: Strain sensor paste development [12]. Noise index (NI) vs. BET surface area of RuO<sub>2</sub>.

In order to improve the  $SNR_{eff}$  [12], compositions were developed as a mixture from RuO<sub>2</sub> (four different particle size distributions, one mixture) as well as two different glasses (five different particle sizes). The aim of these investigations was a TFR sheet resistance of 10 kOhm/sqr.

The results showed that the noise index (NI) and the gauge factor of TFRs are strongly influenced by the particle size distribution of the glasses as well as the conductive phase. Figures 6 and 7 illustrate that there is a

compromise between gauge factor and noise behavior of TFRs.



**Figure 7:** Strain sensor paste development [12]. Longitudinal gauge factor vs. BET surface area of RuO<sub>2</sub>.

However, these developments cannot improve the DP 2041 characteristics regarding the  $SNR_{eff}$

Further activities are planned concerning the development of new glass types, the optimization of firing and the analysis of alternative conductive phases (pyrochlores).

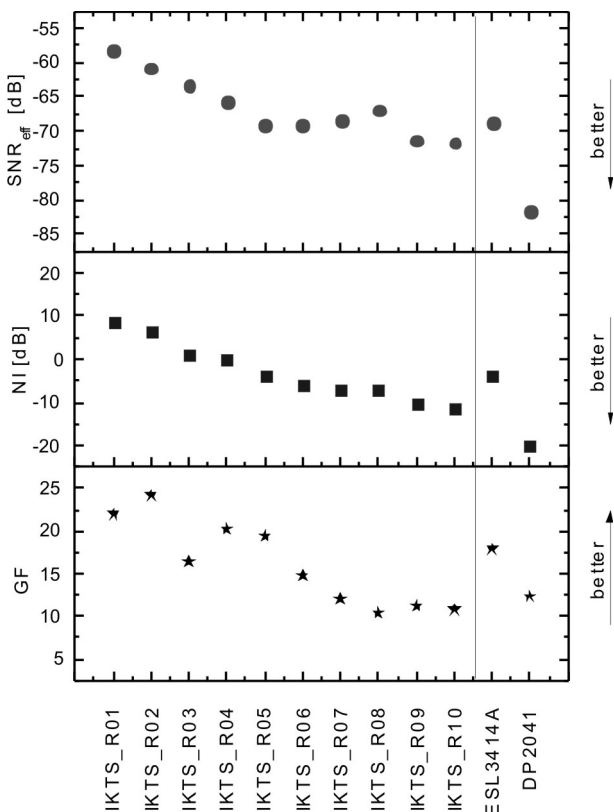


**Figure 8:** Effective signal-to-noise ratio ( $SNR_{eff}$ ) [12]. Comparison of IKTS and commercial pastes.

### 2.2.3 Sacrificial Materials

Sacrificial materials temporarily stabilize functional elements during lamination and sintering. They are removed during or after sintering. Two types of sacrificial materials are differentiated:

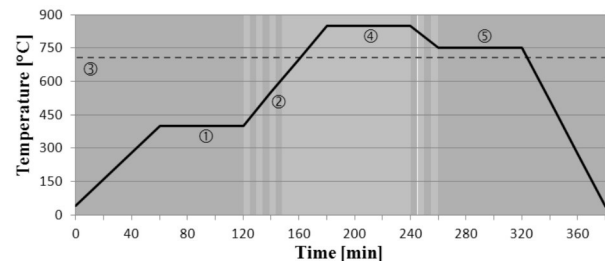
- Mineral sacrificial paste (MSP),
- Fugitive sacrificial paste (FSP).

MSP consists of glass, an active substance and vehicle [13, 14]. The active substance is a mineral filling material. After sintering, the MSP provides a solid layer and can be removed with aqueous acetic acid. MSP suits well for cantilevers and freestanding structures with high level requirements regarding the accuracy. Closed structures are difficult to handle as MSP has to be dissolved with acid.

FSP consists of organic and graphite powder and contains no glass phases [15, 16]. The graphite is oxidized to carbon dioxide at about 700 °C. Thus, it is well suited for closed cavities, channels and diaphragms in LTCC because FSP volatilizes through the porous LTCC or open channels during sintering [15].

In order to stabilize embedded mechanical structures during sintering, FSP oxidation must be prevented using a non-oxidizing sintering atmosphere (e.g. nitrogen). In this case, a “vent” is required for out gassing the carbon dioxide from the embedded structures. The appropriate timing for the change from oxygen to nitrogen and vice versa is a critical issue. It was studied for DP 951 in [17].

The resulting profile is shown in Figure 9. The amount of FSP and the geometry of the embedded structures require an adjustment of the sintering procedure for every component to avoid warping and FSP residue effects.



- ① ... Debinding: 350 °C to 550 °C
  - ② ... Glasmelt: 650 °C to 825 °C
  - ③ ... Carbonoxidation: 700 °C
  - ④ ... Sintering: 850 °C
  - ⑤ ... Burning FSP: 750 °C
- Oxygen atmosphere: 10 slm
  - Nitrogen atmosphere: 40 slm
  - Transition between oxygen and nitrogen and between nitrogen and oxygen, respectively

**Figure 9:** Customized sintering profile for surviving FSP after sintering DP 951 [17].

However, sacrificial materials often require the application of zero-shrinkage techniques [18] because of their unadapted shrinkage behavior in comparison to standard LTCC materials.

### 3. Technological aspects

The higher functional integration in multilayer-based sensors and microsystems complicates their processing compared to that of multilayer substrates for electronic assemblies. Sensors for mechanical quantities, in particular, need (i) functional structures like free-standing deforming bodies, fluidic channels or heating bridges which have to be processed with no sagging or warping, (ii) deforming bodies with reinforced regions for seismic masses or force application, and (iii) low dimensional tolerances of the processed substrates to provide low variances of the performance of the fabricated sensor elements. It is a challenge to customize the standard LTCC technology for these aspects. However, the technology varies according to design, material and dimension of the sensor elements.

#### 3.1 Sagging and warping

Sagging and warping are mainly caused by the lamination and sintering process. Below, some techniques are mentioned in order to reduce these imperfections:

- Cold lamination (uniaxial) at 30 °C reduces sagging.
- An isostatic pre-lamination of the unstructured tapes provides higher stability for the following processes like lamination. However, higher pressure ranges will then be necessary in the following lamination steps.
- A differential shrinkage of several single layers can be achieved by pre-laminating which helps to minimize sagging effects at thin deforming elements (diaphragms, cantilevers) during firing (Figure 10).
- Fixation and support of freestanding structures during sintering reduces sagging. Outer structures can be directly supported on the sintering support. Embedded structures have to be stabilized

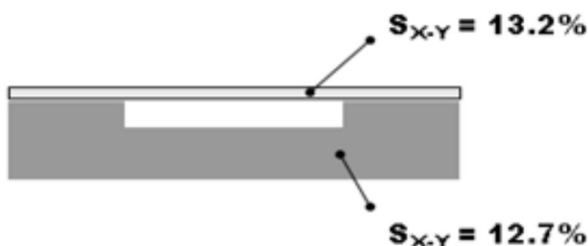


**Figure 10:** LTCC diaphragm: Different pre-lamination steps can minimize sagging effects.

lized using additional layers like MSP or FSP. Customized sintering profiles should then be applied.

- Customized sintering profiles for integrated thick-film metallization reduce warping.

#### 3.2 Structural elements for reinforcement

Some devices require deforming bodies with reinforced structures to supply flexural resistant properties (e.g. accelerometers or force sensors). For a precise and reproducible fabrication special techniques were established to process these bodies in multilayer technology:

- Little bars fix the reinforced regions to the outer frame during stacking and laminating (Figure 11). After laminating or sintering, these bars have to be removed by laser cutting. However, it must be considered that no other functional structures are placed under the bars which might be damaged by the laser.
- Reinforcing layers, e.g. reinforced centers of diaphragms, can also be stacked separately, as shown in Figure 11. However, this technique requires a customized stacking tool and the process gets more complex.

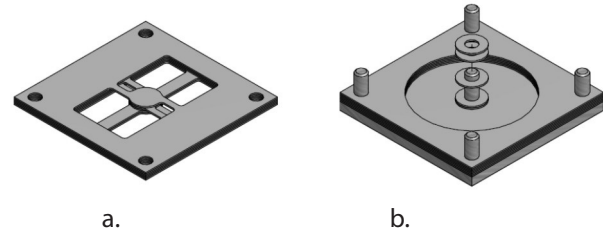


**Figure 11:** Techniques for reinforced regions: a) Fixing bars which are removed after laminating or sintering; b) separate stacking

#### 3.3 Dimensional tolerances

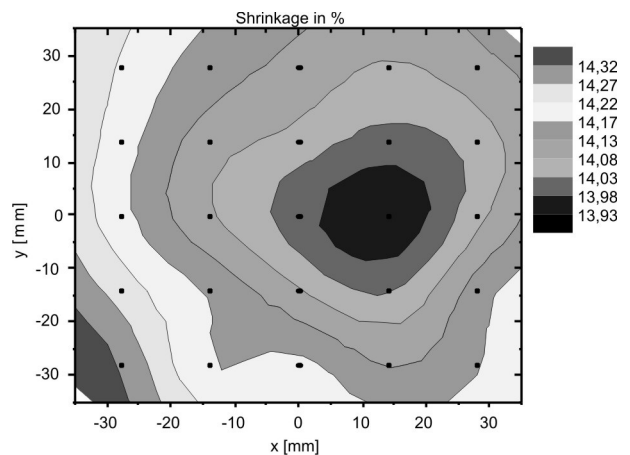


**Figure 12:** Different shrinkage of a DP 951 4-inch substrate - interpolation between 25 data points.

Design miniaturization together with panel production of LTCC microsystems offers low-cost applications. This is one of the advantages of the LTCC technology.

However, small dimensional tolerances have to be met in order to provide reproducible properties of the sensors and to achieve an acceptable yield:

- Low tolerances have to be ensured for the structuring processes (punching, laser structuring, screen printing and stacking) over the whole working space of a multiple printed panel.
- The lamination process has to be controlled (e.g. plan parallelism at the uniaxial lamination press) to ensure homogeneous results.
- The nominal shrinkage varies over the fired substrate up to 0.5% (Figure 12). It depends on the lamination process, the structures [19] and the sintering process. For best results, the variation of the shrinkage over the working space of the panel has already to be considered in the CAD files during the design phase.

#### 4. Sensor design

Even though the LTCC technology provides many different applications for mechanical sensors, the general design process is almost the same (Figure 13).

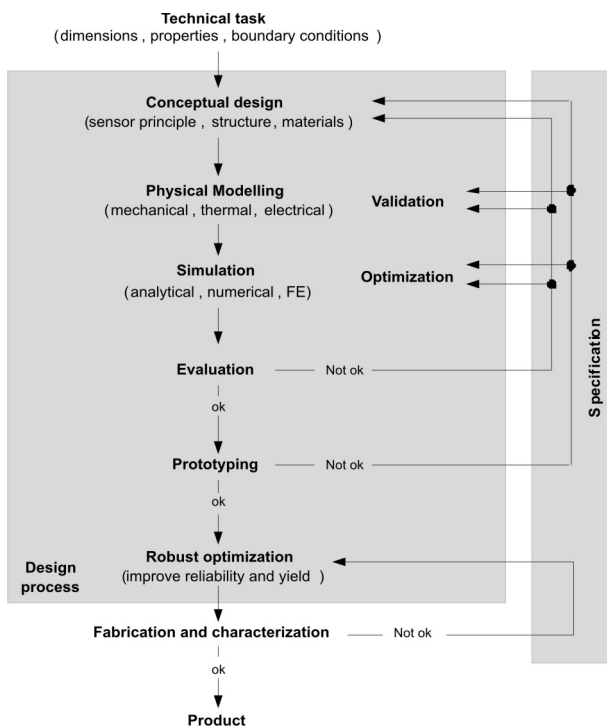


**Figure 13:** General design process for mechanical sensors in LTCC.

At the beginning, technical specifications have to be defined (e.g. sensor properties, dimensions and boundary conditions).

Following that, the conceptual design must be specified regarding producibility of structures and useability of materials. After evaluation and selection, the most suitable conceptual design has to be designed in detail.

Today, model-based design and design optimization is inevitable when designing integrated sensors for mechanical quantities. Therefore, physical models of adequate levels of abstraction (granularity) have to be provided for the conceptual design and the final design step as well.

Afterwards, the final design has to be checked and revised if necessary regarding the required properties. For this purpose, an evaluation step follows which includes fabrication and characterization of prototypes. In case of unsatisfying properties, one or more development loops have to be passed to adapt sensor concept and design and to validate or improve the simulation models as well.

Technology-inherent distributions of dimensions, material properties and process parameters lead to performance variations of a set of sensors even when they all are of the same design and fabrication processes. Performance distributions can be minimized by a further design step which involves the probability distributions of the design and process parameters.

The objective of a so-called robust design optimization is to find a design that fulfills the target requirements specified with minimized scattering of the sensor performance [20, 21]. As a result, an improved yield is to be expected.

#### 5. Applications

##### 5.1 Pressure Sensor

Integrated LTCC-based pressure sensors have many advantages in comparison to classic steel or ceramic-based pressure sensors [22-24] because of the technology-inherent features.

The LTCC technology enables easily variable sensor geometries e.g. different diaphragm thicknesses for different pressure ranges by using different tape thicknesses. All types of pressure sensors (relative, absolute, differential) can be built up. Furthermore, all components of the sensor system (sensor body, pressure con-

nectors/micro piping, and electronic components) can be integrated in the LTCC-based multilayer component.

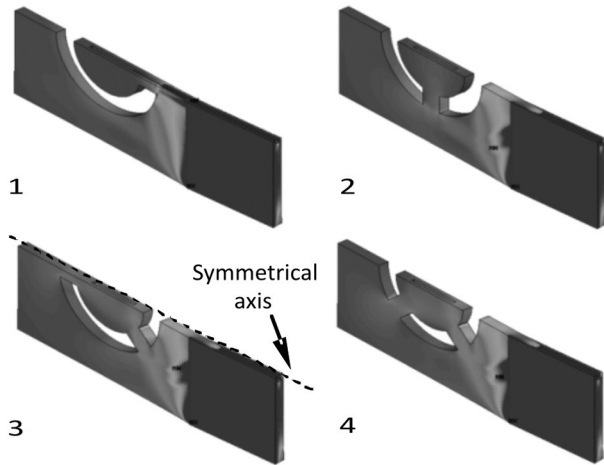


**Figure 14:** Finite elements analyses of different constructional designs (numbers of fixation cantilever): perfect mechanical decoupling of the sensor cell with one or two fixation cantilevers.

In [23] a new LTCC-based pressure sensor concept was presented aiming the improved mechanical decoupling of the diaphragm. The sensor cell is fixed by thin LTCC cantilevers containing micro channels for the pressure connection of the sensor cell.

Using the piezo-resistive measuring principle the strain caused by diaphragm deflection is measured by thick-film resistors, connected to a Wheatstone bridge and screen printed at the surface of the LTCC diaphragm.

FE analyses were carried out for the optimization of the design of the LTCC fixation cantilever [Figure 4].

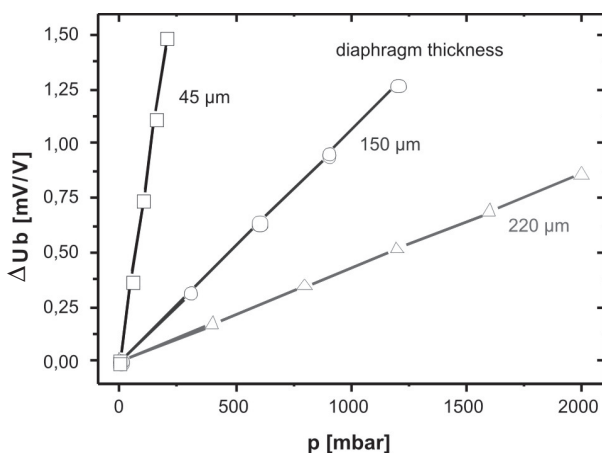


**Figure 15:** Characteristic curves of different sensors (pressure ranges). Shift of bridge voltage ( $\Delta U_b$ ) vs. applied pressure ( $p$ ).

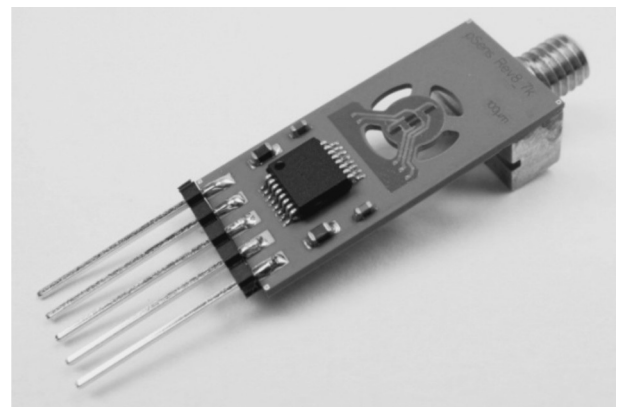
The sensor characterization showed that all sensors have a strongly linear behavior (bridge voltage vs. pressure) and are nearly free of hysteresis (Figure 15).

Table 2 shows the overall characteristics of the sensors for different pressure ranges (0.2, 1.5, 5 bar nominal pressure). The operation pressure of the different sensors was defined by additional burst tests. All sensors have a 4-times overload safety.

**Table 2:** Characteristics of different sensor types according to DIN/ISO 16086 (offset voltage < 25 mV/V, bridge resistance ~ 25 kOhm, T=25 °C). D – diaphragm diameter, d – diaphragm thickness,  $p_{op}$  – operation pressure, S – sensitivity, L – linearity, H – hysteresis; FS – full scale.

Diaphragm		$p_{op}$	S	L	H
D [mm]	d [ $\mu$ m]	[bar]	[mV/Vxbar]	[%FS]	[%FS]
4.5	220	5.0	0.4	0.06	0.05
4.5	150	1.5	1.1	0.04	0.01
4.5	45	0.2	4.6	0.07	0.08

Finally, sensors with integrated signal conditioning electronics (amplifier, temperature compensation) were fabricated (Figure 16).



**Figure 16:** LTCC pressure sensor with integrated electronics for signal condition.

### 5.2 Force Sensor

Force sensors always detect the effect (deformation, stress, strain) of an applied force on a deformable body. The deformation is converted into an electrical signal by transducers working on the principle of e.g. capacitive, piezoelectric or piezo-resistive measurements. Though, the piezo-resistive principle is best suited because of its high accuracy, long-term stability and application range. When this transducer principle is applied, cantilevers and diaphragms obtain the best performance for small nominal loads.

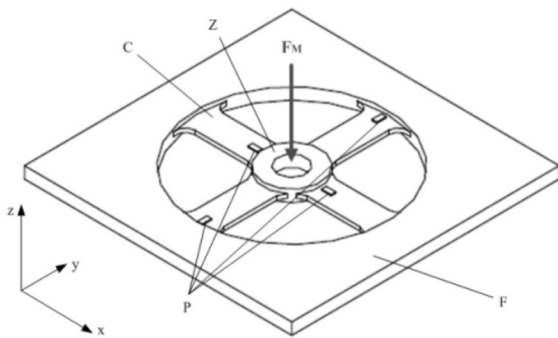


**Figure 17:** The cartwheel structure [8]. C - cantilever; Z - flexural resistant center; P – piezo-resistors; F - frame.

Miniaturized piezo-resistive force sensors for tensile and compressive loads (2 N, 5 N and 10 N) were developed. Compared to the pressure sensor above, the uniform application of the force to be measured in the deforming sensing body is the main challenge of this study. For this purpose, a cartwheel structure was designed (Figure 17). It consists of four identical cantilevers which are combined by a flexural resistant center. A metal pin with thread is mounted axially in the center hole. This structure obtains a uniform distribution of the applied tensile or compressive forces on the cantilevers, avoids angle errors and combines both, the high sensitivity of cantilevers and the robustness against shear forces of diaphragms.

Four piezo-resistors are placed on the cantilevers in areas of maximum strain – two under expansion and two under compression. They are connected to a Wheatstone bridge, thus the bridge voltage composes the sensing signal.

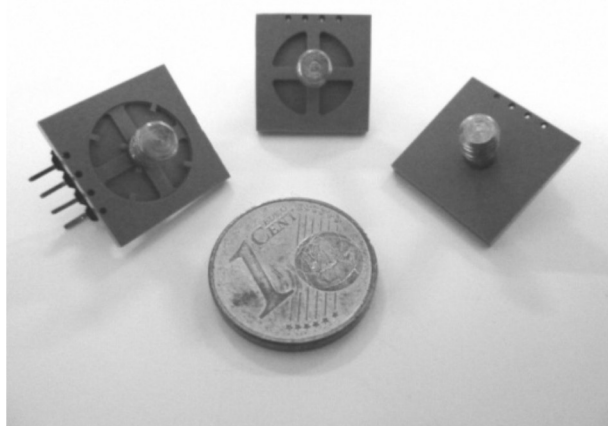


**Figure 18:** LTCC force sensors for three nominal loads (2 N, 5 N, 10 N). Dimensions: 14 x 14 mm<sup>2</sup>.

An analytical model [8] was developed for the dimensioning and simulation of the sensor elements. The

most important restrictions for the design process were (i) to achieve a high grade of miniaturization, (ii) to provide robustness against overloads up to 200% of the nominal load and (iii) an equal layout for the mentioned force ranges except the top layer (Figure 18).

**Table 3:** Measured sensor characteristics (T = 25°C). F<sub>B</sub> – breaking load, S – sensitivity, L – linearity, TC-S – temperature coefficient sensitivity, FS – full scale.

Nominal load F [N]	F <sub>B</sub> [N]	S [mV/(V·N)]	L [%FS]	TC-S [%S/K]
2 N	4	2.6	< 0.6	0.02
5 N	> 10	0.6	< 0.4	0.03
10 N	> 20	0.1	< 1.0	0.02

The designed sensors were fabricated in multiple processing with 25 elements per 4-inch substrate. The techniques: pre-lamination of all sheets, uniaxial cold lamination at 30°C and the fixation of the deformable bodies on the sinter support were used to minimize sagging.

The measured characteristics in Table 3 show the potential of the LTCC as base material for this application. The sensors have a linear behavior and a low temperature drift of the sensitivity. Furthermore, there is a good compromise between sensitivity and breaking load.

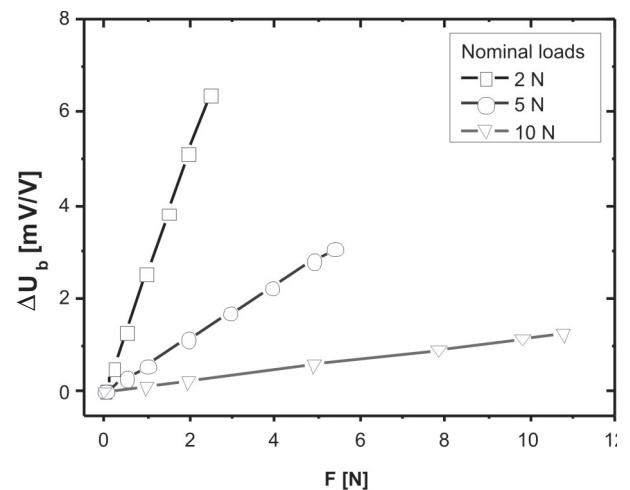


**Figure 19:** Characteristic curves of different sensors (load ranges). Shift of bridge voltage ( $\Delta U_b$ ) vs. applied force (F).

### 5.3 Acceleration Sensor

The measurement of accelerations requires a mass element on a spring. The mass elongates and deforms the spring in response to an applied acceleration. The deformation can be measured e.g. by a piezo-resistive transducer.

Today's acceleration sensors made of silicon offer sufficient functionality in a cost-effective way. In contrast, acceleration sensors made of LTCC work under elevated temperatures, or as an additional feature integrated in LTCC substrates or electronic assemblies.

The LTCC multilayer technology suggests a sensor layout with leaf springs in a layer stressed for bending or for torsion. Thus, an acceleration perpendicular to the layer effects a deformation of the springs which can be measured by piezo-resistive thick-film resistors printed on the springs. The layout has to consider some conflicting requirements, e.g. high resonance frequency, i.e. high stiffness versus high sensitivity, i.e. lower stiffness, or uniform strain in the benders for a high reliability versus high strained areas of the springs for a high sensitivity.

Analytical and finite element models were used to optimize the sensor design. Two parallel trapezoidal benders have advantages as compared to rectangular benders or torsion springs, or the bridge and cantilever structures proposed in [25]. A FEA model of the optimized layout fabricated in LTCC is shown in Figure 20.

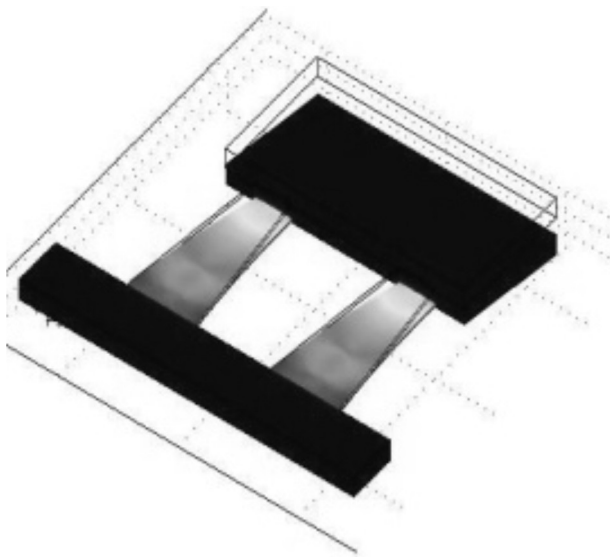


**Figure 20:** FEA model of an acceleration sensor with two trapezoidal benders (equivalent strain).

The first resonance frequency has a strong influence to the working range and is obtained from FEA models. A linear relation between acceleration and deformation can be expected about 50% of the resonant frequency. Resonant excitation would destroy the sensor. Four thick-film resistors, two on the benders and two on the frame are connected to a Wheatstone bridge like it has been done in case of the pressure sensors.

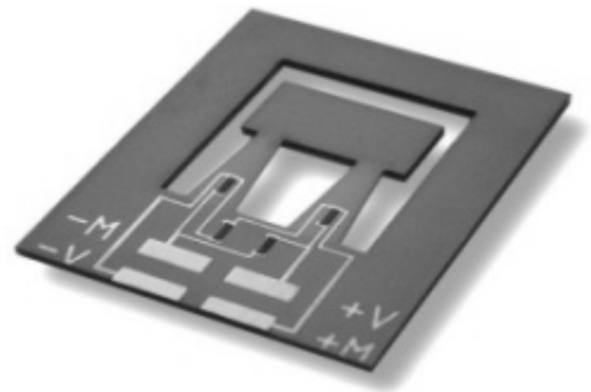


**Figure 21:** LTCC acceleration sensor with piezo-resistors on rectangle leaf springs.

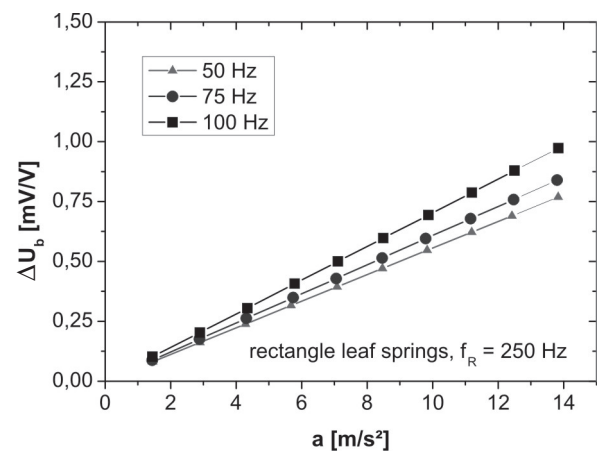


**Figure 22:** LTCC acceleration sensor characteristic curve, bridge voltage ( $U_b$ ) vs. acceleration. Different excitation frequencies.

Figure 21 shows a LTCC acceleration sensor with a resonance frequency of 250 Hz [20]. Excited with 100 Hz the sensor gives a slightly higher signal due to the closer proximity to the resonance frequency as compared to 50 or 75 Hz (Figure 22).

However, the tested sensors are sensitive for large accelerations. Smaller effective ranges or can be designed.

#### 5.4 Flow Sensor

Most of the commercial flow sensors work on the heating wire principle. A thin platinum wire which is heated by a current is placed in a flowing gas. It cools the platinum wire which refers to its resistance and influences the connected Wheatstone bridge. The implementation of a channel system with integrated freestanding heating wire in LTCC is only possible when using a sacrificial material. A thin heater can be realized by overprinting the FSP with a thick-film platinum paste. It enables low power loss and raises the sensitivity.

In order to reach an adjusted shrinkage between LTCC and FSP a zero-shrinkage technique is required. For this purpose, several techniques were investigated:

- The combination of DP 951 with Release-tapes (Ceramtape A, GT 951 RT) indicates delamination and residues at removal respectively.
- The self-constrained LTCC-tape HL2000 (Heraeus) is not suitable to uniaxial lamination process (voids and delamination) which is required and the FSP-paste (residues after firing).
- Best results were achieved with a combination of DP 951 and HL2000 (Figure 23). DP 951 suits to the FSP-paste and stabilizes the HL2000 during the lamination process. The zero shrinkage of the whole substrate is constrained by the HL2000.

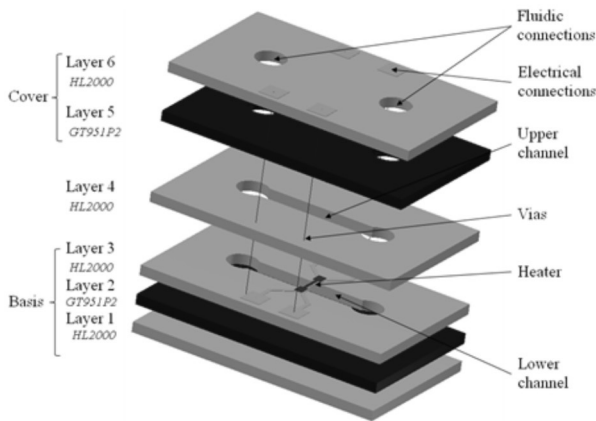


**Figure 23:** Explosion drawing of the LTCC flow sensor.

Figure 23 illustrates the final sensor design [Loh12]. The bottom part of the channel was filled with sacrificial material, which was overprinted by glass and platinum paste to create the heater structure.

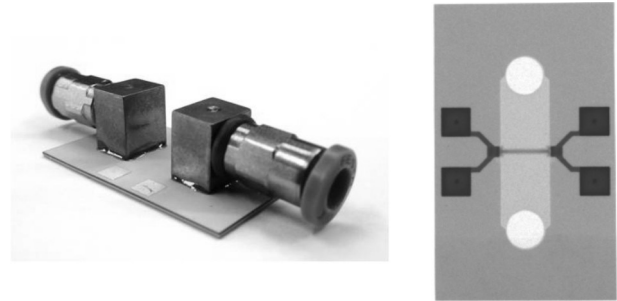
Afterwards, the upper channel part was laminated on top of it so that the heater was centered. With this technique a lot of different heater geometries can be realized.

**Table 4:** Sensor characteristics.  $d_H$  – heater thickness,  $L_H$  – heater length,  $R_{H0}$  – heater resistance ( $T = 25\text{ }^\circ\text{C}$ ),  $R_{H100}$  – heater resistance ( $T = 100\text{ }^\circ\text{C}$ ).

Channel cross section $A_c$	$d_H$ [ $\mu\text{m}$ ]	$L_H$ [mm]	$R_{H0}$ [ $\Omega$ ]	$R_{H100}$ [ $\Omega$ ]
0.8 mm	50	4	2.5	3.1

The prototypes show the expected relation between the current through the heating wire and the fluid flow. Figure 24 shows the characteristic curve of the sensor. In future work, a measuring circuit will be integrated in

the system to complete the sensor and to linearize the current-flow correlation.



Fabricated flow sensor with assembled fluidic adapters

CT-scan of the fabricated flow sensor

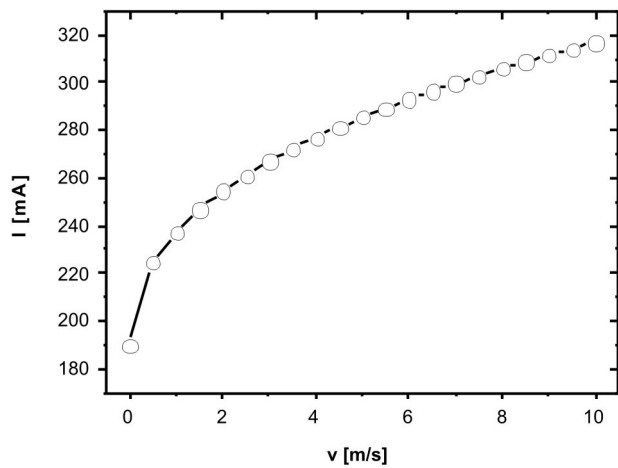


**Figure 24:** LTCC flow sensor and characteristic curve, heater current ( $I$ ) vs. fluid flow ( $v$ ).

## 6. Conclusions

The selected examples show that LTCC is a well suited integration platform for mechanical sensors. Their design and fabrication requires a deep understanding and control of material issues (e.g. material interactions during co-firing, shrinkage behavior, sacrificial layer). Besides this, it is necessary to expand the LTCC process flow on the generation of the required 3D structural elements.

Pressure, force, acceleration and flow sensors were developed following a defined design and manufacturing flow.

It was shown that the sensors have an excellent and stable functionality in all cases. The main advantage of the presented sensors is the quasi-monolithic design. It prevents thermo-mechanical strain which normally occurs when parts of different materials are bonded.

Using the demonstrated material and process expansions and improvements, LTCC-based sensors for mechanical quantities are interesting and cost-effective alternatives to existing technical solutions.

## References

- Jones, W. K.; Liu, Y.; Larsen, B.; Wang, P. and Zampino, M.: "Chemical, Structural, and Mechanical Properties of the LTCC Tapes", *The International Journal of Microcircuits and Electronic Packaging*, Volume 23, Number 4, Fourth Quarter, 2000, S. 469.
- Maeder, T.; Jacq, C. and Ryser, P.: "Long-term mechanical reliability of ceramic thick-film circuits and mechanical sensors under static load", *Sensors and Actuators A*, in press, (2012).
- Duan, K.; Mai, Y.W. and Cotterell, B.: "Cyclic fatigue of a sintered  $\text{Al}_2\text{O}_3 / \text{ZrO}_2$  ceramic", *J. Mater. Sci.*, 30 [20] 5192-5198 (1995).
- Partsch, U.: "Untersuchungen zum Schwindungsverhalten von LTCC-Multilayern" Diploma Thesis 1996, Friedrich-Schiller-Universität Jena.
- Eberstein, M.; Rabe, T. and Schiller, W. A.: "Influences of the Glass Phase on Densification, Microstructure, and Properties of Low-Temperature Co-Fired Ceramics", *Int. J. Appl. Ceram. Technol.*, 3 [6] 428-436 (2006).
- Jau-Ho, J. and Chia-Ruey, C.: "Interfacial Reaction Kinetics between Silver and Ceramic-Filled Glass Substrate", *J. Am. Ceram. Soc.*, 87 [7] 1287-1293 (2004).
- Rabe, T.; Glitzky, C.; Naghib-Zadeh, H.; Oder, G.; Eberstein, M. and Töpfer, J.: "Silver in LTCC – Interfacial Reactions, Transport Processes and Influence on Properties of Ceramics, CICMT – Ceramic Interconnect and Ceramic Microsystems Technology, Denver 2009, Proceedings.
- Lenz, C.; Ziesche, S.; Partsch, U.; Neubert, H.: "Low Temperature Cofired Ceramics (LTCC)-Based Miniaturized Load Cells", *Proc. 35<sup>th</sup> International Spring Seminar on Electronics Technology, ISSE, Bad Aussee* (2012).
- Pike, G. E. and Seager, C. H.: "Electrical Properties and Conduction Mechanisms of Ru-Based Thick Film (Cermet) Resistors", *Journal of Applied Physics*, 12/77, S. 5152.
- Vionnet-Menot, S.; Grimaldi, C.; Maeder, T.; Ryser, P. and Strässler, S.: "Tunneling-percolation origin of nonuniversality: Theory and experiments", *Phys. Rev.B* 71 [6] 064201 (2005).
- Prudenziati, M. (Ed.): "Handbook of Sensors and Actuators 1: Thick Film Sensors", Elsevier Science B.V., 1994.
- Dietrich, S.; Kretzschmar, C.; Partsch, C.; Rebenklau, L.: "Reliability and Effective Signal-to-Noise Ratio of  $\text{RuO}_2$ -based Thick Film Strain Gauges: The Effect of Conductive and Glass Particle Size", *Electronics Technology*, 2009. ISSE2009. 32<sup>nd</sup> International Spring Seminar.
- Maeder, T.; Jacq, C.; Fournier, Y.; Ryser, P.: "Formulation and processing of screen-printing vehicles for sacrificial layers on thick-film and LTCC substrates", 32nd IMAPS – International Microelectronics and Packaging, Pultusk (2008), Proceedings.
- Maeder, T.; Jacq, C.; Fournier, Y.; Hraiz, W.; Ryser, P.: "Structuration of zero-shrinkage LTCC using mineral sacrificial materials", 17<sup>th</sup> EMPC – European Microelectronics and Packaging Conference & Exhibition, Rimini (2009), Proceedings.
- Biol, H.; Maeder, T.; Ryser, P.: "Application of graphite-based sacrificial layers for fabrication of LTCC (low temperature co-fired ceramic) membranes and micro-channels", *J. Micromech. Microeng.*, 17 p. 50-60, (2007).
- Malecha, K.; Maeder, T.; Jacq, C.: "Fabrication of membranes and microchannels in low-temperature co-fired ceramic (LTCC) substrate using novel water-based sacrificial carbon pastes", *Journal of the European Ceramic Society* 32 (12), 3277-3286, 2012.
- Lohrberg, C.: "Entwicklung LTCC-basierter hochempfindlicher Strömungssensoren", Diploma thesis 2012, Dresden University of Technology.
- Rabe, T.; Schiller, W. A.: "Zero Shrinkage of LTCC by Self-Constrained Sintering", *Int. J. Appl. Ceram. Technol.*, 2 [5] p. 374-382, (2005).
- Wagner, M.: "Prozessparameter und ihr Einfluss auf die Schwindungsgenauigkeit von hochintegrierten keramischen Mehrlagenschaltungen", Diss. Thesis of University Erlangen-Nuremberg.
- Neubert, H.; Partsch, U.; Fleischer, D.; Gruchow, M.; Kamusella, A.; Pham, T.: "Thick Film Accelerometers in LTCC-Technology – Design Optimization, Fabrication, and Characterization", *IMAPS Journal of Microelectronics and Electronic Packaging* 5 (2008) 4, 150-155.
- Neubert, H.: "Uncertainty-Based Design Optimization of MEMS/NEMS. In Gerald Gerlach, Klaus Wolter (Eds.): *Bio and Nano Packaging Techniques for Electron Devices - Advances in Electronic Device Packaging* 123. Springer 2012. pp. 119-140
- Slosarcik, S.; Banský, J.; Dovica, M.; Tkáč, M.: "Unconventional Application of Low Temperature Cofired Ceramics for (Under-) Pressure Sensors", *J. Electrical Engineering*, (48) 1997, Nr. 9-10
- Partsch, U.; Gebhardt, S.; Arndt, D.; Georgi, H.; Neubert, H.; Fleischer, D. and Gruchow, M.: "LTCC-

Based Sensors for Mechanical Quantities”, CICMT – Ceramic Interconnect and Ceramic Microsystems Technology, Denver 2009, Proceedings.

24. Fournier, Y.; Maeder, Th.; Boutinard-Rouelle, G.; Barras, A.; Craquelin, N. and Ryser, P.: “Integrated LTCC Pressure/ Flow/ Temperature Multisensor for Compressed Air Diagnostics”, *Sensors* 2010, 10(12), 11156-11173.
25. Thelemann, T.: Die LTCC-Technologie als Basis von sensorischen, aktorischen und fluidischen Komponenten für Mikrosysteme, Diss. thesis of Ilmenau University of Technology 2005

Arrived: 30. 08. 2012

Accepted: 20. 11. 2012

# *Wireless LTCC sensors for monitoring of pressure, temperature and moisture*

*Goran Radosavljevic*

*Vienna University of Technology, Institute of Sensor and Actuator Systems, Vienna, Austria*

**Abstract:** In this paper five different wireless sensors operating in the MHz range are presented. Embedded pressure sensors, temperature sensor and sensor for moisture detection all based on a passive wireless inductor-capacitor resonant circuit are realized, following specifications of the LTCC technology design and fabrication process. Considered resonant sensor principle is based on the passive resonant circuit (LC circuit), where changes are detected by variation of sensor capacitance, while inductor inductance remains invariable.

**Key words:** pressure sensors, temperature sensor, sensor for moisture detection, LTCC.

## *Brezžični LTCC senzorji za merjenje pritiska, temperature in vlage*

**Povzetek:** V članku je predstavljenih pet različnih brezžičnih senzorjev, ki delujejo v MHz področju. Vgrajeni senzorji pritiska, temperature in vlage temeljijo na brezžičnem induktivno-kapacitivnem resonančnem vezju in so izvedeni po specifikacijah LTCC tehnologije in proizvodnega procesa. Način pasivnega LC resonančnega vezja deluje na spremembo kapacitivnosti, pri čemer induktivnost ostaja nespremenjena.

**Ključne besede:** senzorji tlaka, senzorji temperature, senzorji vlage, LTCC.

\*Corresponding Author's e-mail: [Goran.Radosavljevic@tuwien.ac.at](mailto:Goran.Radosavljevic@tuwien.ac.at)

### *1. Introduction*

Monitoring of physical parameters, such as a pressure, temperature, moisture etc. and its measurement are widely employed in different areas of everyday life [1-5]. Precise detection of pressure or temperature variations is important in many applications e.g. automotive or aerospace industry, internal combustion or turbine engines etc. Control of moisture in products can be a vital part of the process of the product. The measurement of moisture has been of interest to building professionals for many years. Development of innovative methods for monitoring and measuring physical parameters in the civil engineering is therefore both commercially and scientifically important.

Sensors should have high sensitivity for the measured parameters and they should be insensitive to the other parameters of environment. Sensitivity should be followed with linearity of measured values in order to simplify the sensing element configuration. Small dimension of the sensors, low cost and non-contact

measurement system for data retrieval are very often required.

Choice of the adequate technology and properties of materials involved in the sensor realizations can ensure its application in chemically aggressive environments and in environments with extreme operating conditions. Since devices fabricated in the Low Temperature Co-fired Ceramic technology (LTCC) are based on glass ceramics they are very well suited for harsh environments. LTCC has been proven as a valuable tool for the realization of three dimensional microsystem structures [4-9]. The variety of available LTCC tapes, as well as a number of methods for substrate patterning, possibility of integration in one LTCC module fluidic channels, heaters, sensors, electronics put LTCC technology in the high-ranking place among technologies suitable for the fabrication of compact sensors devices.

This paper proposes a realization concept of a five resonant sensors configurations. Embedded pressure

sensors, temperature sensor and sensor for moisture detection all based on a passive wireless inductor-capacitor resonant circuit are realized.

In section 2 are presented design, detection principle, fabrication and measured results for pressure sensors. Temperature sensor and sensor for detection of moisture in building materials are presented in Section 3 and Section 4, while in section 5 conclusions are made.

## 2. Pressure sensors

Three pressure sensors are designed and fabricated in the LTCC technology. The sensors are realized as a parallel resonant circuit where pressures changing are detected by variation of capacitance, while inductor remains constant.

### 2.1 Design, geometrical parameters and theoretical model of the pressure sensors

The first sensor can be found suitable for applications in chemically aggressive environments, since sensor membranes are formed as a sandwich composition comprising electrode layers placed between two dielectric tapes and connected in parallel with inductor windings, Fig. 1. The sensor is built up by seven laser

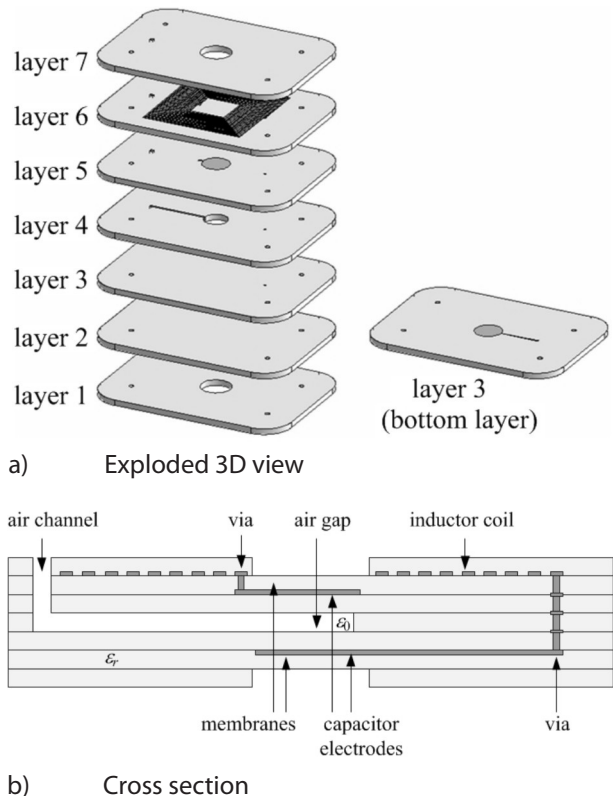


Figure 1: Pressure sensor type 1.

micromachining tapes carrying out vias and holes. Capacitor plates are printed on the top of layer 5 and to the bottom of layer 3, while inductor is placed on the layer 6. Capacitor electrodes are embedded in an each of membranes, which are separated by the cavity. Membranes exposed to the pressure to be measured are formed by the tape layer 2, 3, 5 and 6.

The second design of the pressure sensor incorporates capacitor electrodes that are placed on the outer side of membranes enabling direct application of the pressure to be measured, Fig. 2. Formation of the outer electrodes is attained by implementation of the thin film metallization deposited in the post firing process. This procedure for sensor realization differs from the firstly presented sensor configuration with buried electrodes, resulting in increased sensitivity.

The last sensor design of the pressure sensor was realized with intention to minimize overall sensor dimension. The inductor coil is realized in two layers resulting in miniaturization of the sensor overall dimension, Fig. 3.

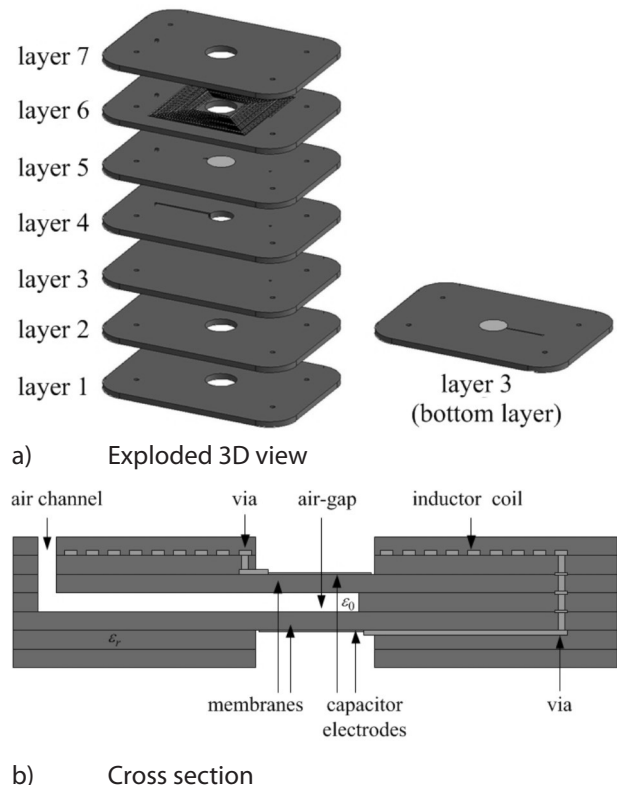
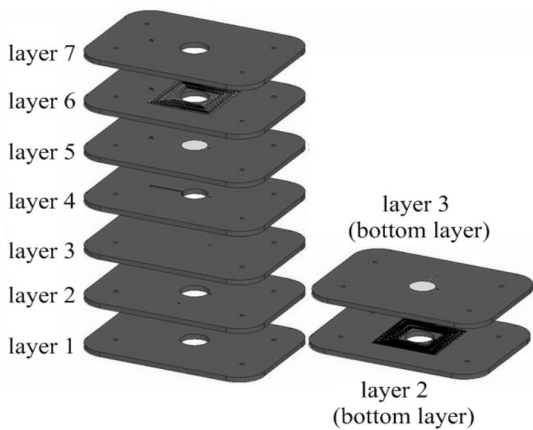


Figure 2: Pressure sensor type 2.

Measured relevant electrical and mechanical characteristic of used LTCC tapes are presented in the Table 1 and Table 2, while geometrical parameters of all sensors are presented in the Table 3 and Table 4.



**Figure 3:** Explode view of sensor type 3.

**Table 1:** Physical properties of LTCC tapes.

Material	Thickness in green state	Thickness after firing
CeramTec GC	100 [μm]	80 [μm]
Heraeus CT707	125 [μm]	95 [μm]

**Table 2:** Measured parameters of LTCC tapes.

Material	Relative permittivity @ 1 kHz	Young's modulus @ 25 °C
CeramTec GC	7.8	61.36 [GPa]
Heraeus CT707	6.39	53.49 [GPa]

**Table 3:** Geometrical parameters of inductors design.

Parameters	Dimension		
	Type 1	Type 2	Type 3
d <sub>in</sub>	10 [mm]	10 [mm]	10 [mm]
s	200 [μm]	270 [μm]	270 [μm]
w	350 [μm]	285 [μm]	285 [μm]
N	17.5	17.5	9.75 (x2)

$d_{in}$  - minimal distance between opposite segments of inner winding,  $s$  - spacing between adjacent segments,  $w$  - width of conductor line,  $N$  - number of windings.

**Table 4:** Geometrical parameters of capacitors design.

Parameters	Dimension	
	Type 1	Type 2 and Type 3
av	3.3 [mm]	3.5 [mm]
a	4 [mm]	4.35 [mm]
tcond	12 [μm]	12 [μm]
tm	80 [μm]	95 [μm]
tg	80 [μm]	95 [μm]

$a_v$  - hole radius,  $a$  - electrode radius,  $t_{cond}$  - conductor thickness,  $t_m$  - tape thickness,  $t_g$  - cavity thickness.

Overall dimensions of the fabricated sensors are presented in Table 5.

**Table 5:** Overall sensors dimension.

Sensor	Dimension
Type 1	35 x 29 x 0.56 [mm]
Type 2	35 x 29 x 0.665 [mm]
Type 3	24.5 x 20.5 x 0.665 [mm]

Theoretical model and wireless detection will be explained for the sensor type 2. Pressure variations are detected by changes in the sensors capacitance during deflection. The sensor capacitance is a complex structure composed from four capacitances - two directly under/above the air-gap ( $C_1$  and  $C_3$ ), the air-gap capacitance ( $C_2$ ) and the annulus capacitance ( $C_4$ ), Fig. 4.

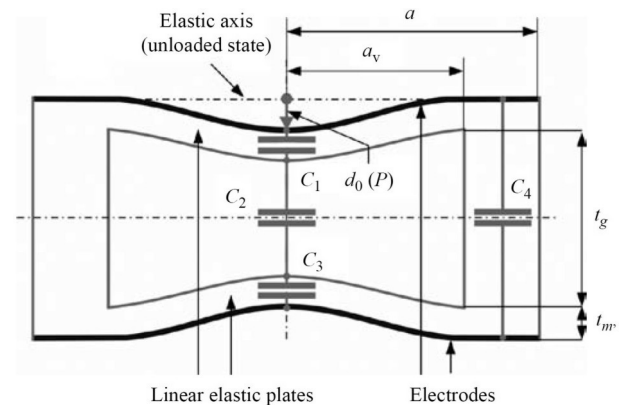


**Figure 4:** Sensor capacitance corresponding to attribution of individual capacitances.

Deflection of membranes occurs when pressure is induced, resulting in the change of the sensor overall capacitance,  $C_s(P)$ . Value of  $C_s(P)$  has been derived in [8, 9] and can be obtained as

$$C_s(P) = C_s(0) \frac{ar \tanh \left( \frac{\sqrt{2d_0(P)}}{\sqrt{t_g + \frac{2t_m}{\epsilon_r}}} \right) + \frac{\epsilon_0 \epsilon_r \pi (a^2 - a_v^2)}{2t_m + t_g}}{\frac{2d_0(P)}{t_g + \frac{2t_m}{\epsilon_r}}} \quad (1)$$

where  $C_s(0)$  is the equivalent capacitance for the sensors at zero pressure can be determined as,

$$C_s(0) = \frac{\epsilon_0 \epsilon_r a_v^2 \pi}{2t_m + \epsilon_r \cdot t_g} + \frac{\epsilon_0 \epsilon_r \pi \cdot (a^2 - a_v^2)}{2t_m + t_g} \quad (2)$$

and  $d_0(P)$  represent the central deflection of membranes.

Values of the membranes central deflection increase under load consequently leading to increase the overall capacitance of the sensor as can be seen from the Fig 5.

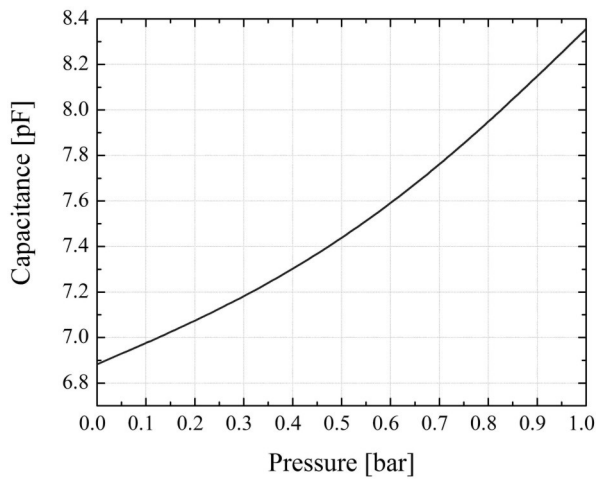


**Figure 5:** Sensor capacitance versus applied pressure.

For the determination of the inductance values monomial expression present in [10] is used.

Sensor resonant nature enables a wireless system for data retrieval using antenna coil, which is present on the Fig 6.

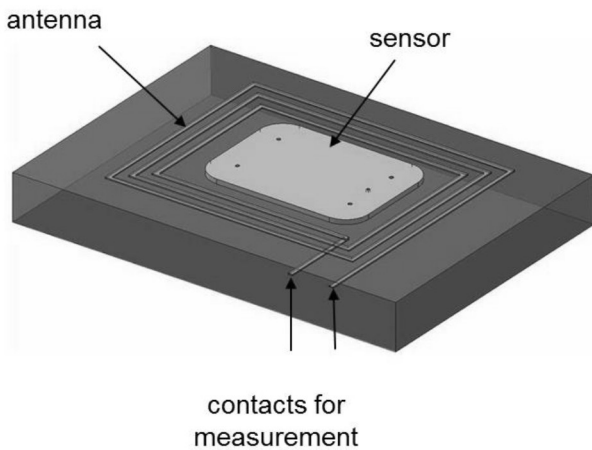


**Figure 6:** Wireless measurement setup scheme.

Resonant frequency of the sensor antenna system is a pressure dependent value and can be determinate from the system input impedance when the imaginary part of that value becomes zero, Fig 7. Dependence of the resonant frequency of the sensor antenna system versus pressure are presented on the Fig. 8 and Fig. 9.

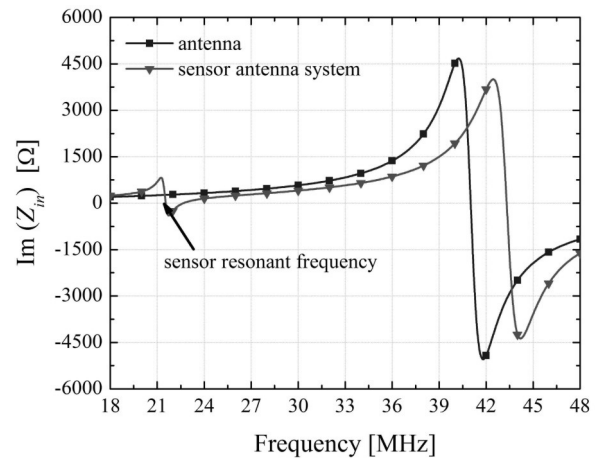


**Figure 7:** Imaginary part of the input system impedance versus frequency for zero pressure.

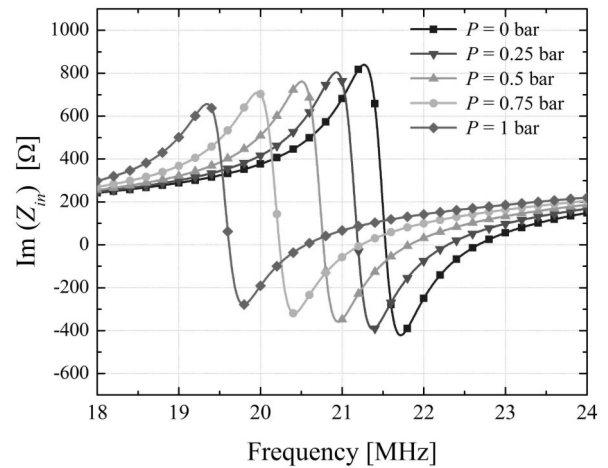


**Figure 8:** Imaginary part of input impedance versus frequency for different pressure values.

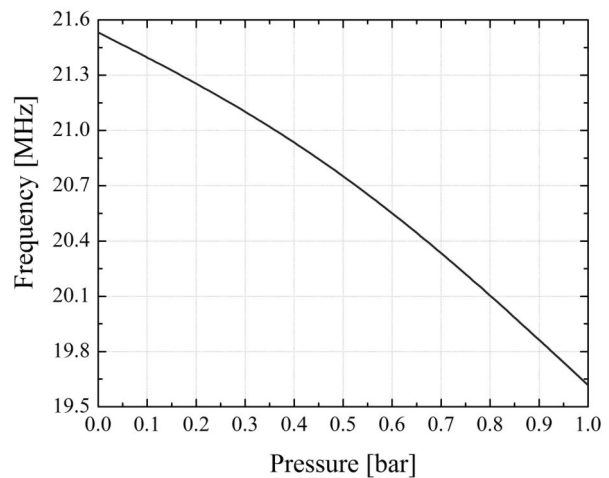


**Figure 9:** Resonant frequency versus pressure

As can be seen from the Fig. 8 and Fig. 9 that pressure variations influence on the capacitance value, resulting in a shift of the sensors resonant frequency.

Increase of the pressure induced onto sensor membranes leads to an increase of the sensor capacitance and consequently results in a decrease of the system resonant frequency value.

### 2.2 Fabrication and measured results

Sensor type 1 is fabricated by application of the standard LTCC technology which covers structuring of tapes using laser micromachining, metalizing, laminating, and finally co-firing the stack of LTCC tape layers. CeramTec GC tapes and compatible silver pastes (Heraeus TC 7303 for line printing and Heraeus TC 7304 for via filling) [11, 12] have been used for the sensor fabrication. Isostatic lamination of the collated LTCC layers has been performed at pressure of 50 bar, temperature of 75 °C, and exposure time of 5 min. Firing of the laminated LTCC stack has been conducted in a six zone belt furnace at peak temperature of 900 °C and total firing cycle time of 210 min.

Sensors type 2 and type 3 is also realized implementing the conventional LTCC technology. Heraeus CT 707 tapes are combined with compatible silver pastes (Heraeus TC 7303A for line printing and Heraeus TC 7304 for via filling) [12] are used for sensor fabrication. Collated tape layers are isostatically laminated at pressure of 70 bar and temperature of 75 °C for 5 minutes. The laminated stack is fired in a six zones belt furnace at peak temperature of 880 °C and total firing cycle time of two hours. This is followed by thin film deposition of silver electrodes onto sensor membranes using the sputtering method.

Resonant operating principle of the sensor allows the possibility for the usage of wireless measurement system for the data retrieval. The measurement setup comprises an antenna and a device for the resonance detection. During the measurement procedure, the sensor is placed in the center of the antenna. The test setup for wireless recording of sensor characteristics is built up by a clamping system where two plates made from acrylic glass, are carrying ducts for the supply of pressurized air, Fig. 10. The exhaust holes for the air in the center of the plates are positioned exactly above the sensor membranes exerting the pressure to be measured. The test setup is additionally equipped with a rectangular antenna coil required for the wireless measurement which is connected to the spectrum analyzer (Anritsu MS620J).

The measured results, compared with the theoretical results for the sensor type 2 are presented in the Fig. 11, while compared measurement results of all sensors are presented in the Fig. 12.

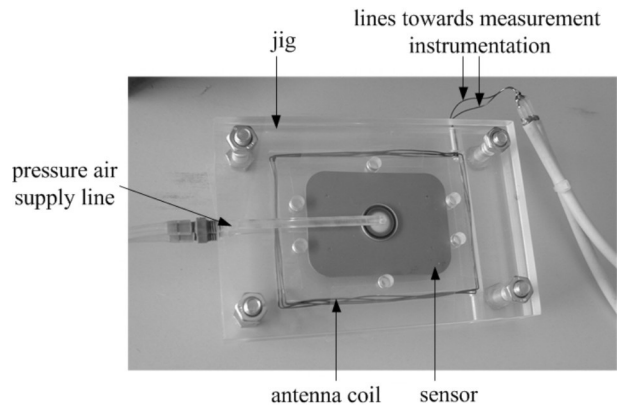


Figure 10: Test setup for the measurement.

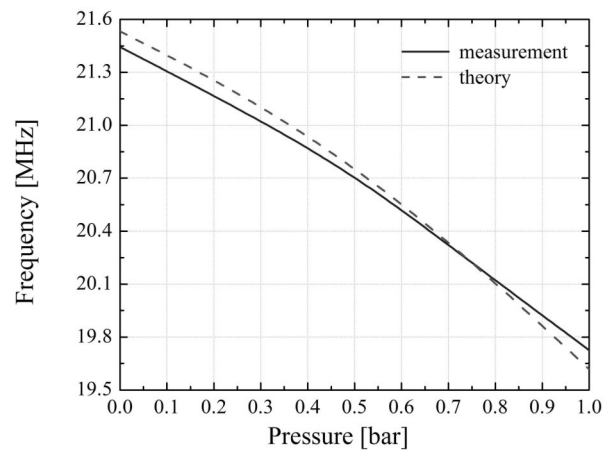


Figure 11: The theoretically and measured results for the pressure sensor type 2.

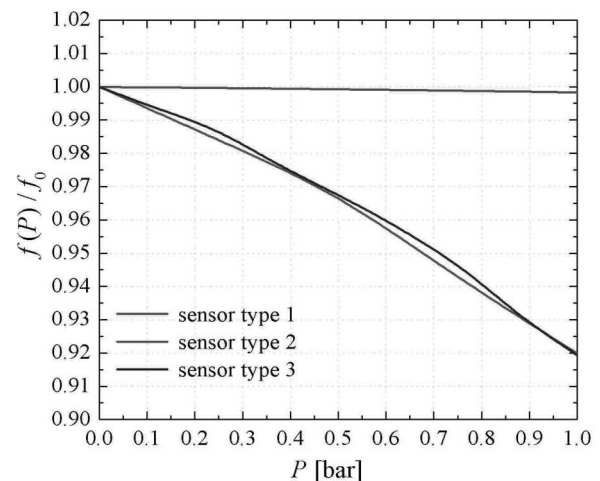


Figure 12: Relative change of sensors resonant frequency versus pressure (measured results).

As can be seen from the Fig. 11 there is a good agreement between theoretical and measured results. It is proved that theoretical model describe sensor antenna system very well.

From the Fig. 12 can be seen that formation of the sputtered thin film electrodes and usage of tapes with higher elasticity significantly contributes to the increase of sensor sensitivity compared to designs for sensor type 1. In addition, 3D realization of inductor coil does not decrease the sensor sensitivity, while the overall dimension of sensor can be significantly reduced.

### 3. Temperature sensor

Temperature measurement is state of the art using many different techniques reaching from thermocouples over resistors (PTC, NTC, Pt100) to fully digital wireless silicon systems. The approach to use a temperature dependent capacitor along a coil to form a resonating structure leads to a wireless temperature sensor that is embedded in a rugged ceramic body and resistant to corrosive environments and can be read by means of an antenna coil.

The sensor introduced in this paper permits temperature measurement in a high pressure, high temperature and even corrosive environment due to its realization in LTCC technology. Design of the temperature sensor is presented on the Fig. 13.

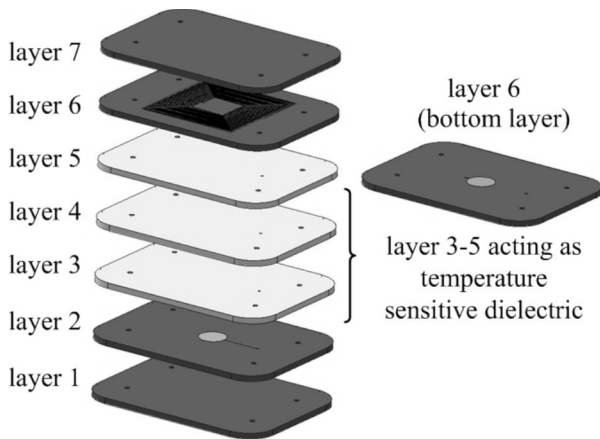


**Figure 13:** Temperature sensor exploded 3D view.

The sensor consists of several layers of LTCC tapes where the inner layers carry the actual sensor components (inductor and capacitor) and additional outer layers increase the mechanical stability of the device. Electrodes of the capacitor are screen-printed on the top of layer 2 and bottom of layer 6, while the square spiral shaped inductor is placed on top of layer 6. For the realization of the sensors, Heraeus CT707 in combination with Heraeus CT765 (sensitive dielectric - ferroelectric) are used. The electrode radius is 4 mm, while geometrical parameters of inductor are presented in the Table 6.

**Table 6:** Geometrical parameters of inductors design.

Parameters	Dimension
d <sub>in</sub>	10 [mm]
s	270 [μm]
w	285 [μm]
N	17.5

$d_{in}$  minimal distance between opposite segments of inner winding,  $s$  - spacing between adjacent segments,  $w$  - width of conductor line ( $w$ ),  $N$  number of windings.

The working principle of the sensor is based on a resonant circuit (inductor and capacitor) and changes its resonant frequency due to thermal expansion of the bulk material and change in permittivity of a special dielectric layer. The capacitance of sensor can be calculated using the following equation [13].

$$C_s = \frac{\epsilon_0 \cdot \epsilon_r(T) \cdot A(T)}{d(T)} \tag{3}$$

where  $A(T)$  is temperature dependent plate area  $d(T)$  temperature dependent plate distance and  $\epsilon_r(T)$  temperature dependent relative permittivity.

The biggest influence on changing the sensor capacitance with the temperature has relative permittivity of the material. Relative permittivity increases if ambient temperature raises leading to increasing the capacitance of the sensor, while value of inductance remains constant, as a result that sensor resonant frequency decrease.

The sensor is fabricated using the standard LTCC fabrication process. Tape layers were first structured with a Nd:YAG laser. After the following screen-printing step using Heraeus TC7304 as via-filler and TC7303 as conductor paste, the layers are dried, stacked in a lamination fixture and laminated for 3 minutes at a temperature of 70 °C and a pressure 60 bar in an isostatic press. Firing of the tapes has been performed in a conventional six zones thick film furnace with a cycle time of 2 h and 880 °C peak temperature. Fabricated sensor element is presented on the Fig. 14.

The measurement set-up shown in Fig. 15 consists of a heat resistant alumina plate that is held 2 cm above a jig that contains a rectangular antenna coil Cu-wire. A hot air stream heats the sensor that is located on the top of the alumina plate and is surrounded by heat resistant insulating bricks (the bricks have been removed for clarity in Fig. 15) to prevent excessive heat loss. Temperature measurement via thermocouples on top and bottom side of the sensor provided defined thermal conditions during measurement.



**Figure 14:** Fabricated temperature sensor (top view).

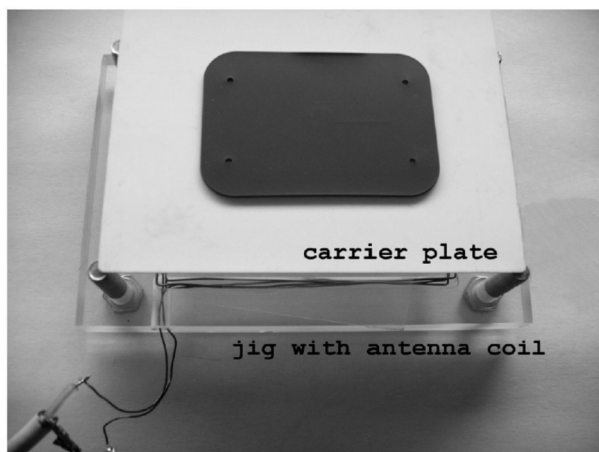


**Figure 15:** Measurement set-up.

For the measurement, a network spectrum analyzer is connected to the antenna coil via two BNC-terminated coax cables (RG58). Measurements are taken as linear magnitude plots in the relevant range. The measured results for the temperature sensor is presented in the Fig. 16.

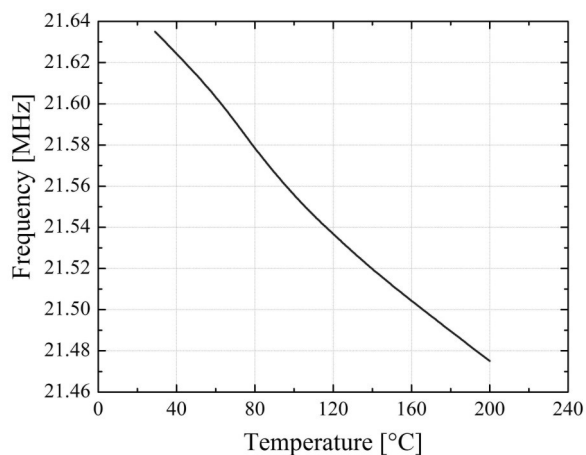


**Figure 16:** Resonant frequency versus temperature.

As can be seen from the measured results that the resonant frequency of the sensor decreasing when ambient temperature increase. Reason for that is the capacitance of the sensor which increases due to the increasing of the relative permittivity of material over the temperature.

#### 4. sensor for detection of moisture in building materials

In order to know the condition of buildings and other construction structures in the construction industry, there is a need to monitor moisture content. In this way, small (and cheap) repairs at the right time, to extend the life time of a building, are ensured. This is especially important for objects which are sensitive to environmental influences.

In this section it will be presents a LTCC sensor for measuring moisture content of building material (clay brick). The proposed sensor consists of two dielectric layers [14], Fig. 17. The LC structure was screen-printed on the first dielectric layer (as a substrate) and the second layer has a window over capacitor's electrodes. Through this window the sensor is exposed to moisture (thanks to the hydrophilic behaviour), which will then cause change of its relative permittivity and total capacitance, and consequently the resonant frequency of the LC sensor.

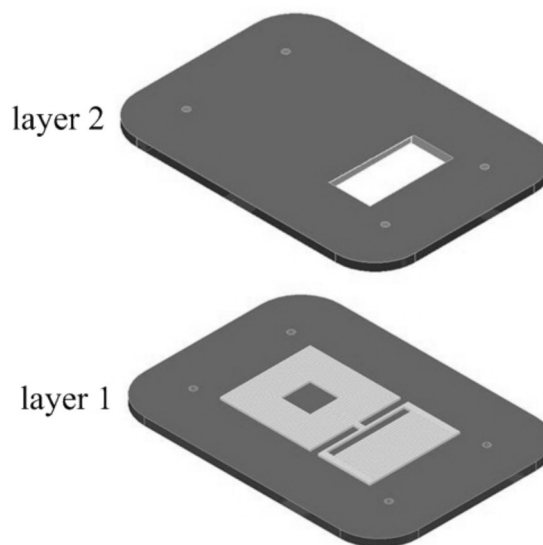


**Figure 17:** Exploded view of the sensor for moisture detection.

This LC sensor is realized that the inductance of the sensor remains constant. The inductive part was covered

with dielectric layer. Contrary to this, the capacitance of the interdigitated electrode system is changed with the variation of the permittivity of the medium (exposed through the small window from the top side of the sensor). This will cause the shift of sensor's resonant frequency. The capacitance of the interdigitated can be calculate using equation proposed in [15, 16],

$$C_s = \frac{\epsilon_{re} \cdot 10^{-2}}{18\pi} \cdot \frac{K(k)}{K'(k)} \quad (4)$$

where  $l$  is length of the fingers expressed in micrometers and  $N$  is number of fingers. The ratio of complete elliptic integral of first kind  $K(k)$  and its complement  $K'(k)$  is given by [4,5].  $\epsilon_{re}$  is the effective dielectric constant of the microstrip line width  $w$ , and define by following equation,

$$\epsilon_{re} = \frac{\epsilon_r + 1}{2} + \frac{\epsilon_r - 1}{2} \cdot F\left(\frac{w}{h}\right) - M \quad (5)$$

$F$  and  $M$  are given explain in [15, 16].

As can be seen from equation (4) and (5) if relative permittivity is higher capacitance of the sensor will be bigger, while inductor remains constant, resulting in a decreasing the resonant frequency of the sensor.

Dimensions of the sensor elements are presented in the Table 7 and Table 8.

**Table 7:** Geometrical parameters of inductors design.

Parameters	Sensor
d <sub>in</sub>	7.6 [mm]
s	100 [µm]
w	500 [µm]
N	13

$d_{in}$  - minimal distance between opposite segments of inner winding,  $s$ - spacing between adjacent segments,  $w$ - width of conductor line,  $N$  - number of windings.

**Table 8:** Geometrical parameters of capacitor design.

Parameter	Dimension
w	500 [µm]
s	100 [µm]
l	13.2 [mm]
N	18
dx	13.2 [mm]
dy	21 [mm]

$w$  - finger width,  $s$  - spacing,  $l$  - length of fingers,  $N$  - number of fingers,  $d_x$  - total length,  $d_y$  - total width

Total dimension of the sensor are (38.2 x 24 x 0.4) mm.

The sensor was fabricated using the LTCC technology, comprising the processing steps of structuring tapes by means of laser micro-machining, metallizing, laminating and co-firing the stack of two LTCC tape layers. For the sensor fabrication Heraeus CT700 [12] dielectric tapes were combined with compatible silver paste Heraeus TC 7303A for conductive line printing. Collated tape layers were isostatically laminated at pressure of 70 bars and temperature of 75 °C for 3 minutes. The laminated stack was fired in a six zones belt furnace at a temperature peak of 880 °C and a total firing cycle time of 2 hours. Fig. 18 illustrates the fabricated sensor. In the Fig. 19 is presented measurement setup and measured results (for the clay brick) are presented in the Fig. 20.

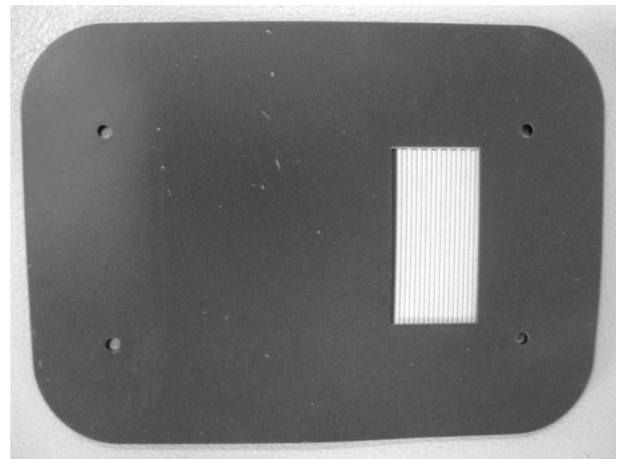


**Figure 18:** Fabricated sensor for moisture detection (top view).



**Figure 19:** Experimental setup for measuring the resonant frequency of the sensor embedded into building material.

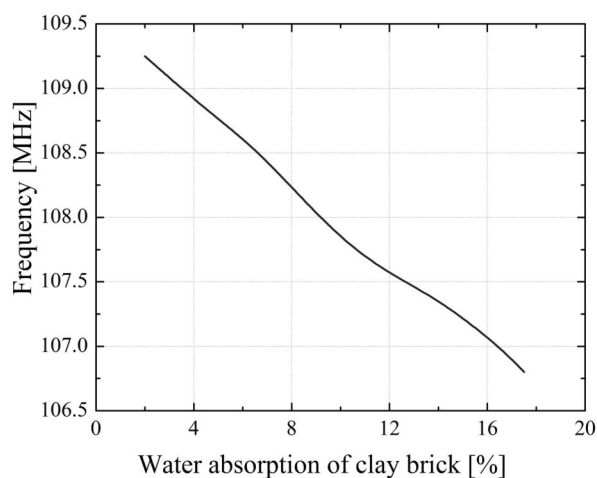


**Figure 20:** Resonant frequency versus percent of water absorption.

The measure results shows that the resonant frequency changes from 109.2 MHz to 106.9 MHz while the percentage of water ranging from 2% to 17.5%. The variation of resonant frequency changes is 2.3 MHz while the change in moisture content is 15.5%. It can also be seen that the deviation of measured values from the ideal linear dependence is very small. The sensitivity of the sensor in this case is 169 kHz/percentage of water content.

## 5. Conclusion

The sensor modules presented in this paper are a passive LC resonant type sensor designed for the operation in MHz range and are fabricated using the conventional LTCC technological process. Three pressure sensors, one temperature and one sensor for the moisture detection are designed and fabricated in the LTCC technology. For all sensors a wireless measurement set-up is used for non-contact retrieval of the measured data.

It is shown that formation of the sputtered thin film electrodes and usage of tapes with higher elasticity significantly contributes to the increase of sensitivity of the pressure sensor. While 3D realization of inductor coil does not decrease the sensor sensitivity, it contributes to the significant reduction of sensor overall dimensions.

The experiments have shown, that LTCC technology offers the possibility to realize different wireless readout sensors with nearly linear characteristics.

## Acknowledgements

This work is done within the scope of the FP7 SENSEIVER project (Low-cost and energy-efficient LTCC sensor/IR-UWB transceiver solutions for sustainable healthy environment project references 289481) and integrated within Scientific and Technological Co-operation between Austria and Romania 2012-2013 (Development of Environment sensors with LTCC technology project number RO 10/2012). The author would like to thank Dr. C. P. Kluge (CeramTec AG) for maintenance of ceramic tapes.

## References

1. Inaudi D, Glisic B and Vurpillot S. "Packaging interferometric sensor for civil structural monitoring," 13th International Conference on Optical Fiber Sensors, Kyongju, Korea, 1999.
2. Soga K, Cipolla R, Bennett P, Seshia A, Middleton C, Wassell I, Stajano F, Hoult N. "Intelligent city - sensors for monitoring civil engineering infrastructure," CamBridgeSens, 2008.
3. Ong J, You Z, Mills-Beale J, Lim Tan E, Pereles B, Ong K G. "A wireless, passive embedded sensor for real-time monitoring of water content in civil engineering materials," IEEE Sensors Journal 2008;8:2053-58.
4. L.J. Golonka, "Technology and applications of Low Temperature Cofired Ceramic (LTCC) based sensors and microsystems", Bulletin of the Polish Academy of Sciences, Vol. 54, No. 2, 2006, pp. 221-231.
5. W. Smetana, "Low temperature ceramic processing for microsystem application," Ceramics Processing in Microtechnology, Whittles Publishing, 2009, pp. 208-225.
6. W. Smetana, B. Balluch, G. Stangl, E. Gaubitzer, M. Edetsberger, G. Köhler, "A multi-sensor biological monitoring module built up in LTCC-technology", Microelectronic Engineering, Vol. 84, No. 5-8, 2007, pp. 1240-1243.
7. M.G.H. Meijerink, E Nieuwkoop, E.P. Veninga, M.H.H. Meuwissen, M.W.W.J.Tijdink, "Capacitive pressure sensor in post-processing on LTCC substrates", Sensors and Actuators A, 2005, pp. 234-239.
8. G. Radosavljević, Lj. Živanov, W. Smetana, A. Marić, M. Unger, L. Nađ, "A wireless embedded resonant pressure sensor fabricated in the standard LTCC technology," IEEE Sensor Journal, Vol. 9 No. 12, December 2009, pp. 1956-1962.
9. G. Radosavljević, W. Smetana, A. Marić, Lj. Živanov, M. Unger, G. Stangl, "Parameters affecting the

- sensitivity of LTCC pressure sensors," *Microelectronics International*, Vol. 27, No. 3, 2010, pp. 159-165.
10. S. S. Mohan, M. D. M. Hershenson, S. P. Boyd, T. H. Lee "Simple accurate expressions for planar spiral inductances," *IEEE Journal Of Solid-State Circuits*, Vol. 34, No. 10, October 1999, pp. 1419-1424.
  11. <http://www.ceramtec.com/ceramtape/>
  12. [http://heraeusthickfilm.com/en/productsapplications/lccmaterials/lcc\\_materials\\_1.aspx](http://heraeusthickfilm.com/en/productsapplications/lccmaterials/lcc_materials_1.aspx)
  13. M. Unger, W. Smetana, G. Radosavljević, Lj. Živanov, L. Nađ, A. Marić, "A Wireless Readout Temperature Sensor Realized in LTCC-Technology," XXXII International Conference of IMAPS - CPMT IEEE Poland, Pułusk 21 - 24 September 2008.
  14. M. Maksimovic, G. Stojanovic, M. Radovanovic, M. Malesev, V. Radonjanin G. Radosavljevic, W. Smetana, "Application of a LTCC sensor for measuring moisture content of building materials," *Construction and Building Materials*, vol. 26 br. 1, pp. 327-333, 2012. ISSN: 0950-0618.
  15. B. Rehak, N. Blaz, M. Damjanovic, A. Maric, Lj. Zivanov, "Influence of variuos parameters on capacitance of Interdigital capacitors" *Proceedings of the 7th International Symposium Nikola Tesla*, Belgrade, Serbia, pp. 65-72, (2011).
  16. Inder Bahl, "Lumped Elements for RF and Microwave Circuits", Artech House, Boston-London, 2003.

Arrived: 22. 08. 2012

Accepted: 22. 11. 2012

# Wide Band-stop Microwave Microstrip Filter on High-resistivity Silicon

Dusan Nesić, Ivana Jokić, Milos Frantlović, Milija Sarajlić

IHTM-CMTM, University of Belgrade, Belgrade, Serbia

**Abstract:** Low-resistivity silicon (standard CMOS-grade silicon) is a troublesome issue for the microwave passive components. One solution is using high-resistivity silicon (HRS). Wide band-stop filter on high-resistivity silicon (HRS),  $5 \text{ k}\Omega\text{-cm}$ , is introduced. The filter is simulated and successfully fabricated in microstrip technology. Relative stop band width is over 70 % for 20 dB suppression. Reflection, S11, in the pass band is -17 dB or lower. Metallization was sputtered aluminum (Al) and silver epoxy was used for bonding.

**Key words:** Microwave, High-resistivity silicon (HRS), Band-stop filter, Sputtered aluminum (Al)

## Širokopasovni zaporni mikrovalovni mikrotrakasti filter na visoko uporovnem siliciju

**Povzetek:** Nizko uporovni silicij (standardni CMOS silicij) ni primeren za mikravalovne pasivne elemente. Ena izmed rešitev je visoko uporovni silicij (HRS). Predstavljen je širokopasoven zapeerni filter na visoko uporovnem  $5 \text{ k}\Omega\text{-cm}$  siliciju. Filter je simuliran in uspešno izveden v mikrotrakasti tehnologiji. Relativna bločna širina je preko 70 % pri dušenju 20 dB. Refleksija S11 v prepustnem pasu je -17 dB ali manj. Metalizacija je izvedena z naprševanjem aluminija, bondiranje pa s srebrno pasto.

**Ključne besede:** mikro valovi, visoko uporovni silicij (HRS), pasovni zaporni filter, napršeni aluminij

\* Corresponding Author's e-mail: nesicad@nanosys.ihtm.bg.ac.rs

### 1. introduction

Microwave passive components on silicon (Si) substrate in microstrip technique are important for microwave integration. Wide band-stop filters are, also, important function of passive components. Si is a vital material for present microelectronics but has some functional problems.

Low-resistivity silicon (standard CMOS-grade silicon, resistivity  $1 - 30 \Omega\text{-cm}$ ) is a troublesome issue for the microwave passive components [1], [2]. Due to high substrate loss it is a problem to fabricate useful traditional passive microwave components on such substrate. One of the solutions is to apply benzocyclobutene (BCB) to serve as the interface layer [2], [3]. BCB has a low dielectric loss and low dielectric constant. The problem is a new material in technology and a weak compactness of the structure due to two substrates. Thin BCB layer, also, need very narrow microstrip lines ( $\ll 100 \mu\text{m}$ ).

Another solution is using high-resistivity silicon (HRS) with resistivity higher than  $2 \text{ k}\Omega\text{-cm}$  [1], [4]-[7]. Simulated and successfully fabricated microstrip attenuator

on high-resistivity silicon (HRS) was presented in [4]. In [4] microstrip lines were fabricated as a metallization of  $2 \mu\text{m}$  thick sputtered aluminum (Al) layer. Examples of the sputtered Al applied to HRS was, also, reported in [5,6]. Aluminum was chosen as the conductor because this is the standard foundry metal [6], even for the band around 30 GHz [5].

The aim of this paper is to simulate and fabricate wide band-stop filter on the HRS substrate. The idea is to simulate circuit with ideal waveguides and to apply it for fabrication of microstrip filter structures [8]. The solution is adjusted to the conditions of HRS and common etching technological ability. The narrowest microstrip line is fixed to  $50 \mu\text{m}$  for the classical etching technology. Metallization is sputtered Al and silver epoxy is used for bonding SMA connectors to the microstrip lines [9, 10].

### 2. Design and simulation

Calculation of the circuit with the ideal waveguide is done according to design curve presented in [8]. The

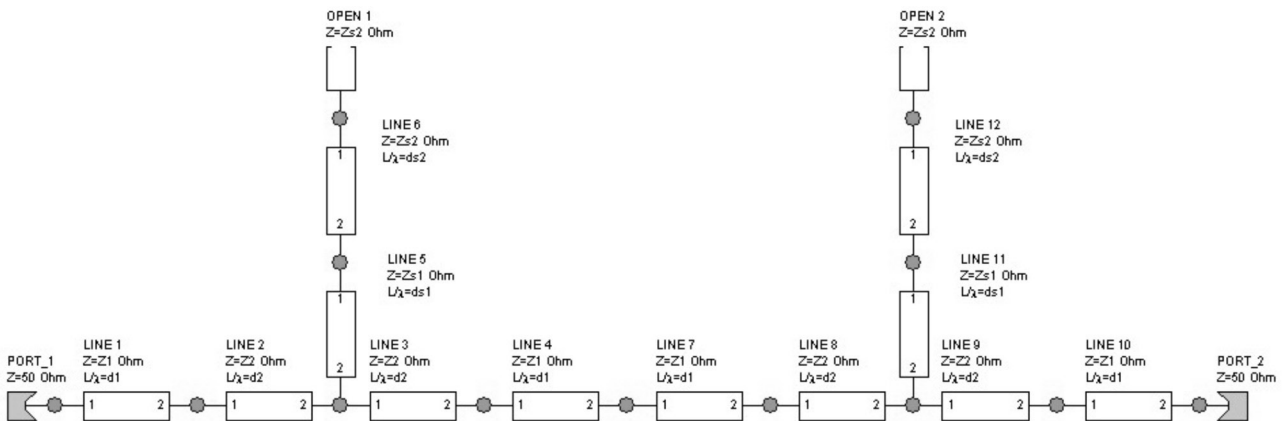


**Figure 1:** Ideal circuit of the introduced low-pass filter,  $Z_2 = Z_{s1} = 84.2 \Omega$ ;  $Z_1 = Z_{s2} = 31.9 \Omega$

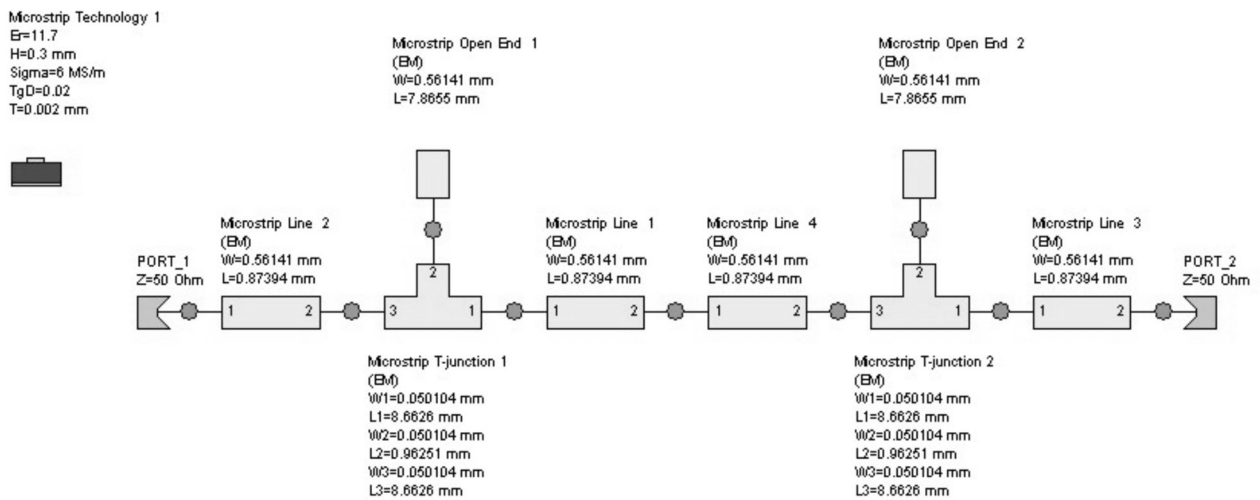
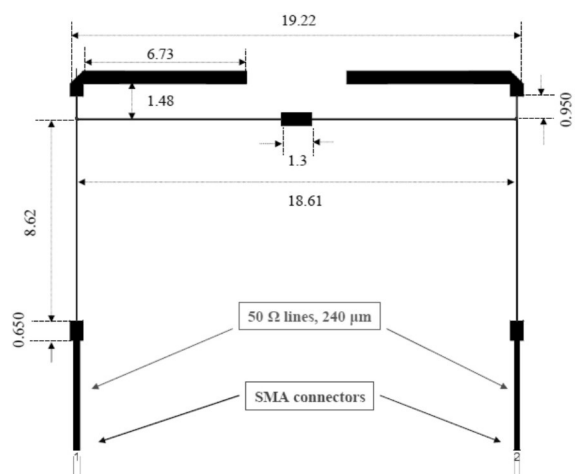


**Figure 2:** Ideal microstrip presentation of the filter (narrow line,  $84.2 \Omega$ , is  $50 \mu\text{m}$ ).

curves present optimal values of the pair of maximum and minimum characteristic impedances.

Characteristics of the used HRS substrate are: substrate height  $h = 300 \mu\text{m}$ , relative dielectric constant  $\epsilon_r = 11.7$  and resistivity is  $\rho = 5 \text{ k}\Omega\text{-cm}$ . Dielectric losses were chosen to be  $\text{tg}\delta = 0.02$ . Metallization is Al thickness  $t = 3 \mu\text{m}$  with chosen conductivity to be low,  $6 \text{ MS/m}$ . The highest characteristic impedance is to adjust common etching technological ability. It is related to the minimum microstrip line width which is chosen to be  $50 \mu\text{m}$  and corresponds to  $84.2 \Omega$ . The lower characteristic impedance is  $31.9 \Omega$ . Ideal filter circuit and the ideal filter in microstrip technology are presented in fig. 1 and fig. 2, respectively.

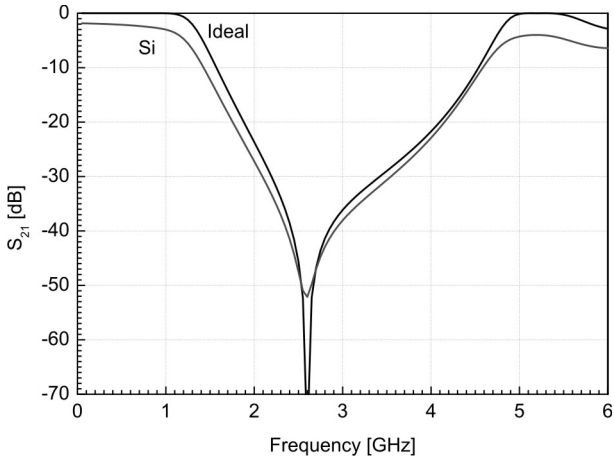
Fig. 3 presents pattern of the introduced filter. Wide microstrip lines are something shortened according to influence of edge effect. Open stubs are folded to reduce the size of the structure.  $50 \Omega$  lines ( $240 \mu\text{m}$  wide) for connectors are included at both ends, as shown in fig. 3.



**Figure 3:** Compact version of the filter ( $19.22 \text{ mm} \times 11.36 \text{ mm}$ ). Narrow lines are  $50 \mu\text{m}$  wide ; wide lines are  $560 \mu\text{m}$  wide.

Simulation results for the ideal model, fig. 1, and 3D electromagnetic simulation (IE3D Zeland Software ver. 10) of the real pattern, fig.3, are presented in fig. 4. They

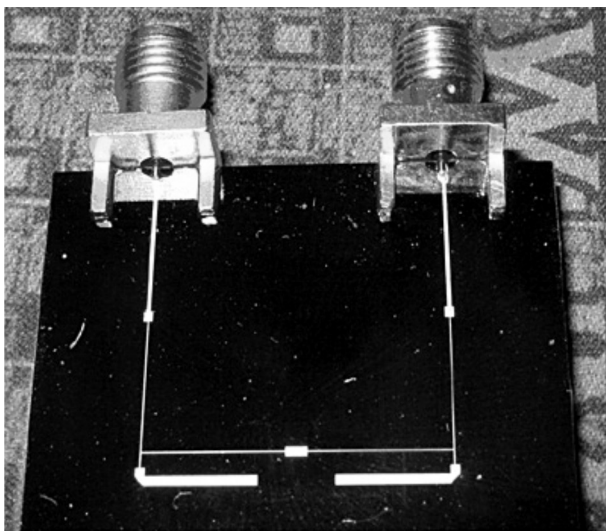
are in agreement for frequency position of the stop-band minimum and the filter shape. Logical difference is for losses, especially in the pass-band region. Relative band-width of the stop band is around 70% for 20 dB suppression.



**Figure 4:**  $S_{21}$  of ideal circuit and 3D EM simulation

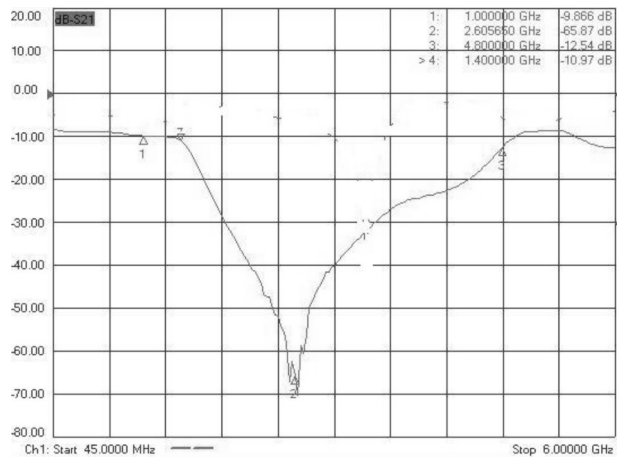
### 3. Fabrication and measurement

Photo of the fabricated filter with SMA connectors is presented in fig. 5. Aluminum (Al) with 1% of Si was sputtered on Si substrate (wafer) to form metallization 3  $\mu\text{m}$  thick. Content of 1% of Si obtains no penetration of Al into the Si substrate. Pattern of the filter, presented in fig. 3, was etched in Al metallization. SMA connectors were bonded on the ends of the 50  $\Omega$  microstrip lines (240  $\mu\text{m}$  wide, fig. 3) using silver epoxy. Ground plane is a brass metal plate bonded to the lower side of the silicon substrate using silver epoxy.



**Figure 5:** Photo of the fabricated filter with SMA connector

It was measured in dark.  $S_{21}$ -parameters for the structure in fig. 5 are presented in fig. 6. Losses in the pass-band are high (-10 dB). Beside that, they are in an agreement with graphics in fig. 4 for frequency position of the stop-band minimum and the filter shape. The problem were only losses. The reason for the high losses was discovered to be out of date (old) silver epoxy.



**Figure 6:** Measured  $S_{21}$  of the filter using out of date (old) silver epoxy

Then, SMA connectors were removed and both the connectors and the contact area on the microstrip were cleaned from the old silver epoxy. The SMA connectors were again bonded using the fresh silver epoxy. It was also measured in dark.  $S$ -parameters for the filter with the fresh silver epoxy are presented in fig. 7.

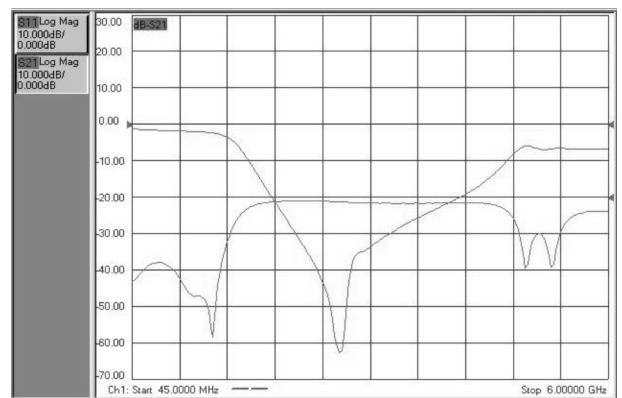


**Figure 7:** Measured (in dark)  $S$ -parameters of the filter using fresh silver epoxy

Measurement under light source illumination can degrade filter characteristics in pass-band. The illumination causes higher losses in the pass-band [11] which is not acceptable for the filter. According to that, operation of the filter is only in dark (protected from light). One example of extreme illumination is presented in fig. 8: filter positioned 1m from 1000 W photo lamp gets totally degraded pass-band. Even small power laser (650

nm, around 1 mW), applied at the end of one microstrip stub, increases losses in the pass-band is near 0.3 dB.

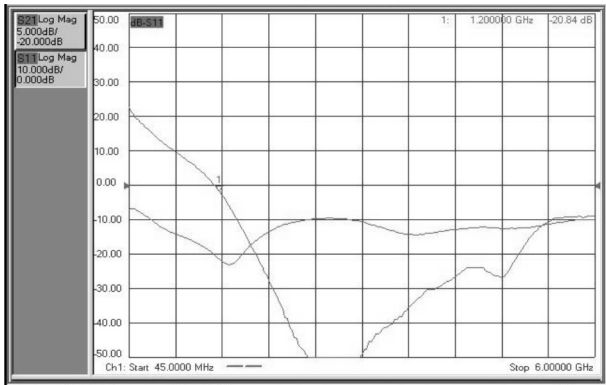


**Figure 8:** Measured  $S$ -parameters of the filter positioned 1m from 1000 W photo lamp. ( $S_{21}$  at 1.2 GHz is near -21 dB comparing with around -3 dB in dark)

Compared  $S_{21}$  parameters for ideal circuit, EM simulation and measured filter are presented in fig.9. All results are in a good agreement. Relative stop band width is over 70 % for 20 dB suppression. Reflection,  $S_{11}$ , in the pass band is -17 dB or lower.

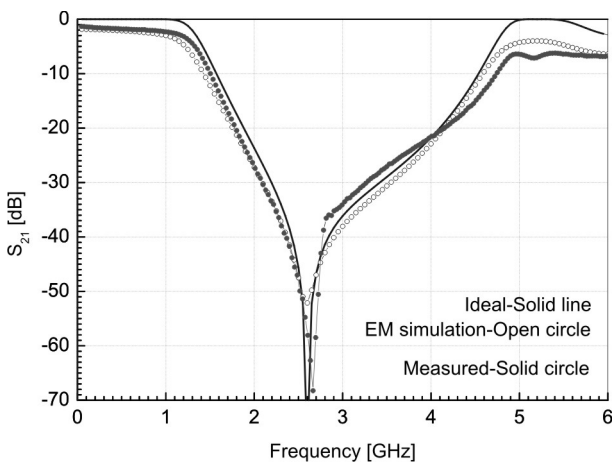


**Figure 9:** Compared results of  $S_{21}$  for ideal circuit, EM simulated and measured filter

Losses in the pass-band can be caused by: 1) connectors, 2) bonding between connectors and Al metallization using silver epoxy, 3) sputtered Al metallization  $t = 3 \mu\text{m}$  thick, 4) Si dielectric losses 5) mismatching and 6) radiation. Parameter  $S_{11}$  in fig. 7 is less than -17 in the pass-band and mismatching is not a problem. Simulation of the same filter structure (and the same Si dielectric losses) with copper (Cu) metallization as an excellent conductor are presented in fig. 10. (Cu metallization is rarely used and is electroplated which is different technology). In fig. 10 pass-band losses are small, below 1 dB, for frequencies below 1 GHz. Radiation is not significant. Differences in the case of our fabricated filter are: 1) losses in the silver epoxy bonding between

SMA connectors and Al metallization and 2) losses in the sputtered Al metallization and its roughness.

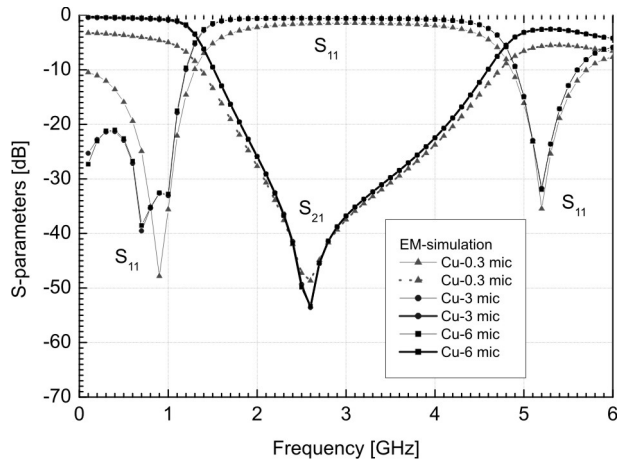


**Figure 10:**  $S_{21}$  of 3D EM simulation with copper (Cu) metallization of various thickness  $t$

Passive intermodulation was measured using signals on 1 GHz and 1.05 GHz with 2 x 4 dBm on input port of the filter. Each signal generator has one circulator for isolation and input into the filter is trough a power divider (from two ports to one). Spectrum analyser is connected to the output of the filter. Intermodulation was not noticed.

#### 4. conclusion

Low-resistivity silicon (standard CMOS-grade silicon) is a troublesome issue for the microwave passive components. One solution is using high-resistivity silicon (HRS). Circuit with ideal waveguides was simulated and successfully applied to band-stop microstrip filter on HRS ( $\rho = 5 \text{ k}\Omega\text{-cm}$ ). The filter was fabricated using aluminum (Al) sputtered metallization and etching of the filter pattern in Al. SMA connectors are bonded using silver epoxy. The fabrication stressed importance of the quality (fresh) silver epoxy for low losses.

There is a high agreement between ideal circuit simulation, 3D electromagnetic simulation in microstrip technology and measured results. Relative stop band width is over 70 % for 20 dB suppression. Reflection,  $S_{11}$ , in the pass band is -17 dB or lower. It means that the sputtered Al and the silver epoxy can be successfully applied for microwave structures on HRS.

#### Acknowledgements

This work was funded by European Commission 7th Framework Programme through the project Regmina,

grant 205533, and by Serbian Ministry of Education and Science, project TR 32008.

The authors are grateful to Institute IMTEL Communications, Belgrade, Serbia, for help in realization process, particularly to: I. Radnovic, N. Popovic and N. Tasic.

strip Load and Stub on Silicon Substrate", *Microwave and Optical Technology Letters*, 2003, vol. 39, no. 4, pp. 271-276.

Arrived: 28. 08. 2012

Accepted: 27. 11. 2012

## References

1. K. Kim, N. Kingsley, M. Morton, J. Papapolymerou, M.M. Tentzeris, and J.-G. Yook, "Fractal-Shape 40 GHz Microstrip Bandpass Filter on High-Resistivity Si for Suppression of the 2nd Harmonic", in *Proc. 35th European Microwave Conference*, Paris, 2005, pp. 825-828
2. L.W.L. Leung, K.J. Chen, X. Huo, and P.C.H. Chan, "Low-Loss Microwave Filter on CMOS-Grade Standard Silicon Substrate with Low-k BCB Dielectric", *Microwave and Optical Technology Letters*, 2004, vol. 40, pp. 9-11.
3. G. Six, G. Prigent, E. Rius, G. Dambrine, and H. Happy, "Fabrication and Characterization of Low-Loss TFMS on Silicon Substrate Up to 220 GHz", *IEEE Trans. Microwave Theory and Techniques*, vol. 53, pp. 301-305, 2005.
4. D. Nesić, "Microstrip Attenuator on Silicon Substrate with a Compact EBG (or PBG) Cell", in *Pro. TELSIKS 2005*, Nis, 2005, pp. 443-444
5. L. Martoglio, E. Richalot, G. Lissorgues-Bazin and O. Picon, "Low-Cost Inverted Line in Silicon/Glass Technology for Filter in the Ka-Band", *IEEE Trans. Microwave Theory and Techniques*, vol. 54, no. 7, pp. 3084-3089, 2006.
6. N. Thomson and J.-S. Hong, "Micromachined Interdigital Filter on Silicon", *Microwave and Optical Technology Letters*, 2006, vol. 48, pp. 1862-1866
7. M.-L. Ha, and Y.-S. Kwon, "Ku-Band Stop Filter Implemented on a High Resistivity Silicon with Inverted Microstrip Line Photonic Bandgap (PBG) Structure", *IEEE Microwave and Wireless Components Letters*, 2005, vol. 15, pp.410-412
8. D. Nesić, "Structures with One-dimensional Electromagnetic Bandgap in Microwave Technique", *PhD dissertation*, University of Belgrade, 2011.
9. F. Zhong, B. Zhang, Y. Fan, M. Zhao and K. Xu, "Development of an Improved Sub-Harmonic Mixer Based on Planar Schottky Diodes at 94 GHz", *Research Journal of Applied Science, Engineering and Technology*, 4 (13), 1895-1898, 2012
10. <http://www.aeroconf2012.org/resources/junior-engineering/16%20Amyantennas.ppt>
11. A. Bhadauria, Nasimuddin, A. K. Verma, E. K. Sharma and B. R. Singh, "Optically Controlled Micro-

## *In memoriam Marija Kosec*

*Professor Dr. Marija Kosec passed away after a brief and serious illness on 23 December 2012.*



Professor Marija Kosec was a very active and strong supporter of Society for Microelectronics, Electronic Components and Materials MIDEM and its long-term member. In the years 1996-2005 she was the President, and in the periods 1989-1996 and 2005-2011 the Vice-President of the society.

She studied chemical technology at the University of Ljubljana and obtained a PhD degree in chemistry in 1982. Since 1971 she was employed at the Jožef Stefan Institute, and since 2002 she was Head of the Electronic Ceramics Department. In 2007 – 09 she was the President of the Scientific Council of Jožef Stefan Institute.

In the years 2004 – 09 she was leading the Centre of Excellence Materials for electronics of next generations and other emerging technologies and since 2009 the Centre of Excellence Advanced Materials and Technologies for the Future NAMASTE.

Since 1999 she was Professor of Materials Science at the University of Ljubljana and the vice-president of Jožef Stefan Postgraduate School. She was visiting professor at Ecole Polytechnique Fédérale de Lausanne, Switzerland, Shizuoka University, Japan and for short periods

at a number of other schools. She was Adjunct Professor at Xi'an Jiaotong University, China.

She was the only female member of Slovenian Academy of Engineering since its establishment in 1995 and in 2005 – 06 its President.

Prof. Kosec supported the European Cooperation in Science and Technology framework COST for many years, actively participating in COST Actions since 1991. Until 2010 she represented Slovenia in the COST Materials Nanosciences Physics Domain Committee (MPNS DC). In 2010 she was nominated MPNS DC expert for Slovenia.

Since 1999 she was the member of the European Liaison Committee of International Microelectronics and Packaging Society and since 2001 the member of the Ferroelectrics Committee at IEEE.

Prof. Kosec was Ambassador of Science of Republic of Slovenia (2003). She was the recipient of the Zois award, the highest national science award in 2006. In 2009 she received Puh recognition for the implementation of research results in industry.

In 2010 she received the Ferroelectrics Recognition Award, IEEE Ultrasonics, Ferroelectrics, and Frequency Control Society for her significant contributions to the processing science and technology of ferroelectric powders, bulk ceramics, thin and thick films.

Her research interest was in synthesis and characterization of electronic ceramics, particularly piezoelectrics and ferroelectrics in bulk, thin and thick film form. Her contribution to science was in understanding phenomena of ceramics processing of application-important multi-component systems. Her mission was to merge basic research with applied research and development. She participated, as member or principal investigator, in more than 20 European framework or international projects and she had more than 40 contracts with industry.

She was author or co-author of more than 300 scientific papers in international journals with more than 2000 citations. She gave more than 150 invited talks at international conferences and at different research institutions including Max Planck Institut, MIT, Tokyo Institute of Technology, and at important Japanese producers of electronic components including Murata, TDK, Panasonic and Toshiba.

She chaired the international conference Electroceramics VII in 2000, the European conference Processing of

Electroceramics in 2003 and the 4th European Microelectronics and Packaging Symposium in 2006.

In an effort to strengthen the cooperation between science and industry she organized, together with the Technology Centre SEMTO, a series of meetings where researchers, developers and users could present results, discuss, and exchange ideas. In 2012 she was the chair of the 48<sup>th</sup> International Conference on Microelectronics, Devices and Materials with the Workshop on Ceramic Microsystems and she managed to attract many participants from Slovenian industry.

The world of science lost not only a great scientist, but also a woman who was able to accept challenges and solve them with optimism and a positive approach. One of her acquaintances from abroad wrote that she was a sunny personality. Professor Marija Kosec was, if I may borrow the words of the current President of the MIDEM Society, Professor Marko Topič, a bright star in the sky of Slovenian science.

She will be missed by her colleagues and friends both at home and in the international communities.

Prof. Dr. Barbara Malič  
Jožef Stefan Institute

## MIDEM 2013

49<sup>th</sup> INTERNATIONAL CONFERENCE ON MICROELECTRONICS, DEVICES AND MATERIALS WITH THE WORKSHOP ON DIGITAL ELECTRONIC SYSTEMS

### CALL FOR PAPERS

**Announcement and Call for Papers**  
**September 25<sup>th</sup> – 27<sup>th</sup>, 2013**  
**Hotel Larix, Kranjska Gora, Slovenia**

**ORGANIZER: MIDEM Society** - Society for Microelectronics, Electronic Components and Materials, Ljubljana, Slovenia

**CO – ORGANIZER: CO NAMASTE** - Centre of Excellence, Ljubljana, Slovenia

**CONFERENCE SPONSORS:** Slovenian Research Agency, Republic of Slovenia; IMAPS, Slovenia Chapter; IEEE, Slovenia Section; Zavod TC SEMTO, Ljubljana.

#### GENERAL INFORMATION

The 49<sup>th</sup> International Conference on Microelectronics, Electronic Components and Devices with Workshop on Digital Electronic Systems continues the tradition of the annual international conferences organised by MIDEM, Society for Microelectronics, Electronic Components and Materials, Ljubljana. The conference will be held in **Kranjska Gora**, Slovenia, well-known ski resort and conference centre, from **SEPTEMBER 25<sup>th</sup> – 27<sup>th</sup>, 2013**.

Topics of interest include but are not limited to:

- Novel monolithic and hybrid circuit processing techniques,
- New device and circuit design,
- Process and device modelling,
- Semiconductor physics,
- Sensors and actuators,
- Electromechanical devices, Microsystems and nanosystems,

- Optoelectronics,
- Photovoltaic devices,
- New electronic materials and applications,
- Electronic materials science and technology,
- Materials characterization techniques,
- Reliability and failure analysis,
- Education in microelectronics, devices and materials.

#### ABSTRACT AND PAPER SUBMISSION:

Prospective authors are cordially invited to submit up to 1 page abstract before **May 1<sup>st</sup>, 2013**. Please, identify the contact author with complete mailing address, phone and fax numbers and e-mail address.

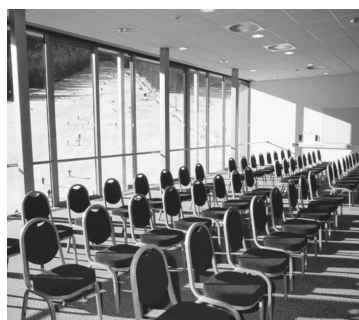
After notification of acceptance (**June 1<sup>st</sup>, 2013**), the authors are asked to prepare a full paper version of six pages maximum. Papers should be in black and white. Full paper deadline in PDF and DOC electronic format is: **August 1<sup>st</sup>, 2013**.

#### IMPORTANT DATES:

- Abstract deadline: **May 1<sup>st</sup>, 2013** (1 page abstract or full paper)
- Notification of acceptance: **June 1<sup>st</sup>, 2013**
- Deadline for final version of manuscript: **August 1<sup>st</sup>, 2013**

Invited and accepted papers will be published in the conference proceedings.

Detailed and updated information about MIDEM Conferences is available at:  
<http://www.midem-drustvo.si/> under Conferences.





# *Boards of MIDEM Society | Organi društva MIDEM*

## *MIDEM Executive Board | Izvršilni odbor MIDEM*

### **President of the MIDEM Society | Predsednik društva MIDEM**

Prof. Dr. Marko Topič, University of Ljubljana, Faculty of Electrical Engineering, Slovenia

### **Vice-presidents | Podpredsednika**

Prof. Dr. Barbara Malič, Jožef Stefan Institute, Ljubljana, Slovenia

Dr. Iztok Šorli, MIKROIKS, d. o. o., Ljubljana, Slovenija

### **Secretary | Tajnik**

Olga Zakrajšek, UL, Faculty of Electrical Engineering, Ljubljana, Slovenija

### **MIDEM Executive Board Members | Člani izvršilnega odbora MIDEM**

Prof. Dr. Slavko Amon, UL, Faculty of Electrical Engineering, Ljubljana, Slovenia

Darko Belavič, In.Medica, d.o.o., Šentjernej, Slovenia

Prof. Dr. Bruno Cvikl, UM, Faculty of Civil Engineering, Maribor, Slovenia

Prof. Dr. Leszek J. Golonka, Technical University Wroclaw, Poland

Leopold Knez, Iskra TELA d.d., Ljubljana, Slovenia

Dr. Miloš Komac, UL, Faculty of Chemistry and Chemical Technology, Ljubljana, Slovenia

Prof. Dr. Marija Kosec, Jožef Stefan Institute, Ljubljana, Slovenia

Prof. Dr. Miran Mozetič, Jožef Stefan Institute, Ljubljana, Slovenia

Jožef Perne, Zavod TC SEMTO, Ljubljana, Slovenia

Prof. Dr. Giorgio Pignatelli, University of Perugia, Italia

Prof. Dr. Janez Trontelj, UL, Faculty of Electrical Engineering, Ljubljana, Slovenia

## *Supervisory Board | Nadzorni odbor*

Prof. Dr. Franc Smole, UL, Faculty of Electrical Engineering, Ljubljana, Slovenia

Mag. Andrej Pirih, Iskra-Zaščite, d. o. o., Ljubljana, Slovenia

Dr. Slavko Bernik, Jožef Stefan Institute, Ljubljana, Slovenia

## *Court of honour | Častno razsodišče*

Emer. Prof. Dr. Jože Furlan, UL, Faculty of Electrical Engineering, Slovenia

Prof. Dr. Radko Osredkar, UL, Faculty of Computer and Information Science, Slovenia

Franc Jan, Kranj, Slovenia

**Informacije MIDE**  
*Journal of Microelectronics, Electronic Components and Materials*  
ISSN 0352-9045

*Publisher / Založnik:*  
*MIDEM Society / Društvo MIDE*  
*Society for Microelectronics, Electronic Components and Materials, Ljubljana, Slovenia*  
Strokovno društvo za mikroelektroniko, elektronske sestavne dele in materiale, Ljubljana, Slovenija

[www.midem-drustvo.si](http://www.midem-drustvo.si)